The Reliability Margin of the Direct Strength Method Prediction Model for Cold-Formed Steel Members

by

Alexander Bauer

Thesis presented in partial fulfilment of the requirements for the degree of Master of Engineering (Structural) in the Faculty of Engineering at Stellenbosch University

Department of Civil Engineering.
University of Stellenbosch.
Private Bag X1, 7602 Matieland, South Africa.

Supervisors: Dr. C. Viljoen
Mr. E. van der Klashorst

March 2016

The financial assistance of the National Research Foundation (NRF) towards this research is hereby acknowledged. Opinions expressed and conclusions arrived at, are those of the author and are not necessarily to be attributed to the NRF.

Declaration

By submitting this thesis electronically, I declare that the entirety of the work contained therein is my own, original work, that I am the sole author thereof (save to the extent explicitly otherwise stated), that reproduction and publication thereof by Stellenbosch University will not infringe any third party rights and that I have not previously in its entirety or in part submitted it for obtaining any qualification.

Date: .....

Abstract

SANS 10162-2, the South African standard for structural purpose cold-formed steel, allows for design of members to resist loading of compression, bending and combinations of these among others. The focus of this research is to determine the reliability of member strength design according to the standard, following the Direct Strength Method (DSM) for beams and columns. The DSM is an empirical design prediction model that has been developed through testing and from prediction curves based on the Effective Width Method (EWM). Member strength from the DSM is dependent on three dominant buckling modes. The design failure capacity considers local, distortional and global (flexural, torsional or torsional-flexural) buckling. For the local and distortional buckling cases some post buckling reserve consideration is incorporated by the DSM. To attain the reliability margin for the design of members using the DSM, the First Order Reliability Method (FORM) was implemented in combination with the semi-empirical Finite Strip Method (FSM). The FSM allows prediction of the elastic buckling loads, which are necessary for the capacity prediction, as well as buckling modes and shapes. A FSM model can therefore be used to numerically determine the directional derivatives of the limit state function necessary for the FORM and allows for a unique approach to conventional FORM. Based on literature, probabilistic parameters that form part of the investigation presented are: the yield stress, the thickness and the model factors for the prediction curves.

The integrated DSM-FORM procedure was used to determine the reliability margin for various member lengths with idealised pin-pin ended boundary conditions. A typically used lipped C-section, which conforms to the geometric limitations of the DSM, was investigated for the design of concentric axial compression and pure laterally unrestrained bending. Normal probability distributions were used for the thickness and model factor variables. A lognormal distribution and a design yield strength of 300 MPa was assumed for all members. Discrete member lengths ranging from 0.1 m to 4 m were investigated to determine the reliability across multiple failure modes.

For the members designed in compression, reliability indices as low as $\beta_R = 1.31$ were obtained relating to local buckling capacity prediction. A minimum reliability index of $\beta_R = 1.32$ was found by the FORM for compression

members failing due to global buckling. No reliability index was found as a result of the distortional buckling failure mode, since the lipped C-section analysed does not fail from this buckling mode.

Members designed for uniform laterally unrestrained bending were analysed for failure from all buckling modes, depending on member length. A minimum reliability index of $\beta_R = 1.69$ was found for members designed to resist distortional buckling failure. From the local-global buckling interaction assumed in the DSM bending capacity equations, a minimum reliability index of $\beta_R = 1.45$ was obtained for both failure modes as a result of the analyses.

The findings of this thesis show that the level of reliability achieved by the DSM is not consistent across all modes of failure. This is largely attributed to the fact that one partial factor is used in the design process, to ensure reliability across all failure modes of the design resistance. It may be more appropriate to apply different partial factors to the three failure modes. Also, the reliability indices across all modes of failure were shown not to conform to the targeted reliability from calibration. The assessed reliability indices in addition do not conform to the conservative resistance based target of $\beta_{t_R} = 2.4$ for the South African structural design standard. Due to the South African loading code not covering the sensitivity of the resistance targeted by the currently provided partial factors for the DSM, lowering of the partial factors is recommended.

Acknowledgements

The compilation of this document would not have come about were it not for a specific number of people. Their involvement in my life during the course of this project must be mentioned in order to attribute to the achievement that this work presents.

First and foremost I want to thank Etienne van der Klashorst for providing me with the opportunity to receive funding during my post graduate studies. I would also like to mention the significant impact he has had on my academics, by introducing me to the theory behind steel member design and by his supervision during the progress of this thesis.

Secondly I have to express my appreciation to Dr Celeste Viljoen, whom I was introduced to in my first year of studies as the lecturer for Strengths of Materials. Without her supervision, progress towards completion of this document would never have taken the course that it did.

Furthermore I would like to thank both my parents for ensuring everything they did that has made it possible for me to reach this point in my life. They always supported the decisions that I have made and have cheered me on after making them. I would also like to acknowledge my mother Jasmin Kötting-Bauer for the hours that she spent proof reading my thesis.

Lastly I need to thank some of my friends for their support during my 6 years of being a student: Oliver Lerch, Jonathan Edmunds and Arnim Ritter. Also thanks to all of the Masters students sharing my office with me and for their opinion when I required it. Finally thanks must be given to Olaf Diener, for hearing me out all the time and for making sure that my student life will never be forgotten.

Contents

List of Figures

List of Tables

Nomenclature

Acronyms

AISI	American Iron and Steel Institute
AS	Australian Standard
B	Bending
CA	Canada
cFSM	constrained Finite Strip Method
COV	Coefficient of variation
D	Distortional deformation
DOF	Degree of Freedom
DSM	Direct Strength Method
EN	Eurocode
EWM	Effective Width Method
FORM	First Order Reliability Method
FSM	Finite Strip Method
G	Global deformation
GBT	Generalised Beam Theory
ISO	International Standards Organisation
L	Local deformation
LN	Lognormal probability distribution
MPP	Most Probable Point
N	Normal probability distribution

NZS New Zeeland Standard

PS Plane stress

SANS South African National Standard

SASFA South African Light Steel Frame Building Association

ST Transverse shear deformation

USA United States of America

VaP Variable Processor

Symbols

$[\Lambda]$ Diagonal matrix of eigen-values

$[\Phi]$ Matrix of eigen-modes

$[D]$ Material matrix relating to generalised Hook's law

$[K_e]$ System elastic stiffness matrix

$[k_e]$ Strip element elastic stiffness matrix

$[K_g]$ System geometric stiffness matrix

$[k_g]$ Strip element geometric stiffness matrix

$[R_M]$ Modal constraint matrix

α_E Sensitivity of the load effect

α_n Sensitivity of a random variable

α_R Sensitivity of the resistance

β Reliability index

β_R Reliability index from resistance based analysis

β_t Overall target reliability index

β_{tR} Target reliability index for the resistance side of the margin

δ_D Bias factor of the dead load

δ_E Bias factor of the load effect

δ_I Bias factor of the imposed load

δ_R Model factor of the resistance

δ_W	Bias factor of the wind load
ϵ	Normal strain
γ	Shear strain
κ_x	Curvature along x-axis
λ	Plate slenderness
λ_d	Distortional buckling slenderness
λ_g	Global buckling slenderness
λ_l	Local buckling slenderness
λ_n	Load level
μ_D	Mean value of the dead load
μ_E	Mean value of the load effect
μ_G	Mean value of reliability margin
μ_I	Mean value of the imposed load
μ_n	Mean value of a random variable
μ_R	Mean value of the resistance
μ_W	Mean value of the wind load
μ_{δ_R}	Mean model factor of the resistance
μ_{δ_t}	Mean value of the bias factor for the thickness
∂	Partial derivative operator
Φ	Cumulative probability density function
ϕ_b	Partial factor for members subjected to bending
ϕ_c	Partial factor for members subjected to compression
π	Mathematical constant for denoting the ratio of a circle's circumference to it's diameter
ρ	Correlation coefficient
σ	Stress
σ_E	Standard deviation of load effect

σ_G Standard deviation of the reliability margin

σ_n Standard deviation of a random variable

σ_R Standard deviation of the resistance

σ_{δ_R} Standard deviation of the model factor of the resistance

σ_{δ_t} Standard deviation of bias factor for the thickness

$\sigma_{\delta_{f_y}}$ Standard deviation of the bias factor for the yield stress

σ_{cr} Critical buckling stress

σ_e Effective stress

τ Convergence criteria for the reliability index

θ Local rotational deformation about the y-axis

φ Probability density function

$\{\alpha\}$ Sensitivity factor vector for all random variables

$\{\epsilon\}$ Cauchy strain vector

$\{\phi\}$ Eigen-mode vector

$\{D\}$ Directional derivative vector

$\{d\}$ Deformation vector

$\{u\}$ Vector of realisation of standardised variable

$\{X\}$ Vector of random variables

$\{x\}$ Vector of realisations of random variables

$\{x^*\}$ Vector of realisations of random variables at the design point

$\{x_d\}$ Vector of realisations of values used in design

a Finite strip length term; Skewness of probability density function

A_g Gross cross-section area

b Plate width

B_e Effective dimension parameter

b_e Effective plate width

B_g Gross dimension parameter

D	Dead load
D_n	Nominal dead load
E	Load effect
E	Young's Modulus of elasticity
E_n	Nominal load effect
f	Applied stress
$F_{cr,d}$	Member elastic critical buckling stress due to distortional buckling
$F_{cr,l}$	Member elastic critical buckling stress due to local buckling
$F_{cr,n}$	Mode dependant member elastic critical buckling stress
F_e	Member effective stress
F_g	Member capacity stress
F_{model}	Predicted capacity by model
F_n	Member uniform capacity stress
F_{test}	Tested capacity
f_{y_d}	Yield stress used for design
F_y	Section steel yield stress
f_y	Yield stress
G	Limit state function
G	Shear modulus
h	Finite difference length
I	Imposed load
i	Index of load effect considered
I_n	Nominal imposed load
k	Effective slenderness factor
L	Physical length
l	Centreline lip length
M	Applied bending moment

m	Longitudinal strip number
$M_{cr,d}$	Distortional buckling based bending moment capacity of a beam
$M_{cr,e}$	Global elastic critical bending capacity of a beam
$M_{cr,e}$	Global elastic critical bending moment capacity of a beam
$M_{cr,l}$	Local buckling based bending moment capacity of a beam
M_{cr}	Elastic critical buckling bending moment
M_{nd}	Distortional buckling based bending moment capacity of a beam
M_{ne}	Global buckling based bending moment capacity of a beam
M_{nl}	Local buckling based bending moment capacity of a beam
M_{test}	Bending moment beam capacity from testing
M_y	Moment of first yield
n	Index
P	Axial load
p_f	Probability of failure
$P_{cr,d}$	Distortional elastic buckling capacity of a column
$P_{cr,e}$	Global elastic buckling capacity of a column
$P_{cr,l}$	Local elastic buckling capacity of a column
P_{cr}	Elastic critical axial buckling load
P_{nd}	Distortional buckling based axial capacity of a column
P_{ne}	Global buckling based axial capacity of a column
P_{nl}	Local buckling based axial capacity of a column
P_{test}	Axial column capacity from testing
P_y	Column squash load
Q	Variable load
q	Total longitudinal strip number
R	Resistance
r	Centreline corner radius

r_d Deterministic load effect

R_n Nominal resistance

T Traction or edge load

t Thickness

t_d Thickness used for design

U, V, W Global deformation variables

u, v, w Local deformation variables

U_n Standardised variable

u_n Realisation of standardised variable

v Poisson's ratio

V_n Coefficient of variation of random variable

V_{δ_E} Coefficient of variation of the load effect

V_{δ_R} Coefficient of variation of the resistance

V_{δ_t} Coefficient of variation of the bias factor for the thickness

$V_{\delta_{f_y}}$ Coefficient of variation of the bias factor for the yield stress

V_t Coefficient of variation of the thickness

W Wind load

w Member element centreline length

W_n Nominal wind load

X, Y, Z Global left hand rule coordinates

x, y, z Local left hand rule coordinates

X_n Random variable

x_n Realisation of random variable

Z_g Gross section modulus

Z_y Section modulus of first yield

Chapter 1

Introduction

Introducing new and improved design procedures into codified design standards requires fundamental understanding of the reliability of such methods. Determining the full extent of the reliability that a new design procedure presents, requires complex probabilistic analysis covering the influence of the structural design variables. Investigation into the influence of these variables should therefore be conducted, to establish what aspects in the design process impact the reliability outcome. Factors attributed to the required level of reliability are branches such as ethics, the environment and economics.

Cold-formed steel is used as a building material in structures ranging from office buildings to storage warehouses. Due to the light weight of cold-formed steel and its slenderness, wind loading generally dominates the structural design. Consequences of failure of these structures may be the loss of human life, environmental pollution or simply damage to financial assets.

A new design method for cold-formed steel members has been developed over the last two decades. This so called Direct Strength Method combines an integrated process that requires computer aided output with codified design equations. The reliability achieved by member design according to this design model is relatively un-established within the South African design context and is therefore investigated.

1.1 Motivation

The reliability implied in a member resistance design code is based on partial factor calibration. Since the South African National Standard 10162-2 (from here on referred to as SANS 10162-2) for structural use of cold-formed steel members has been introduced to the South African structural design codes, some level of reliability is associated with the use of this standard. However, the code is an adaptation of the Australian/New Zealand Standard (AS/NZS

4600) and the inherent level of reliability does not conform to the required level of reliability of $\beta_t = 3.0$ of the South African Standard. The aimed reliability of the partial factors currently included in the adopted standard are based on a significantly basic calibration and target a level of reliability of $\beta_t = 2.5$. This is a cause for concern and requires investigation.

Once the influences on the reliability are understood, future research regarding calibration of the reliability level to the norm of the South African basis of structural design can be conducted. This thesis should provide the necessary discussions to contribute to such a development.

1.2 Aims and objectives

The main objective of this thesis is to determine the reliability of member design according to the Direct Strength Method. Since the method allows for the design of column as well as beam members, the reliability from these design procedures is specifically of interest.

A model for the reliability analysis needs to be formulated in terms of multiple random variables to allow for insight into how these parameters affect the reliability. Furthermore the limits and extents of the influences need to be examined and presented.

Due to the nature of the design method, various numerical techniques have to be combined to determine the reliability. This thesis aims to provide and document the required procedure for a relatively basic limit state model associated with member design according to the Direct Strength Method.

Once all of the above is achieved, the reliability behaviour results must be produced from analysis and must be critically evaluated.

1.3 Method

To understand all parameters that affect the reliability, this investigation starts by determining the origin and principles of the Direct Strength Method as a design procedure. This includes presenting the knowledge necessary to make use of the Finite Strip Method. The direct link between these two methods is explained in depth.

Thereafter, the First Order Reliability Method is used to determine the reliability index of resistance-design from the Direct Strength Method. The unique feature, which is that the Direct Strength Method requires a numerical

method-based input, is exploited to calculate arithmetically finite differences of the capacity prediction. This is done to determine directional derivatives required in a FORM procedure. A case specific cross-section is used to determine the reliability of column and beam member design. By means of an explicit performance surface for 1 m member length, the FORM procedure implemented is confirmed by comparing reliability index results with those obtained from the well-established reliability analysis program VaP. Then the author's analysis algorithm is used to analyse reliability associated with member design for increased lengths. This is necessary to cover the full design equation spectrum associated with the Direct Strength Method. In order to understand the implications of the results, background to the reliability analysis procedure is also presented. All basic assumptions for this analysis are also examined in this document. Multiple preliminary investigations are performed, before the final results are presented and discussed.

1.4 Limitations

Determining the reliability that results from using a specific design procedure such as the Direct Strength Method requires a full probabilistic load effect and resistance analysis. However, the focus of this research will be limited to the reliability achieved from member resistance design only.

The Direct Strength Method only applies to pre-qualified cross-sections as well as a limited scope of steel grades. Only conventionally available 300 MPa cold-formed steel complies with the limitations of both compression and flexural members and is therefore investigated. Also all geometric limits set out by the Direct Strength Method are adhered to. Furthermore only design for strong axis bending is considered for beam members.

All design processes are based on the South African National Standard 10162-2 for cold-formed steel member design. Steps and model input used in this thesis comply specifically to this standard.

1.5 Outline of the thesis

Chapter 2 starts by presenting the development and fundamentals behind the Direct Strength Method and explains the tools required for an analysis of this strength prediction model. First plate stability together with the Effective Width concept are explained. The research development of the Direct Strength Method and the links to the Effective Width are elaborated thereafter. The numerical Finite Strip Method is then presented for determination of the critical elastic buckling coefficients used in the Direct Strength Method.

Lastly, Chapter 2 explains the First Order Reliability Method for determining the reliability index. Together with this a literature comparison is made to establish what probabilistic variables were considered in the calibration of the partial factor.

Chapter 3 presents the limit state function which the Direct Strength Method proposes. The interaction between the numerical methods and the limit state function is then defined. All analysis critical parameters are addressed and formulated. Thereafter basic assumptions regarding model input are addressed based on literature. A performance surface is used to verify the interactive FORM analysis and initial reliability results are produced. These results are then compared to the target reliability.

Chapter 4 presents reliability results from an increasing member length. All results are discussed based on capacity predictions for the case-specific cross-section. Lastly the results are once more compared to the targeted reliability.

Chapter 5 concludes the most important outcomes of the results based on the discussion of the previous chapters. Recommendations are made for future research in the field based on the conclusions.

Chapter 2

Background into Cold-Formed Steel and Structural Reliability

2.1 Cold-formed steel in the South African design context

Cold-formed steel building construction originated from the American timber structure industry. According to Schafer (2011) cold-formed steel members can be summarized as having three main load bearing applications:

1. Framing
2. Metal buildings with clear spans
3. Storage racks

Cold-formed steel can be made by one of two processes; either from break-pressing or cold-rolling. For both methods thin sheet steel is used which is produced from cold rolling of steel plates up to 25.4 mm thick (Yu and LaBoube, 2010). Members are considered highly slender, which means that the thickness in relation to the width is quite small. Since the sheet steel is generally less than 6.35 mm, but larger than 0.378 mm thick (Yu and LaBoube, 2010), it can be bent into any shape imaginable and the possible cross-section shapes are endless. Research has already been conducted by Li *et al.* (2014) and Gilbert *et al.* (2012) into optimal shapes for various bearing applications with some symmetry and sectional property constraints. However, conventional cross-sections used in the South African industry are the well known: C-Section, Lipped C-Section, Hat-Section and Z-Section.

Built-up members of the above mentioned profiles also exist. Figure 2.1 depicts various possible member sections, including the above mentioned cross-sections.

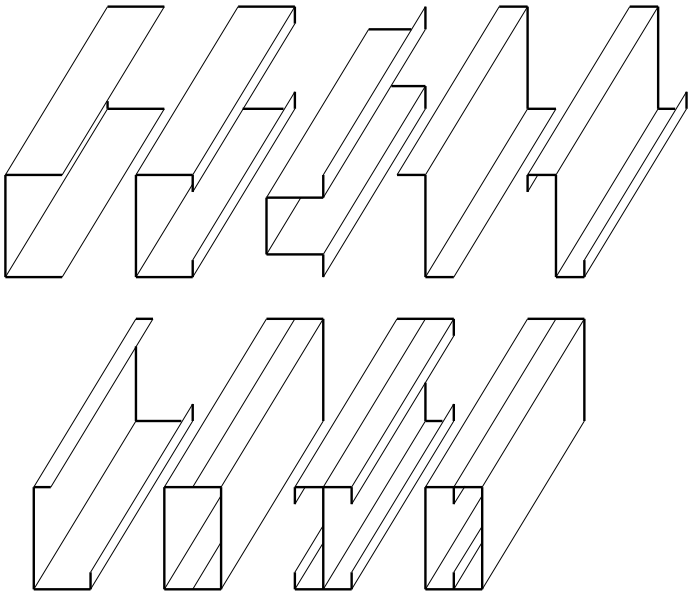

Figure 2.1: Various cold-formed steel member shapes

The basis for structural member design in South Africa is the SANS 10162-2 standard which is a direct adaptation of the Australian/New Zeeland Standard AS/NZS 4600 of 2005, adopted in 2011. The major origin of the standard's equations and specifications can be traced back to the research for the American Iron and Steel Institute, Canadian Standards Association and Camara Nacional de la Industria del Hierro y del Acero's standard for cold-formed steel members, also referred to as the North American Specification or AISI-S100-07 (2012).

SANS 10162-2 defines member strength and built-up member strength of C250 to C450, and G250 to G550 grade steel for: tension, compression, bending, shear and combined loading. The standard allows member design from two different methods, namely: the Effective Width Method (from here on referred to as EWM) and the Direct Strength Method (referred to as DSM).

The latter design procedure is a relatively new development based on research conducted over the last two decades and allows for member design in compression and bending. As mentioned in the introductory chapter these two forms of loading are the focus of this research. Furthermore the Direct Strength Method has some geometrical limitations for the mentioned standard cross-sections as well as the members' yield strength and these are addressed at a later stage.

2.2 Stability of cold-formed steel members

2.2.1 Introduction

To understand the mechanics behind the failure of cold-formed steel, basic stability of members must first be discussed. According to the Guide to Stability Design Criteria for Metal Structures (Ziemian, 2010), instability is the condition where a compressed structural element loses its ability to resist an increase in load. Hence the element loses its ability to resist load altogether, which results in collapse in service. As both columns and beams may need to resist compressive stress in the member, stability is typically the limiting strength design parameter for both of these structural members.

The generalised behaviour of compressive and flexural structural components is that members first deform axially and at a point during loading start to deform in some other deformation mode such as lateral bending, also referred to as buckling. The terminology used when referring to the compressive load against axial-deflection peak before the onset of the lateral form of deformation starts in members such as columns, cylindrical shells and plates, is referred to as the critical load or the equilibrium bifurcation point. This concept is an idealised model which assumes that before the onset of the critical load, the element behaves elastically. However, this simplification does not represent the true behaviour of members. True non-linear behaviour of the member needs to be considered and additional factors effecting the real behaviour, such as initial out of straightness, imperfect loading and material imperfection, must also be taken into account in the model. Incorporating these imperfections predicts the true behaviour of a compressed member, with minor lateral deformation onset visible at early stages of loading. Furthermore the point of loss of stability is often associated with the critical load. However, instability with the connotation of limit of strength is also affected by the effective slenderness.

Figure 2.2 shows a graph of lateral deflection against the load and the onset of buckling of various types of structural elements, for both the idealised and the imperfect state. In the graph the effect of three types of structural elements having different effective slendernesses is visible, with the perfect state represented by solid lines and the imperfect sate by dashed lines. The point of instability for a thin-walled cylinder can be seen at it's peak axial load. Thin-walled cylinder stability behaviour is also refereed to as unstable buckling. The point of instability for the slender column is clearly set out by the idealised column line. Elastic buckling in slender columns is also known as stable buckling. However, only the onset of instability for the thin stiffened plate is shown in the figure, with the true instability associated with the peak load not visible. This behaviour is also referred to as possessing a post buckling reserve. Cold-formed steel members are allowed to be simplified to thin plates that are supported along the bends and thus exhibit the compressive behavioural

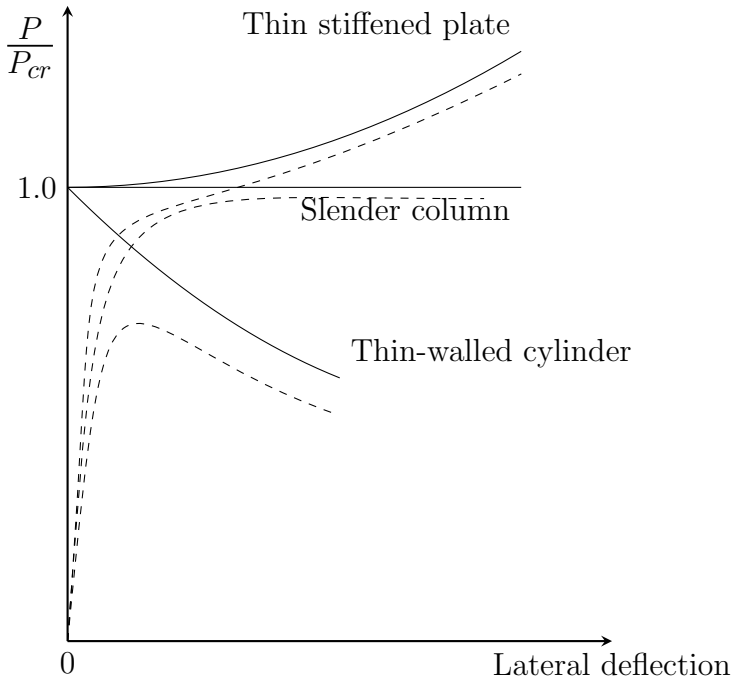

Figure 2.2: Elastic post buckling curves for compressed elements (Ziemian, 2010)

properties of edge supported, in other words stiffened, plates. Thus a more in-depth explanation for the stability behaviour of thin plates is presented next.

2.2.2 Stability of thin plates

Plates are prone to buckling when subject to loading of either direct compression, bending or a combination of these. This follows from the fact that in-plane stresses at some orientation form principle stresses of either pure tension and compression, or pure shear. The compressive principle stress direction is nevertheless responsible for the buckling phenomenon.

The buckling stress for slender plates with long loaded edges was investigated by Timoshenko and Gere (1961), who formulated a differential equation for behavioural predictions. The fundamental solution to the equation and the associated stress causing the onset of bucking and how it depends on the edge restraint is given by Equation 2.1.

$$\sigma_{cr} = k\frac{\pi^2 E}{12(1-v^2)(b/t)^2} \tag{2.1}$$

In Equation 2.1 the critical buckling stress (σ_{cr}) is a function of the plate length (b) to plate thickness (t) ratio. Material behaviour is assumed to be

linear-elastic and isotropic and the parameters of modulus of elasticity as well as Poisson's ratio (v) effect the buckling stress accordingly. The predicted deformation resulting from the solution to the differential equation show that deformation takes place in the form of sinusoidal half-wavelengths. If the length to thickness ratio of the loaded edge is decreased, the solution approaches the Euler buckling solution for a slender plated-column. At the same time the buckling solution is still influenced by the plate buckling slenderness factor (k), which depends on the width to hight ratio. The plate buckling slenderness factor can further be used for predicting the critical load of plates subject to other forms of planar loading, with pure bending being another major load condition of interest. The k-factor also takes the edge restraint effect into account. Various k values and their influence on buckling have been studied and are listed by the SANS standard and various other literature.

Plate capacity is also limited by yielding, or inelastic buckling, depending on the slenderness of the plate. The critical buckling stress from Equation 2.1 is only valid for elastic behaviour and is used as an idealized reference for the capacity. The buckling phenomenon is once again amplified in real plate behaviour by imperfections before the point of instability or ultimate strength is reached. Yet, as mentioned, plates may be able to resist loads even after the onset of elastic local buckling. This post buckling reserve is only observed in plates that have some restraint on the effective slenderness. All elements in cold-formed members exhibit this restraint attribute to a certain extent. A good conceptual illustration that shows the effect restrained edges have on the effective slenderness is presented by the grid analogy.

Figure 2.3 shows this illustrative example where a simply supported plate resists some edge loading. As the vertical struts in the plate start to buckle laterally, a tension field of horizontal ties is developed by the restrained edges. This tension field is responsible for the post buckling reserve in the elastic range as the effect of the field increases from additional loading long before the material has failed. The membrane tension field developing perpendicular to the direction of the compressive load follows from the principle compression stress orientation. From the grid it is additionally visible that the restraint provided by the ties is larger, closer to the restrained edges. Thus the load resisted by the edges of the plates is larger than at the already deformed centre. At the supported edges, portions of the plate may start yielding at an applied stress lower than the elastic buckling stress. That is why it is difficult for certain plates to define their buckling behaviour as being either perfectly elastic or inelastic. The early lateral deformation onset by imperfections causing geometrically non-linear behaviour makes it difficult to predict the ultimate resistance of plates exhibiting post buckling capacity. This true deformation behaviour observed in real plates is the basis for the Effective Width Method (from here on referred to as EWM) as a design procedure.

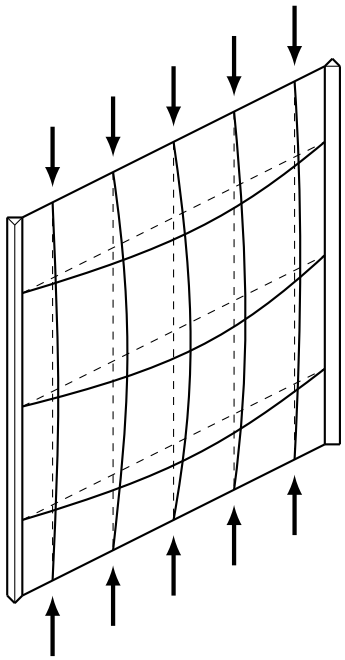

Figure 2.3: Analogous grid of a plate for uniform edge loading illustrating post-buckling reserve (American Iron and Steel Institute *et al.*, 2012)

2.2.3 Effective Width Method

The first strength design procedure for thin walled, cold-formed steel was developed by the American Iron and Steel Institute in 1946 (Ziemian, 2010). It incorporated the post buckling reserve observed in highly slender cold-formed steel profiles. All major developments in the design for cold-formed members specification including countries such as Canada (S136), Australia and New Zealand followed from the AISI development (Yu et al., 2005), the latter design specification being the fundamental origin of the South African Standard. The basis for this now well established procedure is the so called "Effective Width".

As has already been introduced, the most important factor which contributes to the post buckling behaviour is the fact that the restrained edges allow for stress redistribution after a section in the plate starts to buckle. The stress distribution for a slender plate with edge restraints (see Figure 2.3) as loading increases is idealized in Figure 2.4.

The stress distribution starts off as uniform through the width b of the plate, before the onset of local buckling. As soon as buckling starts, at the idealized elastic critical buckling stress, the stress is redistributed towards the edges. Finally the stress in the member approaches the material yield stress at the edges with a non-uniform stress distribution throughout the rest of the plate width. The stress that the entire section resists can be idealized as some linearised stress in a certain part of the plate width only. An effective

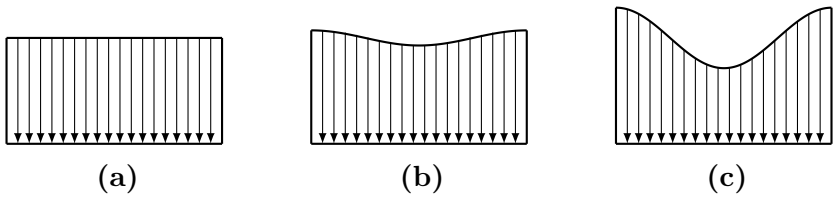

Figure 2.4: Development of stress distribution through the plate width in stiffened compression elements (Yu and Schafer, 2005). (a) uniform stress level of σ, (b) stress level of $\sigma > \sigma_{cr}$ and (c) outer edge yields ($\sigma = \sigma_e$).

width (b_e), composing of two edge parts, where full plasticity at supported edges is allowed to develop, is now conceptualized and is visible in Figure 2.5. The associated deformation can be predicted by Green's large deformation theory, but is too complicated to be applied in practical design (Ziemian, 2010).

The first method to predict b_e was proposed by von Kármán in 1932 (Ziemian, 2010). Equation 2.2 gives the prediction model suggested by him and follows from rearrangement of Equation 2.1, to make the width the subject. What is more, the procedure was suggested for the simply supported-edge case where $k = 4$. The edge stress σ_e in the equation is the maximum stress at which the specific length of b_e has developed and at ultimate strength represents the yield point.

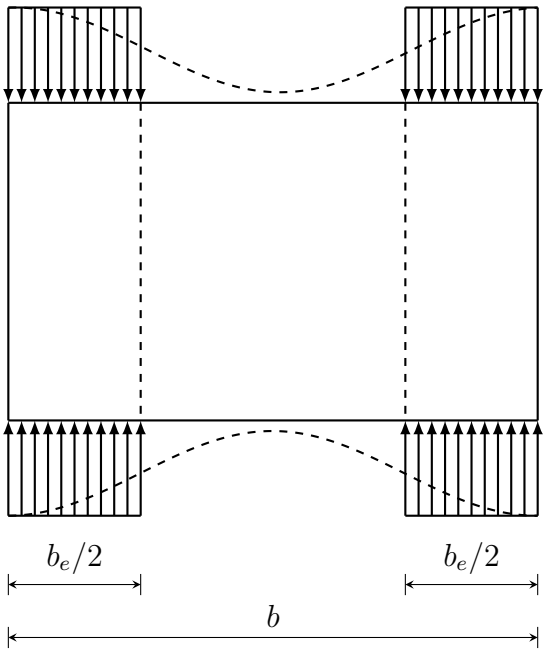

Figure 2.5: Idealized stress distribution after buckling and formation of effective width (Ziemian, 2010)

$$b_e = t\left[\frac{\pi}{\sqrt{3(1-v^2)}}\sqrt{\frac{E}{\sigma_e}}\right] \tag{2.2}$$

For the Effective Width approach first presented in the AISI design specification, the equation developed by Winter at the University of Cornell was used. Winter's equation was developed as a result of multiple tests and studies and is therefore a semi-empirical equation (Ziemian, 2010). Although investigations were based on $k = 4$, the generalised Winter's equation from 1942 can be expressed as given in Equation 2.3.

$$b_e = t\left[0.95\sqrt{\frac{kE}{\sigma_e}}\right]\left(1 - 0.2375\sqrt{\frac{kE}{\sigma_e}}\frac{t}{b}\right) \tag{2.3}$$

When comparing, one can see that the first part of Winter's equation represents the effective width suggested by von Kármán (see Equation 2.2). However, the commonly displayed case of the equation shown here includes a 0.95 coefficient that results from substitution of v and π value. This same substitution is shown for the slenderness ratio (λ) in Equation 2.4, which is often used to similarly express the formula. The second part of Winter's equation is merely a reduction factor based on testing, that includes the effects of imperfections, such as initial out-of-straightness (Ziemian, 2010). The reduction in effective width is only applicable for the case where $\lambda > 0.673$, otherwise the full width is able to resist the applied load.

$$\lambda = \frac{b}{t}\sqrt{\frac{12(1-v^2)\sigma_e}{k\pi^2 E}} = \frac{b}{t}1.052\sqrt{\frac{\sigma_e}{kE}} \tag{2.4}$$

In 1968 the reduction coefficient in Winter's equation was modified to the version displayed in Equation 2.5 and shows the design procedure as it is presented in the South African design standard in terms of the slenderness ratio (Ziemian, 2010).

$$b_e = t\left[0.95\sqrt{\frac{kE}{\sigma_e}}\right]\left(1 - 0.209\sqrt{\frac{kE}{\sigma_e}}\frac{t}{b}\right) = \frac{b}{\lambda}\left(1 - \frac{0.22}{\lambda}\right) \tag{2.5}$$

Equation 2.6 shows the same equality used in Equation 2.5 in a different form, by simplifying with Thimoshenko's solution for the critical buckling stress. Rearranged in this manner the equation is useful for the understanding of the DSM and shows how the ratio of reduced section width to full width behaves.

$$\frac{b_e}{b} = \sqrt{\frac{\sigma_{cr}}{\sigma_e}}\left(1 - 0.22\sqrt{\frac{\sigma_{cr}}{\sigma_e}}\frac{t}{b}\right) \tag{2.6}$$

From the equation it can be seen that the resistance of a member as an assembly of plate elements depends predominantly on the yield stress, the critical

buckling stress and cross-section dimensions, $R = f(\sigma_e, \sigma_{cr}, b, t)$ (resistance is a function of the underlying variables).

A plot to show the behaviour of Winter's equation against the commonly used basis for strength approximation, the elastic critical buckling stress (Equation 2.1), is shown in Figure 2.6 below. From the graph the region where the post-buckling reserve comes into effect is visible. It is seen as the region to the right of the intersection between the EWM equation by Winter and the elastic critical buckling equation by Timoshenko.

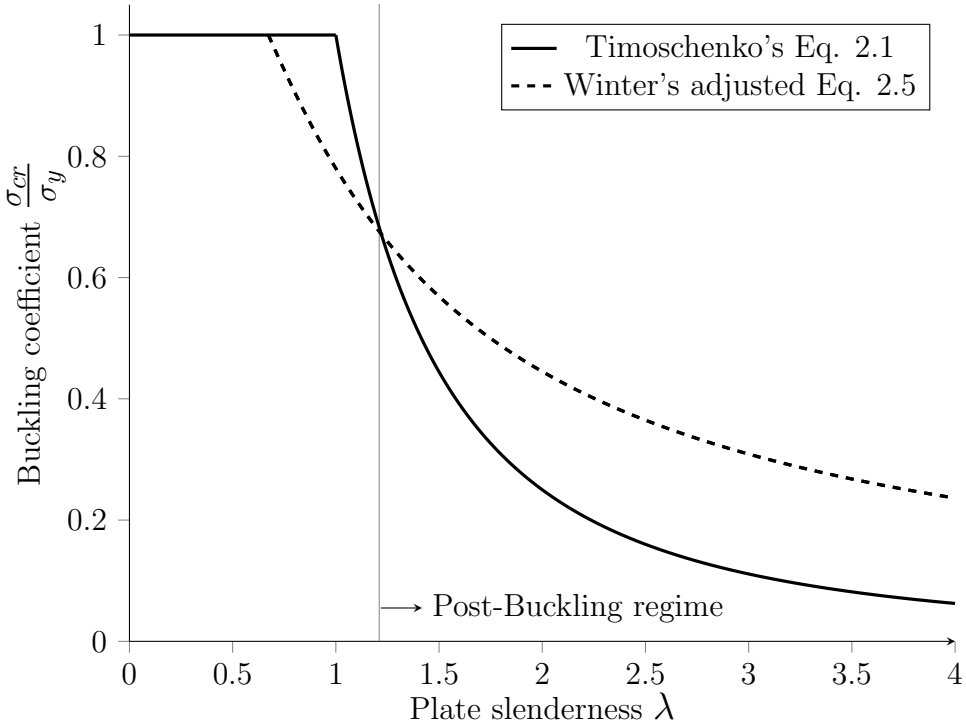

Figure 2.6: Non-dimensional buckling curves for uniform edge-loaded plates in compression

For more complex cold-formed members such as those that have a C-section, shown in Figure 2.7, the effective width must be determined for each compressed plate element in the assembly. The resistive load of the section can then be obtained as the sum of the sections able to resist load. Sections unable to resist load are shaded in on the figure.

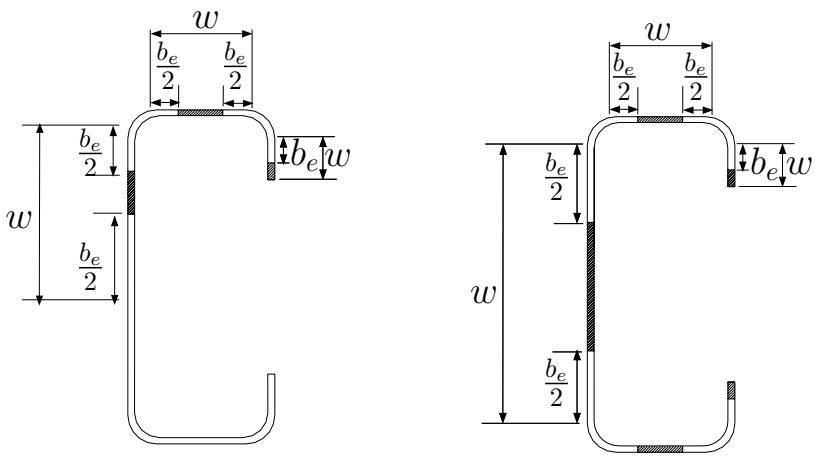

(a) Bending **(b)** Compression

Figure 2.7: Effective Width of a C-section (shading denotes ineffective regions) (Yu and Schafer, 2005)

2.2.4 The Direct Strength Method

As discussed, the EWM allows a designer to calculate element plate capacity of cold-formed members based on their local buckling behaviour. The sum of element capacities makes up the member capacity, but it may still be limited to overall member stability or global buckling. However, a failure mode that was observed in research but over-conservatively predicted by local buckling behaviour and not predicted by global instability, was the phenomenon of distortional buckling. Another factor that the effective width concept could not predict accurately was the interaction between plate elements of thin walled members. Furthermore the EWM required cumbersome iterative procedures to determine even basic member resistance (Schafer, 2006*b*). This difficulty led to the preference of hot-rolled steel over cold-formed steel members by design engineers in most situations (Ziemian, 2010). All of the above factors, including performance optimization of sections by introduction of stiffeners, resulted in the development and adoption of the Direct Strength Method (from here on referred to as DSM) by the AISI in 2004 (Yu and Schafer).

2.2.4.1 Buckling modes of cold-formed elements

From the development of the DSM three main basic stability modes that are key to member strength for cold-formed steel, were newly defined. The definitions are introduced next and are adapted from the SANS, but are equivalent to the definitions given by the AISI Specification for the Design of Cold-formed Steel Structural Members (2012):

2.2.4.1.1 Local Buckling: This is the buckling of elements only within a section, where the line junctions between elements remain straight and angles between elements do not change. In addition, the half-wavelength associated with local buckling should not exceed the largest straight line element dimension of the member (Schafer, Design Guide, 2007). A depiction of this local buckling mode description for a lipped C-section can be seen in Figure 2.8.

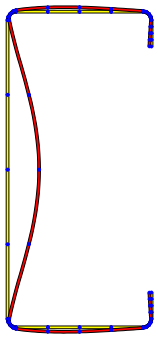

Figure 2.8: Local buckling for a lipped C-section

2.2.4.1.2 Distortional Buckling: A mode of buckling involving change in cross-sectional shape, excluding local buckling. Unlike with local buckling the bends of the member cross-section are allowed to change in angle and are allowed to rotate. The half-wavelength of deformation for this mode should be larger than that for local buckling, but smaller than that of global buckling (Schafer, Design Guide, 2007). Figure 2.9 below also depicts this behaviour as observed for a lipped C-section.

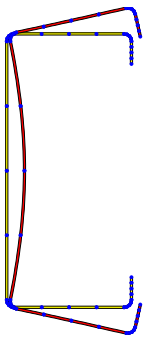

Figure 2.9: Distortional buckling for a lipped C-section

2.2.4.1.3 Global Buckling: A buckling mode of a member involving deflection out of the plane of bending (translation) occurring simultaneously with twist about the shear centre of the cross section. The cross-section for

this buckling mode does not deform in shape and is associated with flexural, torsional, torsional-flexural buckling for columns and with lateral-torsional buckling for beams. The associated half-wavelength is dependent on the end restraints of the member, but is at maximum the physical length of the column while having pin-ended boundary conditions (Schafer, Design Guide, 2007). Translation and rotation of the cross-section for this buckling mode is shown in Figure 2.10 for a lipped channel section.

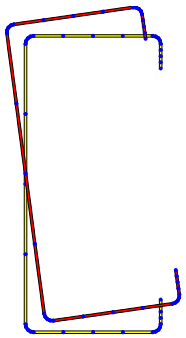

Figure 2.10: Global buckling of a lipped C-section

The fundamental basis of the DSM is the empirical EWM. As mentioned, the element stability limit could be obtained by iteration form Winter's equation. Similarly the DSM assumes member stability to result from a member's element critical elastic buckling load (σ_{cr}) for an assembly of elements, as well as from the material yield strength (σ_e). The newly developed DSM equations obtain member strength (resistance) for compressive and flexural members as a function of these two plate element parameters. In other words the DSM takes the same approach as the EWM, but applies it to the entire cross-section. Thus, similarly as for the EWM, it can be said that the DSM capacity $R = f(\sigma_e, \sigma_{cr}, b, t)$ and offers a good prediction model. Exact member strength resulting from material non-linearity and member out of straightness are momentarily only predictable by advanced finite element models (Ziemian, 2010). Nevertheless, to incorporate long member stability, the concept of interaction of effective cross-sections-curves and global stability predictors for member strength was introduced with the DSM. This means that the resistance model is based on a set of statistical data from testing. It includes data from a select type of sections that limit the use of the equations. Nevertheless the elastic instability modes mentioned are obtained from a linear elastic finite element analysis and these are key in the formulation of the DSM. The subsequent equations thus resulted from a combination of these concepts and the procedure is therefore limited for quite specific use.

At this point it is useful to observe that considering the DSM equations used for local and distorional buckling in terms of the critical elastic cross-sections stresses ($F_{cr,n}$) for both columns and beams, makes their origins from the EWM more understandable. Consider Equation 2.7 compared to the arrangement of the EWM Equation 2.6, where critical elastic cross-section stress has replaced the plate element critical buckling stress.

$$\frac{F_n B_e}{F_e B_g} = \left(\frac{F_{cr_n} \cancel{B_g}}{F_e \cancel{B_g}}\right)^{c_1} \left(1 - c_2 \left(\frac{F_{cr,n} \cancel{B_g}}{F_e \cancel{B_g}}\right)^{c_1}\right) \tag{2.7}$$

The equation shows a generalised format of the upcoming DSM member strength equations for local and distortional buckling in terms of critical elastic cross-sections stresses ($F_{cr,n}$). To generalise for both the distortional and the local buckling case of both columns and beams, the dimension component is represented by B. The effective dimension component is denoted with a subscript e, whereas the full dimension component is denoted with a g. For columns B describes the cross-sectional area (A) and for beams it symbolises the section modulus (Z). Since the full dimension symbol B_g is present in the slenderness factor of the DSM equations, recognizable by the power coefficient c_1, the dimension component can be cancelled out for comparison purposes. Now the comparison to Equation 2.6 is more understandable, especially if the DSM equations are also divided by the limiting section stress strength $F_e B_g$. Depending on local or distortional bucking, F_e can be either the section yield strength F_y or the section global-strength F_{ne}, which is the global capacity stress. The ultimate uniform stress carried by the section multiplied with the effective dimension component is referred to as the member capacity ($F_n Be$).

The two coefficients c_1 and c_2, obtained empirically for the case of Winter's equation, are addressed together with the presentation of the DSM equations.

2.2.4.2 Limitations

The limitations for the procedure are well known and a summary adopted from the Direct Strength Method Design Guide is listed below. They are as follows (Schafer, 2006*a*):

- No shear provisions
- No web crippling provisions
- No provisions for strength increase due to cold-work of forming
- Overly conservative if very slender elements are used
- Shift in the neutral axis is ignored

- Empirical method calibrated only to work for cross-sections previously investigated
- Limited number/geometry of pre-qualified members

The pre-qualification limits set out are the same for the North American Specification as they are for the SANS. They are based on the range of dimension which tested sections used for the calibration of the DSM strength curves conform to. Consequently, these pre-qualification limits should maintain the required level of reliability used for the calibration. The sections allowed for the use with the DSM are as follows;

for compression members:

1. Channel sections including lipped and web-stiffened channels
2. Z-sections
3. Rack sections
4. Hat section

for flexural members:

1. Channel sections including lipped and web-stiffened channels.
2. Z-sections
3. Hat section
4. Complex hats or Trapezoids with stiffened flanges

Additionally, the applicability of the DSM for members in compression and bending is also limited by the design yield strength. The limiting value varies for the structural member under consideration and results from the original testing used for calibration of the equations (American Iron and Steel Institute *et al.*, 2012).

Although the newest version of the AISI specification for cold-formed steel members includes the DSM for members with holes, these added equations are not considered here. This is due to the scope of this research being limited to the South African specification currently in place. The procedure for the design with holes is therefore not given any further consideration.

The DSM equations are subsequently presented.

2.2.4.3 Columns

2.2.4.3.1 Global buckling The nominal axial resistance of a column, P_{ne}, for global buckling is defined as:

$$P_{ne} = \begin{cases} \left(0.658^{\lambda_c^2}\right) P_y & \text{for } \lambda_c \leq 1.5 \quad (2.8a) \\ \left(\frac{0.877}{\lambda_c^2}\right) P_y & \text{for } \lambda_c > 1.5 \quad (2.8b) \end{cases}$$

where

$$\lambda_c = \sqrt{\frac{P_y}{P_{cr,e}}} \quad (2.9)$$

$$P_y = A_g F_y \quad (2.10)$$

and $P_{cr,e}$ is the elastic critical load obtained from the lesser of the weak axis elastic flexural, torsional or torsional-flexural buckling loads. A_g is the total cross-sectional area based on design and F_y is the member yield strength.

The elastic global critical buckling load ($P_{cr,e}$) according to the DSM procedure is obtainable from either rational buckling analysis or from a closed form solution. This closed form solution was developed by solving of a set of coupled deferential equations by Timoshenko (1945) and it is the same for all the pre-qualified cross-sections. The applicable equations necessary for obtaining the global buckling load are available in SANS 10162-2 and are not only specific to the DSM.

Unlike the other prediction equations of the DSM, the set of equations used for global buckling is not a new development. Equations 2.8a and 2.8b are a result of the research based on the work by Bjørhovde from 1972, to find a deterministic column curve based on the probabilistic factors influencing the strength (Ziemian, 2010). Bjørhovde created 112 strength column curves from testing of various shapes and types of cross-sections. Additional factors affecting strength design that were considered in his study, are effects from residual stress, initial out-of-straightness and end restraints. In order to not have a single equation that was over-conservative for some cases and non-conservative for others, the data was split into three categories of sub-column curves, with each having its own average strength prediction curve. The groups were based on similar cross-section attributes used for the establishment of the column curves.

The second group consisting of 70 out of the 112 column curves with an assumed initial mean out of straightness of 1/1470 of the column length resulted in the equations used for the DSM. The equation is presented in two parts based on the slenderness of the section. The former equation (2.8a) applies to inelastic buckling and the latter equation (2.8b) applies to the elastic

buckling of the column. The latter equation approaches the Euler buckling curve for large slenderness. Noteworthy to state is that the equation is based on average strengths that were calculated for 70 column curves with equal dispersion on the 9 different slenderness ratios investigated for the strength variable. Also, the mean of the 70 column curves is captured in Equations 2.17a and 2.17b such that the variables of cross-section properties and yield strength are denoted by the arithmetic mean of measured data (Bjørhovde, 1972 p-143).

2.2.4.3.2 Local buckling The nominal axial resistance of a column, P_{nl}, for local buckling is defined as:

$$P_{nl} = \begin{cases} P_{ne} & \text{for } \lambda_l \leq 0.776 \quad (2.11a) \\ \left[1 - 0.15\left(\frac{P_{cr,l}}{P_{ne}}\right)^{0.4}\right]\left(\frac{P_{cr,l}}{P_{ne}}\right)^{0.4} P_{ne} & \text{for } \lambda_l > 0.776 \quad (2.11b) \end{cases}$$

where

$$\lambda_l = \sqrt{\frac{P_{ne}}{P_{cr,l}}} \tag{2.12}$$

$$P_{cr,l} = A_g F_{cr,l} \tag{2.13}$$

P_{ne} is the nominal axial resistance of a column for global buckling as defined in Equations 2.17a and 2.17b of Section 2.2.4.3.1. Again A_g is the total cross-sectional area based on design and $F_{cr,l}$ is the section stress at which elastic local buckling occurs. This stress needs to be determined using a finite strip buckling analysis among other.

The basis for the set of equations comes from the equation used for local buckling strength prediction of beams and this is elaborated in the beam local buckling DSM Section, 2.2.4.4.1. Noteworthy to point out is that the equations assume global and local buckling interaction to incorporate global stability (P_{ne}) in the strength equation. The origin of the equation is from experimental testing performed by Schafer and is based on the section effective stress concept by Winter (Ziemian, 2010). The only probabilistic measure for calibration of the curves that could be found is the mean model factor (μ_{δ_R}) or mean test to predictor ratio. It is based on a set of 187 column tests subject to the limitations section of this thesis (Schafer, 2008). The noticeable effect is that coefficients c_1 and c_3 for Equation 2.11b change from Winter's equation to 0.4 and 0.15 respectively, to produce the DSM predictor equation. The influence of the model factor on the reliability is discussed in the subsequent chapter.

2.2.4.3.3 Distortional buckling The nominal axial resistance of a column, P_{nd}, for distortional buckling is defined as:

$$P_{nd} = \begin{cases} P_y & \text{for } \lambda_d \leq 0.561 \quad (2.14a) \\ \left[1 - 0.25\left(\frac{P_{cr,d}}{P_y}\right)^{0.6}\right]\left(\frac{P_{cr,d}}{P_y}\right)^{0.6} P_y & \text{for } \lambda_d > 0.561 \quad (2.14b) \end{cases}$$

where

$$\lambda_d = \sqrt{\frac{P_y}{P_{cr,d}}} \tag{2.15}$$

$$P_{cr,d} = A_g F_{cr,d} \tag{2.16}$$

P_y is the section squash load as defined in Equation 2.10. Again A_g is the total cross-sectional area based on design and $F_{cr,d}$ is the section stress at which elastic distortional buckling occurs. This stress needs to be determined using a finite strip buckling analysis or other numerical methods.

Calibration of the equations resulted from research conducted by Hancock, Kwon and Bernard (1994). Multiple research had shown an undesired tortional-local mode that could not be predicted by local behaviour theory. Among other research Thomasson investigated web stiffened lipped C-sections showing the then unidentified, but now known, distortional buckling mode. Thomasson avoided the mode by placing closely spaced bracing to the test columns resolving the distortion effect. Hancock found a rack section that exhibited this distortional behaviour and used it for the basis of his investigation. Although both yield strength and thickness were treated as probabilistic variables the resulting equation is a deterministic equation based on the regression analysis for mean test to predictor ratio (δ_R). The influence that the yield stress and thickness have on the deterministic variable based equation is not distinguishable. Again it could be found that the equations were based on Winter's effective width concept when considering the research by Hancock *et al.* (1994). The idea to use the concept resulted from good prediction behaviour of the elastic distortional buckling load to test sample strengths (Hancock *et al.*, 1994). According to Hancock *et al.* the adjustment of the coefficients c_1 and c_2 to 0.6 and 0.25 in Equation 2.14b, yielded more conservative results (1994). Lipped C-sections, hat sections and stiffened lipped C-sections that exhibited a distortional failure also contributed to the calibration. It is however stated by Hancock *et al.* (1994) that this form of the equation incorporated conservative results for members that showed indistinct local or distortional failure. That is also why the yield strength is used as member strength basis ($P_{nd} = f(P_y, P_{cr,d})$), as to not include a local-dirtortional buckling interaction. No influence on the coefficient choices

due to probabilistic factors could be found, to which the conservatism refers. It is however natural to assume that similarly to local buckling, coefficient c_1 and c_2 choices resulted from the mean model factor being closer to unity. This implies a more accurate model.

The sample basis for the 249 tests used in calibration for both local and distortional buckling can be found in the Commentary to the North American Specification (American Iron and Steel Institute *et al.*, 2012). Figure 2.11 below shows a plot of the individual test result set, as well as the DSM design curves for local and distortional buckling. It is important to consider, when looking at the reference y-axis, that it is plotted showing different normalizing strengths; P_{ne} and P_y are used to determine member stability for the two cases. Clearly visible from the graph for the empirical strength equations is that a large number of local buckling test results for a slenderness of about 1.2 do not seem conservative. However, the curve does not consider the slenderness as probabilistic variable, but rather the model factor for tested data. That is why the graph does not pass through the middle of these points. The effect that the model factor was used as calibration measure is not easily quantifiable from this graph.

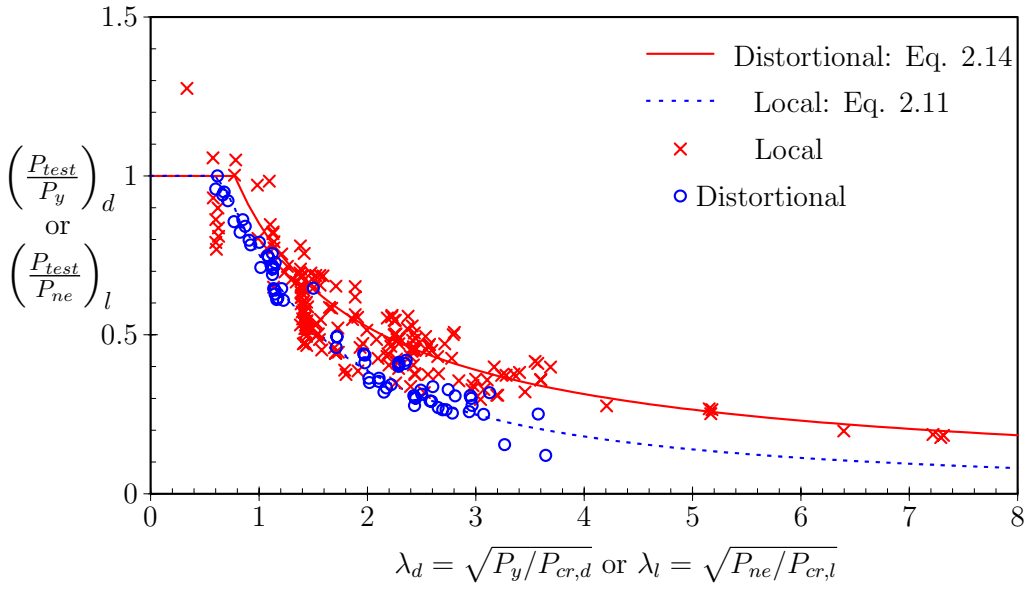

Figure 2.11: Comparison of the DSM predictor curves to test data used for calibration (American Iron and Steel Institute *et al.*, 2012)

In contrast to Figure 2.11, Figure 2.12 shows the calibration effect of the two coefficients from the point of the model factor. This graph pertains to the test performed on lipped channel columns only and is only applicable for the model factor including both local and distortional buckling effects. The test-to-predictor ratio in Figure 2.12 indicates a conservative mean model factor

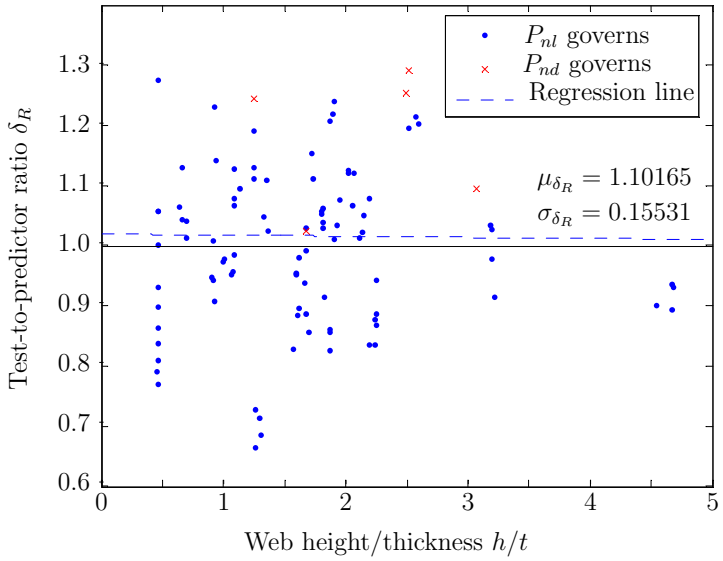

Figure 2.12: Comparison of the DSM predictor curves to test data for lipped C-sections used in calibration (American Iron and Steel Institute *et al.*, 2012)

across various plate slenderness ratios. This implies that the predictability of the new DSM equations are good and conservative for lipped C-sections in compression. For interpretation purposes it should be noted that a model factor larger than unity relates to a conservative predictor.

2.2.4.4 Beams

2.2.4.4.1 Global buckling The nominal member moment capacity of a beam, M_{ne}, for lateral-torsional buckling is defined as:

$$M_{ne} = \begin{cases} M_{cr,e} & \text{for } M_{cr,e} < 0.56M_y \quad (2.17a) \\ \dfrac{10}{9}M_y\left(1 - \dfrac{10M_y}{36M_{cr,e}}\right) & \text{for } 0.56M_y \leq M_{cr,e} \leq 2.786M_y \quad (2.17b) \\ M_y & \text{for } M_{cr,e} > 2.78M_y \quad (2.17c) \end{cases}$$

where

$$M_y = Z_f F_y \tag{2.18}$$

and $M_{cr,e}$ is the elastic critical lateral torsional buckling moment obtained from analytical solution to the boundary value problem. Z_f is the section modulus with the outer most fibre at first yield and F_y is again the section yield strength.

Again the elastic critical moment, $M_{cr,e}$, according to the DSM procedure is obtainable from either rational buckling analysis or from the closed form

solution by Timoshenko (1945). Similarly the closed form solution was developed by solution of a set of coupled deferential equations and it is the same for all the pre-qualified cross-sections. The equations are once more not only part of the DSM and can be found in SANS 10162-2.

The origin of the resistance equations can be traced back to a statistical analysis based on work by Baker and Kennedy from 1984 (Ziemian, 2010). The probabilistic procedure used to set up Equation 2.17 followed a similar procedure as the one Bjørhovde used for columns (Ziemian, 2010). Equation 2.17b was developed for rolled I-sections tested by Dibley in 1969, however this equation allowed for the full section to become plastic. In other words maximum strength was obtained by allowing the section to develop full plasticity through its depth. This is commonly the design strength for laterally braced hot-rolled profiles. For thin walled members the basis was however changed to the moment of first yield, M_y, as seen in the equation. This change was made to incorporate the effects of local buckling on the global strength as not to increase the prediction strength of the global case too much by making use of the plastic moment (Ziemian, 2010).

2.2.4.4.2 Local buckling The nominal moment of resistance of a beam, M_{nl}, for local buckling is defined as:

$$M_{nl} = \begin{cases} M_{ne} & \text{for } \lambda_l \leq 0.776 \quad (2.19a) \\ \left[1 - 0.15\left(\frac{M_{cr,l}}{M_{ne}}\right)^{0.4}\right]\left(\frac{M_{cr,l}}{M_{ne}}\right)^{0.4} M_{ne} & \text{for } \lambda_l > 0.776 \quad (2.19b) \end{cases}$$

where

$$\lambda_l = \sqrt{\frac{M_{ne}}{M_{cr,l}}} \tag{2.20}$$

$$M_{cr,l} = Z_g F_{cr,l} \tag{2.21}$$

M_{ne} is the nominal moment resistance of a beam for lateral-torsional buckling as defined in Equations 2.17a to 2.17c. Z_g is again the section modulus of first yield in the outer most fibre and $F_{cr,l}$ is the stress at which elastic local buckling occurs in the section. This stress, once more, needs to be determined using a finite strip buckling analysis.

The beam related local buckling strength of the DSM was extensively developed by Schafer and Peköz in research presented in 1998 (Schafer and Peköz, 1998). Again locational buckling interaction is assumed by Equation 2.19 and therefore limited to the maximum lateral-torsional buckling strength of

the long beam, M_{ne}. This local-global interaction was assumed from the findings for columns and was extended to DSM prediction for beams (Schafer, 2008). The first suggestion for a prediction model where local buckling failure occurred, was presented by the two authors with the same c_1 and c_2 coefficients as Winter's equation, as well as the same slenderness limit of applicability. However, the equation yielded over-conservative predictions (Ziemian, 2010). A new slenderness limit was suggest by Schafer and Peköz together with the improved coefficients as seen in Equation 2.19b. The improvement was based on an increased probabilistic model factor (δ_R or test-to-predictor ratio) performance as a result of 574 test samples, including beam tests performed by Winter in 1946 (Schafer and Peköz, 1998). Sections that were included in the study were various arrangements of C-sections. This included lipped, unlipped, sloping lip and lipped with web stiffened channels. The improved prediction equation was then adopted in the AISI specification (Ziemian, 2010).

2.2.4.4.3 Distortional buckling The nominal moment of resistance of a beam, M_{nd}, for distortional buckling is defined as:

$$M_{nd} = \begin{cases} M_y & \text{for } \lambda_d \leq 0.673 \quad (2.22a) \\ \left[1 - 0.22\left(\frac{M_{cr,d}}{M_y}\right)^{0.5}\right]\left(\frac{M_{cr,d}}{M_y}\right)^{0.5} M_y & \text{for } \lambda_d > 0.673 \quad (2.22b) \end{cases}$$

where

$$\lambda_d = \sqrt{\frac{M_y}{M_{cr,d}}} \tag{2.23}$$

$$M_{cr,d} = Z_g F_{cr,d} \tag{2.24}$$

M_y is the moment of first yield in the top fibre as defined in Equation 2.18. Again Z_g is the section modulus of first yield in the top fibre. This stress ($F_{cr,d}$) once more needs to be determined using a finite strip buckling analysis or other rational analysis.

Hancock, Kwon and Bernard (1994) first suggested this equation. It was proposed from their research into distortional column buckling. Since the effective width concept had revealed conservative results, the procedure was directly extrapolated to beam behaviour with the generalised dimension factor B in the equation for bending replaced by the section modulus Z. This was presented with substitution for both the effective dimension factor B_e and the full section factor B_g. The slenderness limit to which the equation was applicable (presented in Hancock *et al.*'s proposal), was however different to how it appears in the equation above.

For the calibration of the DSM beam strength equations, 559 specimen were used for the calibration from various research (American Iron and Steel Institute *et al.*, 2012). The largest contributions leading to the equations' inclusion in the AISI specification were made by Schafer (American Iron and Steel Institute *et al.*, 2012). Extrapolated from the research on columns, the interactions between distortional-global buckling and local-distortional buckling have been ignored in the beam design procedure (Schafer, 2008). Furthermore, most of the research that was conducted on beams, was for laterally restrained members. This came as a direct result of the distortional buckling strength buckling prediction presenting some difficulty when investigated for the laterally unrestrained case.

Figure 2.13 shows a plot of the individual test results as well as the DSM design curves for local and distortional buckling. Attention should again be directed at the y-axis for this plot, since it is only normalized by the section yield moment M_y. This is as a result of the experimental testing being performed for laterally braced cases. A remarkable behaviour which can be seen from the graph, is that more sections failed in distortional than in local buckling. This observation is related to the fact that most testing was done on C-sections, Z-sections and rack sections. These members are simply more prone to distortional buckling failure and are represented accordingly (Schafer, 2008). Lastly with respect to the DSM calibration, it is noted in literature that large parts of the research were performed on strong axis bending, more specifically the strong axis bending of C-sections and Z-sections. The procedure was once more extrapolated to weak axis bending due to the fact that hat sections and deck sections are included in the calibration data which were tested about their weak axis, since they are loaded in this manner in practice (Schafer, 2008).

Similarly as for the case of compression, a graph that shows the calibration effect of the two coefficients c_1 and c_2 of the generalised equation, by using the model factor as a performance measure, is found in Figure 2.14. This graph pertains to the full set of test-sections, for all cases of local and distortional buckling studied by Schafer. It should however be noted that this graph's reference predictor strength (M_n), is only the equation for local buckling from bending of beams. Again for interpretation purposes it should be stated that a model factor larger than unity relates to a conservative predictor.

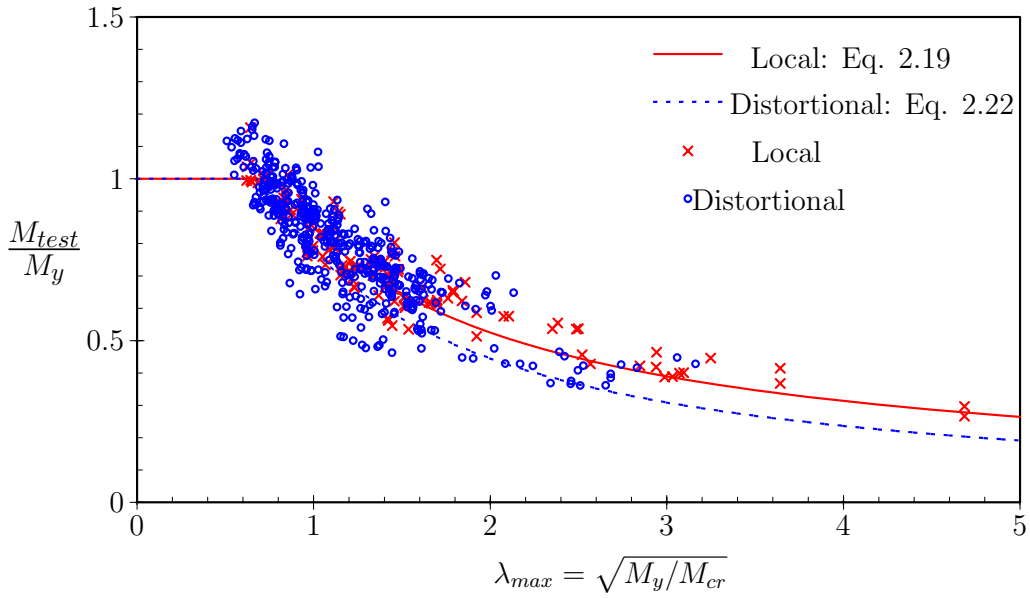

Figure 2.13: Comparison of the DSM predictor curves to test data for calibration (American Iron and Steel Institute *et al.*, 2012)

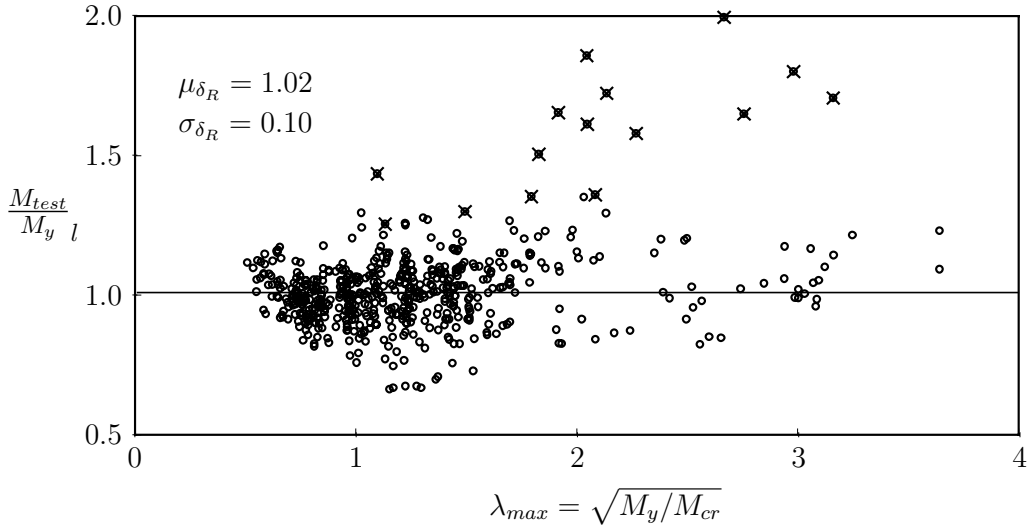

Figure 2.14: Comparison of only the DSM local buckling predictor curves to all test data used in calibration (Schafer and Peköz, 1998)

In summary the DSM provides a tool with which to predict member stability with relative ease. The basis of the procedure is to find the elastic buckling limits based on the cross-section properties and the global slenderness. Simply put, once all three elastic buckling limits $F_{cr,n}$ and the section strength based on the material properties F_y have been found, the stability load F_n can be predicted as a function of those parameters. Or similarly $F_n = f(F_{cr,l}, F_{cr,d}, F_{cr,g}, F_y)$. This is true for both beams and columns.

2.3 The Finite Strip Method

2.3.1 Classic Finite Strip Analysis

Modelling of the response of thin-walled cold-formed steel elements is a complex procedure even for simple cross-section geometry. The Finite Strip Method (from here on referred to as FSM) was publicized in 1974 by Plank and Wittrick and is one procedure that allows elastic behavioural prediction (Ziemian, 2010). Hancock and collaborating researchers introduced the notion to use the numerical method to determine elastic buckling stresses of cold-formed sections and combine these with true stability behaviour and strength prediction as elaborated in the previous section. One of the major contributing attributes that led to a demand for the development of the procedure, was accurate prediction of the plate buckling coefficients with minimal effort. The simplified assumptions of the classical FSM found in most literature, which make the method pleasant and easy to use, also bring about one of the largest limitation of the method's applicability. That is, that the procedure does not allow any tapering of a member along its length (Li, Abreu, Leng, Ádány and Schafer, 2014). The reason for this limitation is evident from the subsequent review of the fundamental theory.

Discretization (also referred to as meshing) takes member geometry and splits it into a finite number of parallel strip elements. Furthermore a finite number of repeated strips along the length, remarked by the m variable (up until q) may be considered. An illustration of the strip elements placed in a member for the $m = 1$ case is illustrated in Figure 2.15 below. In the figure the degrees of freedom (from here on referred to as DOF) nomenclature and directionality with respect to the strip element is furthermore annotated. It is important to point out, that the deformation variables unconventionally follow the left hand rule as indicated by the axis system in the figure. The variable a and b refer to the length and width of the one strip respectively, as illustrated in the figure.

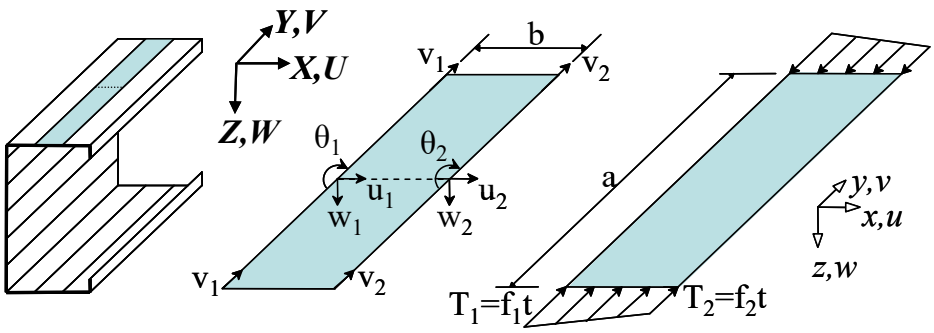

Figure 2.15: Coordinates, Degree of Freedom and loads of a typical finite strip model (Schafer and Ádány, 2006)

Interpolation of the displacement fields in one full- length strip is done by summing the shape functions over all strips in the length, from m up to q. The vector of the general displacement field can be written as: $\{d\} = [u\ v\ w]^T$, where u is the displacement in the transverse-, v in the longitudinal- and w in the lateral-direction. The summation along the length of a member in terms of the nodal DOF $u_{i[m]}$, $v_{i[m]}$, $w_{i[m]}$, $\theta_{i[m]}$ are given in Equations 2.25 to 2.27, where θ is the rotational deformation of the plate (Li and Schafer, 2010). The i term indicates the left or right longitudinal edges incrementing in the positive x-direction.

$$u = \sum_{m=1}^{q} \left[\left(1 - \tfrac{x}{b}\right) \quad \tfrac{x}{b}\right] \begin{Bmatrix} u_{1[m]} \\ u_{2[m]} \end{Bmatrix} Y_{[m]} \tag{2.25}$$

$$v = \sum_{m=1}^{q} \left[\left(1 - \tfrac{x}{b}\right) \quad \tfrac{x}{b}\right] \begin{Bmatrix} v_{1[m]} \\ v_{2[m]} \end{Bmatrix} Y'_{[m]} \frac{a}{m\pi} \tag{2.26}$$

$$w = \sum_{m=1}^{q} \left[\left(1 - \tfrac{3x^2}{b^2} + \tfrac{2x^3}{b^3}\right) \quad x\left(1 - \tfrac{2x}{b} + \tfrac{x^2}{b^2}\right) \quad \left(\tfrac{3x^2}{b^2} - \tfrac{2x^3}{b^3}\right) \quad x\left(\tfrac{x^2}{b^2} - \tfrac{x}{b}\right)\right] \{d_{w[m]}\} Y_{[m]} \tag{2.27}$$

The term $\{d_{w[m]}\} = \begin{bmatrix} w_{1[m]} & \theta_{1[m]} & w_{2[m]} & \theta_{2[m]} \end{bmatrix}^T$ is the nodal displacement vector for bending and term $Y_{[m]}$ is the longitudinal shape function which is dependant on the boundary conditions. For the simply supported end-boundary condition case, the $Y_{[m]}$ term is presented in Equation 2.28. Alternative shape functions for other boundary conditions have also been developed and can be found in Li and Schafer (2010) and Li *et al.* (2014). However, for research comparison purposes only the simply supported case is considered. This end-boundary condition case is the most repeatable in experimental processes and is therefore generally considered. In addition to this, the simply supported boundary condition allows for a lower limit solution for all cases except the clamped-free boundary condition, and is therefore a favourable investigative basis. Additionally shown in Figure 2.15 is the applied traction T_i, which is the product of the applied nodal stress f_i and the strip thickness t.

$$Y_{[m]} = \sin\left(\frac{m\pi y}{a}\right). \tag{2.28}$$

Shape functions for the displacement field are unique in the way that they are the same as for beam finite elements in the transverse direction (x), but trigonometrical for the longitudinal direction (y) (Li *et al.*, 2014).

The stain-displacement relationship that is used for finite strip theory is a combination of a generalised plane strain membrane theory (referred to with a subscript PS) and Kirchoff thin plate theory for bending (referred to with

a subscript B). Both deformation theories are based on small displacement theory of Cauchy. The DOF for plane strain are associated with displacement u and v, where as the Kirchoff plate DOF is the displacement w. The combined deformation relationship is shown in Equation 2.29 and requires the left hand rule of coordinate systems to work.

$$\{\epsilon_M\} = \begin{Bmatrix} \epsilon_x \\ \epsilon_y \\ \gamma_{xy} \end{Bmatrix}_{PS} + \begin{Bmatrix} \epsilon_x \\ \epsilon_y \\ \gamma_{xy} \end{Bmatrix}_{B} = \begin{Bmatrix} \frac{\partial u}{\partial x} \\ \frac{\partial v}{\partial y} \\ \frac{\partial u}{\partial y} + \frac{\partial v}{\partial x} \end{Bmatrix}_{PS} + \begin{Bmatrix} \frac{-z\partial^2 w}{\partial x^2} \\ \frac{-z\partial^2 w}{\partial y^2} \\ 2\frac{z\partial^2 w}{\partial x \partial y} \end{Bmatrix}_{B} \tag{2.29}$$

It is assumed that the strip size is small relative to the displacement field, which allows small deformation theory to prevail instead of large deformation theory by Green (Cook *et al.*, 2007).

From the integral form of the differential equation of structural mechanics that defines equilibrium, two energy terms can be formulated to solve the differential equation; the internal energy term and the potential work or external energy term. Given the previous assumption about the size of the strip, the work term can be calculated with reference to the local coordinate system without the need of large deformation theory. The internal strain energy is denoted by the symbol U and the integral form to solve the differential equation for the internal strain energy term is shown in Equation 2.30 below.

$$U = \frac{1}{2}\int \{\sigma\}^T\{\epsilon\}dV = \frac{1}{2}\int \{\epsilon\}^T[D]\{\epsilon\}dV = \frac{1}{2}\{d\}^T\left\{\int \{B\}^T[D]\{B\}dV\right\}\{d\} \tag{2.30}$$

The $[D]$ matrix represents generalized Hooke's law for the two dimensional orthotropic case and together with the strain term ($\{\epsilon\}$) replaces the stress vector $\{\sigma\}$. Additionally the $\{B\}$ vector results from the strain-displacement relationship of Equation 2.29. Thus solving the integral form, by summing over the volume of the strip, the elastic stiffness matrix , $[k_e]$, can be obtained as seen in Equation 2.31. This must be done for both the PS and the B case separately and thereafter they can be summed. Both matrices are of size $8q \times 8q$ for the full member length and are presented in Schafer and Ádány (2006) exactly.

$$[k_e] = \int \{B\}^T[D]\{B\}dV \tag{2.31}$$

The matrix is then transformed from the local axis (x, y, z) to the global axis (X, Y, Z) to form the global stiffness matrix. The global elastic system matrix $[K_e]$ is then a $4n_sq \times 4n_sq$ matrix, where n_s is the number of strip lines in the cross-section.

By integrating the potential work done by the strips as the plate shortens, an expression for the geometric stiffness matrix, $[k_g]$ can be derived. Equation 2.32 shows this integration over the volume of the strip. The traction T is a linear function in the x-direction dependant on the two nodal magnitudes. The second order strain term is denoted by ϵ_y^{II} and can follow one of two possibilities: either it is modelled using second-order theory of beams or second-order theory of plates (Li *et al.*, 2014).

$$W = \int T\epsilon_y^{II} dV = \frac{1}{2}\int T\{d\}^T[G]^T[G]\{d\}dV = \frac{1}{2}\{d\}^T\left\{\int T[G]^T[G]dV\right\}\{d\} \tag{2.32}$$

Conventionally the second order beam theory is implemented, but it may for shorter buckling lengths produce incorrect buckling factors for thicker strips (Li *et al.*, 2014). Nevertheless the relation between the displacement field and the second-order strain term in its generalised form, is captured by Equation 2.32. Finally the geometric stiffness matrix in terms of the second-order strain-displacement relationship, $[G]$, is given in Equation 2.33 below.

$$[k_g] = \int T[G]^T[G]dV \tag{2.33}$$

Again as for the internal strain the geometric stiffness matrix is expressed in terms of the PS membrane and plate bending (B) terms. Thus the size of the global geometric stiffness matrix $[K_g]$ is the same as mentioned for the elastic stiffness matrix earlier.

If the member is now loaded with an arbitrary traction load, scaled by $[\Lambda]$, and one performs a linear analysis, the geometric stiffness contribution is also scaled by the same level $[\Lambda]$. The elastic stiffness contribution remains unchanged due to the linear behaviour assumed. Since the buckling deformation $[\phi]$ takes place relative to the reference deformations, the well known eigen-buckling problem of Equation 2.34 occurs.

$$([K_e] - [\Lambda]\,[K_g])\,[\Phi] = 0 \tag{2.34}$$

The roots of the equation are the buckling coefficients or load levels, λ_n of the reference traction and are associated with a reference buckling deformation, ϕ_n, as presented in matrix form in Equation 2.35. The buckling coefficients are also known as the eigenvalues and the buckling shape as the eigen-vectors of the eigen-value problem. The buckling coefficients are an important integral part of the DSM and their role is explained at the end of this section.

$$[\Lambda] = diag\begin{bmatrix}\lambda_1 & \lambda_2 & \dots & \lambda_{4n_sq}\end{bmatrix},\ [\Phi] = \begin{bmatrix}\{\phi\}_1 & \{\phi\}_2 & \dots & \{\phi\}_{4n_sq}\end{bmatrix} \tag{2.35}$$

2.3.2 The Constrained Finite Strip Method

The previous section regarding the classical FSM has limitations when trying to identify the deformations associated with the eigen-buckling shapes or eigen-modes of the member. An additional feature to the classical FSM was added, to enable the identification of the three known elastic buckling deformations associated with cold-formed steel. Simply put, the procedure uses mechanical assumptions to constrain the deformations to a desired set of criteria associated with elastic deformation modes (Li and Schafer, 2010). Thus the procedure is referred to as the constrained finite strip method or from here on abbreviated as cFSM. The constraints are known to come from the Generalised Beam Theory and are presented in Table 2.1. cFSM constraints are categorized into global (G), distortional (D), local (L) and transverse shear deformation space (ST) (Li and Schafer, 2010). No explicit influence on the shape function is given here, but the generalized concept is illustrated by Equation 2.36.

$$\{d\} = [R_M]\{d_M\} \tag{2.36}$$

The system deformations, $\{d\}$, are post multiplied with the constraint matrix, $[R_M]$, where the subscript M refers to the deformation mode (G,D,L,ST). Inclusion of this concept has a significant influence on the eigen-buckling problem given previously in Equation 2.34. The transformed arrangement to include the deformation constraints is given in Equation 2.37. This process is also referred to as modal decomposition of the eigen-value problem.

$$[R_M]^T [K_e] [R_M] [\Phi_M] - [\Lambda] [R_M]^T [K_g] [R_M] [\Phi_M] = 0 \tag{2.37}$$

Effectively the constraint matrix reduces the problem size to the size of the M space. The solution space is therefore decomposed to only include the desired constrained deformations and only those are solvable. The constraint matrix may contain individual modes, such as global or distortional, but may also be used to determine a combined modal deformation.

Table 2.1: Criteria for decomposition of field (Li and Schafer, 2010)

Mechanical criteria	G	D	L	ST
Vlasov's hypotheses: $(\gamma_{xy})_{PS} = 0$, $(\epsilon_x)_{PS} = 0, v$ is linear	Yes	Yes	Yes	No
Longitudinal warping: $(\epsilon_x)_{PS} \neq 0$	Yes	Yes	No	-
Undistorted section: $\kappa_x = 0$	Yes	No	-	-

In essence this development allows the decomposition of the entire deformation spectrum into its various modal parts. The cFSM can then be used to identify the contributions of a mode to the total deformation field.

2.3.3 CUFSM

CUFSM is an open source implementation of the constrained finite strip method based in the MATLAB programming environment. The software is freely distributed by Benjamin Schafer, a professor at Johns Hopkins University in Baltimore, USA (Li and Schafer, 2010). The current version, CUFSM 4.05, which was also used for the purpose of this research, allows elastic buckling analysis for thin walled members for general end boundary conditions based on the theory discussed in the classical FSM section. The program furthermore includes the feature of modal decomposition based on the theory previously elaborated in the cFSM section. This section deals with an introduction to CUFSM to explain the results that are obtained from the program, which helps to put the results into context for the use with the DSM. The explanation that follows is based on the interpretation of results for the simply supported boundary condition as this provides basic insight needed in the methodology chapter.

For the simply supported case, with the number of longitudinal strips $m = 1$, a buckling analysis can be performed by variation of the strip element length a. If the fundamental buckling coefficient, also the lowest buckling coefficient out of the set of buckling solutions for a fixed length (λ_1), is plotted against various physical lengths a, the well established signature curve is developed (Li *et al.*, 2014). The solid blue line in Figure 2.17 shows an example of a signature curve. The figure also shows higher buckling load levels associated with the second and third buckling deformation shape. Inflection points in the figure are critical points for member buckling, each associated with some cross-section deformation.

For the simply supported case a repetition of the buckling shape and load factor can be obtained by doubling the number of longitudinal elements ($q = 2$) with each strip having lengths of a, but half-waves developing at half-the physical length analysed $\left(\frac{L}{2} = a\right)$. An illustration of this can be seen in Figure 2.16, where the deformed shape is however only drawn for a two dimensional line segment for conceptual purposes.

For this example the fundamental buckling shape (ϕ_1) of the line segment is in the form of one half-sine curves for the $m = 1$ case, with the strip length being alternated to produce a signature curve. For the second case where $m = 2$, the fundamental buckling shape is a full sine curve, however the physical length at which fundamental buckling load is reached, is $2a$ of the previous analysis. If now only the fundamental buckling mode of the second example, $m = 2$, is plotted against the half-wavelength of the buckling length, the same plot as with the $m = 1$ case is produced. This is why the signature curve is plotted by means of the half-wavelength rather than the physical length. Such a plot shows the fundamental buckling load with the shortest arrangement

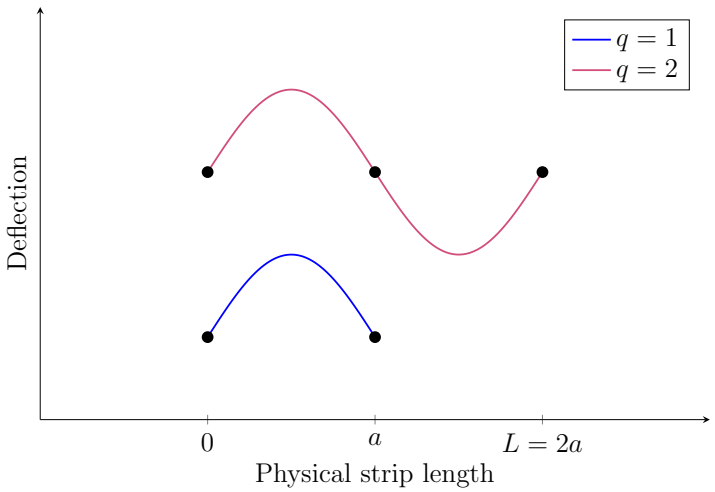

Figure 2.16: Buckling shape for the case of the strip $m = 1$ and $m = 2$

of buckling half-wavelength and reflects real propagation behavoiur. Figure 2.17 shows the $m = 2$ case with a visible phase shift of the buckling length exactly double that of the $m = 1$ case. As mentioned, the half-wavelength plot for both cases coincide. Thus, when analysing the simply supported boundary condition member, only the $m = 1$ case needs to be considered for member elastic stability.

For alternative boundary condition cases the significance of the signature curve is however lost as different m values may produce lower fundamental buckling coefficients (Li and Schafer, 2010). An alternation of the participation of the named elastic buckling modes takes place for the same physical length with alternating m cases. Thus for alternate end boundary conditions the longitudinal m terms must additionally be varied and participations of pure elastic deformation kinds must be identified parallel to this for the various buckling modes (λ_1 to λ_{4qn_s}). Only the lowest buckling coefficient from such an analysis is applicable for use in the DSM. CUFSM allows for the predictions of the m term to be included in the alternated length analysis to find pure elastic modes for alternate end boundary conditions. This feature is however not significant for simply supported conditions and is therefore not considered further.

Identification of the critical buckling factor for the three pure elastic buckling cases is however difficult from the FSM signature curve. For simple sections the identification can easily be done by the criteria outlined under the elastic stability mode section (2.2.4.1). Minima on the signature curve, as shown in Figure 2.17, are associated with pure local or distortion critical buckling coefficients. These minimum buckling coefficient values are directly used for local, distortional and global buckling strength prediction in the DSM. The half-wavelengths at which pure elastic deformations are produced can be

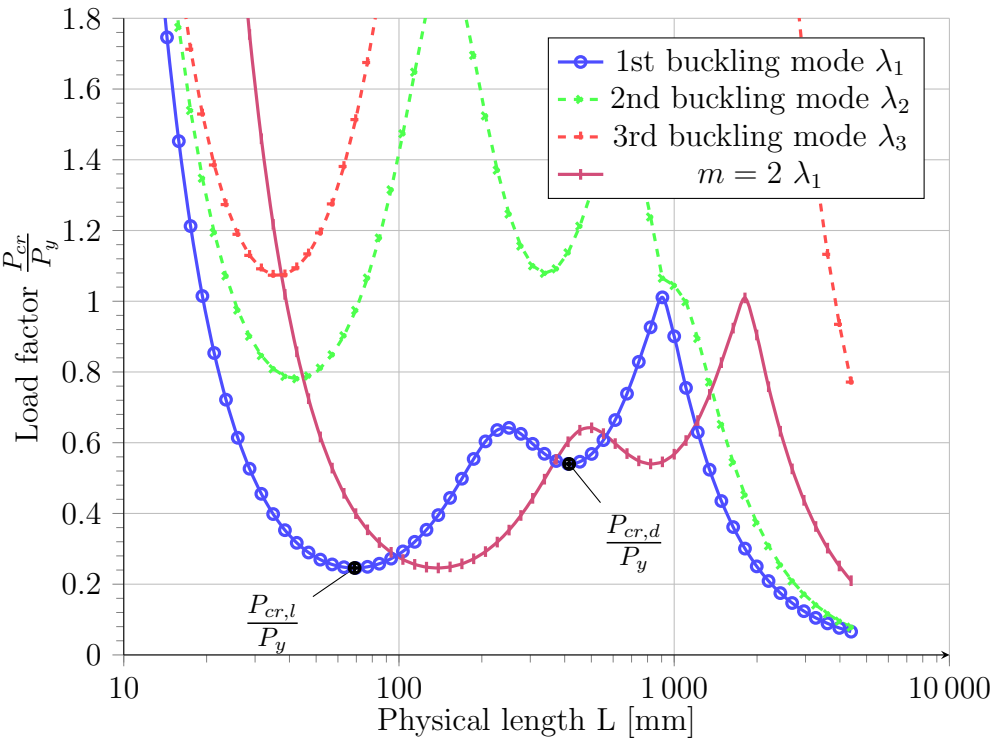

Figure 2.17: Signature curve showing different eigen-buckling loads

additionally checked together with minima to identify the critical buckling coefficient respective to each deformation mode. Global buckling coefficients for lengths where the influence from distortional buckling is not prevalent may also be used from the signature curve.

Figure 2.18 shows the signature curve for a lipped C-section where the three elastic critical buckling cases for thin walled members are easily identified. Cross-section deformation plots are also provided, which show the pure elastic buckling criteria in the cross-section at the critical points. Before the introduction of cFSM, the final check for associating the critical buckling mode with the correct pure elastic deformation, was limited to these visual identifiers. For more complex sections the local minima are not necessarily pronounced, as stiffeners may present an unclear signature curve for the classical FSM case. Expert cross-section case studies were developed by Schafer (2006*a*) to overcome this identification predicament. This ultimately led to the development of the cFSM to aid in the identification process.

Using the constraint conditions of cFSM, additional pure mode signature curves are determinable to find half-wavelengths associated with the pure deformation modes. An example of this is shown in Figure 2.18 with the three contained signature curves plotted for the local, distortional and global buckling case in red, green and cyan respectively. Now critical wavelengths can

be used to find the critical buckling factors from the full member deformation behaviour signature curve (shown in blue in the figure). The development of the pure elastic buckling mode constrained signature curves is a difficult process as round corner models present solver inaccuracy for constrained buckling analyses. Sharp corner models first need to be investigated as these remove interaction of deformation mode between elements (Schafer, 2008). Round corner model elastic mode participation plots are also problematic as they may falsely present dominant distortional buckling participation for the entire half-wavelength spectrum.

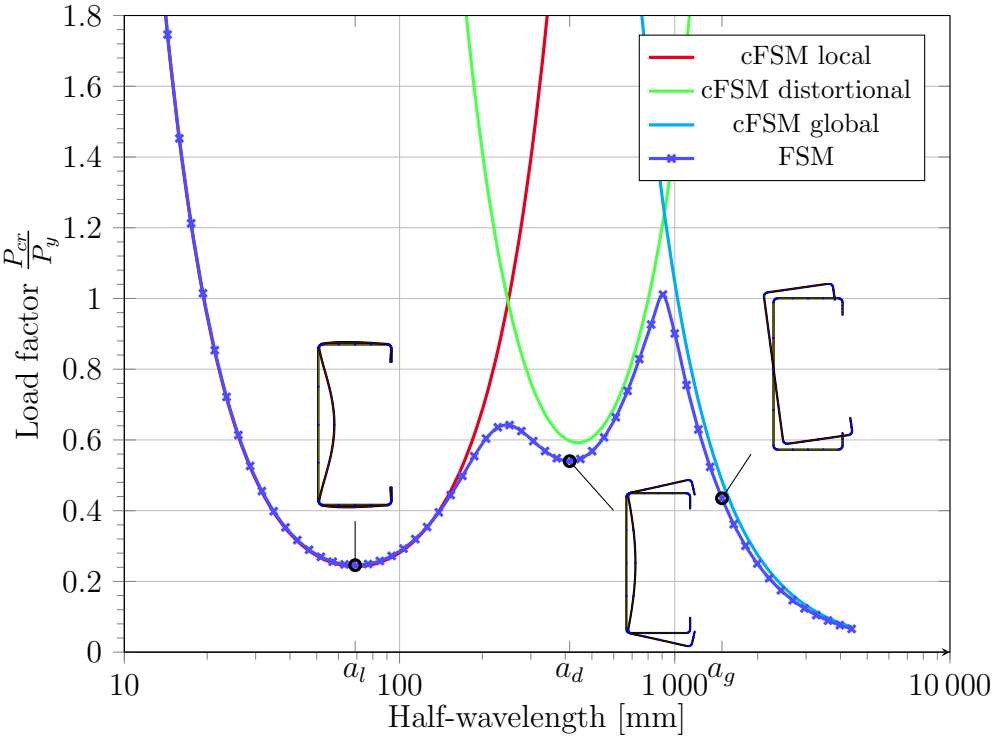

Figure 2.18: Signature curve decomposed deformations of local, distortional and global buckling

In summary half-wavelengths are key identifiers for pure mode elastic buckling behaviour. They may be determined using cFSM features in CUFSM; however, the combination of three identifiers need to be checked to establish pure elastic local, distortional and global buckling coefficients. Recapped again, the identifiers are for the simply supported end condition boundary case; (1) inflection points on the full model together with, (2) wavelengths associated with pure elastic buckling deformation modes, identified by (3) sharp-corner-model equivalent pure elastic-mode buckling signature curves or (4) sharp corner model elastic buckling mode wavelength participation plots.

2.4 Reliability theory

2.4.1 Basic reliability theory

Limit-state design is the governing condition for design of structures or structural members. For any structure the limit-state represents a point of non-exceedance at which a structure is classified safe or acceptable to human comfort levels. The limit-state condition in structures is separated into the ultimate limit-state and the serviceability limit-state conditions. Exceeding the serviceability limit-state is physically related to excessive defections, vibration or cracking in a structure. The focus of this research is on the ultimate limit-state of thin-walled cold-formed steel members. The ultimate limit-state relates to the point of load distribution that results in the loss of safety of a structure caused by loss of static equilibrium or stability.

The simplified safe-load condition for the ultimate limit state of a member can be expressed by Equation 2.38. A favourable state is expressed by determining that the load effect, E, experienced by the member, does not exceed the structural resistance (or strength), R.

$$E \leq R \tag{2.38}$$

Additionally the safe condition may be expressed by stating that the mathematical difference between the resistance, R, also known as the capacity of the system, and the load effect, E, also known as the demand on the system, must be larger or equal to null. This is represented by rearrangement of Equation 2.38 to Equation 2.39. The equality, $G = 0$, describes the boundary of the safe state and is referred to as the limit state function, performance function or reliability margin.

$$G = R - E \geq 0 \tag{2.39}$$

Conversely the region of failure can be expressed by Equation 2.40.

$$G(R, E) < 0 \tag{2.40}$$

Since the two variables that the limit state equation depend upon are associated with uncertainty, the entire problem becomes a probabilistic one. Both load effect (E) and strength (R) are not deterministic variables and this fact has led to the inclusion of probability theory in design codes to account for this property. Probability theory allows for the uncertainty to be incorporated in the design procedure. Uncertainties that arise and affect the design procedure due to variability in the load, variability in resistance and uncertainties in the modelling are explained as follows (Nowak and Collins, 2012):

1. Loads: Long term loads and self-weight are fairly accurate to predict, nonetheless when considering the density of a material, it cannot be

said that the value of this property is exact throughout the entirety of a structure. Even more so, imposed loads such as traffic and wind load are almost impossible to predict exactly at any given time.

2. Resistance: To assume that the material properties such as yield strength and thickness are uniform throughout a section is unmotivated. Thickness is only exact to the limits of the measurement instrument by which it is manufactured and the yield strength is highly dependent on the chemical composition of a section throughout its entirety.

3. Modelling and analysis: Since modelling is only an approach to simulate the behaviour of a structure, the true nature of the mobilisation of forces from that model to the members is further associated with large uncertainty depending on the applicability of the approximation.

The load effect and the resistance are functions of various underlying n-number of variables. Randomness in both system demand and capacity come from theses underlying variables. The limit state function can thus similarly be expressed as seen in Equation 2.41 bellow:

$$G = g(X_1, X_2, X_3, ..., X_n) \tag{2.41}$$

Once the n-number of random parameters have been addressed, the probability density functions for both variables of load effect and resistance can be obtained by probability theory and the respective distribution functions are shown in Figure 2.19.When looking at Figure 2.19, it is clear that the load effect and resistance variables can attain various possible magnitudes and the figure show the non-deterministic attribute of the variables. Additionally it is visible form the figure that combinations of realisations for the variables exist, that do not satisfy the limit state condition. The associated probability condition, denoted as p_f, which relates to the probability of failure can be expressed by Equation 2.42

$$p_f = p(E > R) \tag{2.42}$$

The equation shows that some realisations of the random variables exist, where the load effect exceeds the resistance of the member and the possibility of this situation comprises the probability of failure. Probability of failure, set out by Equation 2.42 for n continuous random variables, may be attained by the integration procedure in Equation 2.43 (Haldar and Mahadevan, 2000):

$$p_f = \int ... \int_{g()<0} \varphi_X(x_1, x_2, x_3, ..., x_n) dx_1 dx_2 ... dx_n \tag{2.43}$$

For the equation above, φ_X is the joint probability density function from the x_n probability density functions of the n-number of random variables, which

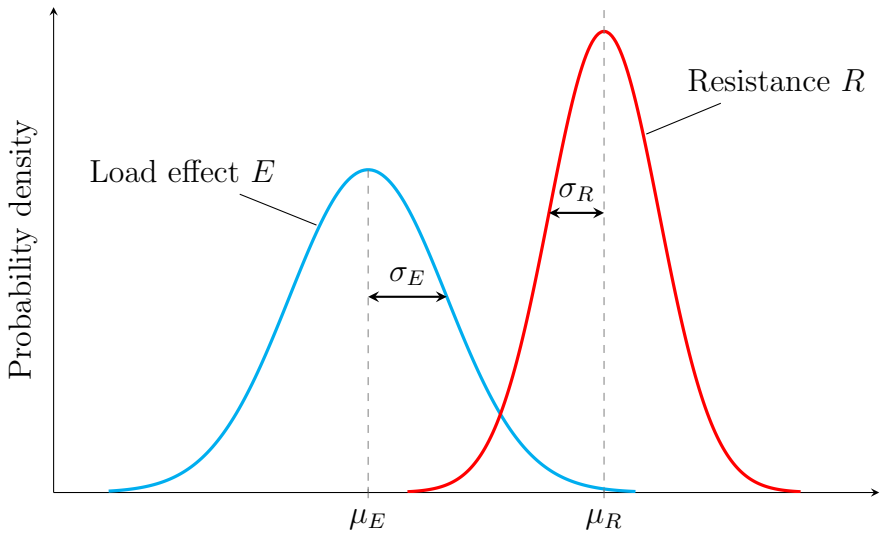

Figure 2.19: Risk from load effect and resistance as random variables

are integrated over their full domain of possible realisations. If the variables are statistically independent, then the integral may be replaced by the product of the individual cumulative probability functions Φ_{x_n} (Nowak and Collins, 2012). "Independent" in probability terms means that the variables are not functions of one another.

1. The relative position of the two curves. If the relative distance between the two curves decreases, the likelihood of failure increases and the reliability decreases. The position of the curves may be represented by the mean values (μ_E and μ_R) of the two random variables.

2. The dispersion of the two curves. If the probability density functions are narrower, the region of failure decreases. A measure of dispersion for the two curves is the standard deviation (σ_E and σ_R).

3. The shape of the two curves. The shapes of the probability density function of each variable affects the size of the region of intersection. The statistical moment parameter that impacts the shape of the distribution is the coefficient of skewness for the curves (a_E and a_R), but is not exclusively determined by this parameter.

Each of the above named parameters are also indicated in Figure 2.19 and are also referred to as the statistical moment parameters.

2.4.2 Alternative reliability measure from two normally distributed random variables

As the complexity of probability theory and the probability of failure is not easily understood by engineers, a different measure of reliability was formalized that is based on the statistical moment parameters outlined in the previous section. This alternative measure can be best explained in a simplified manner, if the load effect and resistance probability density functions both follow the symmetrical normal probability density function.

From the property that both variables are normally distributed, the mean value (μ_G) and the coefficient of variation (σ_G) for the reliability margin are calculated as presented in Equations 2.44 and 2.45:

$$\mu_G = \mu_R - \mu_E \tag{2.44}$$

$$\sigma_G^2 = \sigma_R^2 + \sigma_E^2 + 2\rho_{RE}\sigma_R^2\sigma_E^2 \tag{2.45}$$

where $2\rho_{RE}\sigma_R^2\sigma_E^2$ is the correlation coefficient of the random variables of load effect and resistance. The two equations above have now reduced the reliability problem to that of one variable.

As mentioned the probability of failure, stated in Equation 2.42 previously, can be expressed as the intersection probability that the resistance is exceeded by the load effect. This can now simply be expressed in terms of the reliability margin (G). This rearrangement of the probability of failure condition is given in equation 2.46.

$$p_f = p((R - E) < 0) \tag{2.46a}$$
$$= p\left(G(R, E) < 0\right) \tag{2.46b}$$
$$= \Phi_G(0) \tag{2.46c}$$

In Equation 2.46 the probability of failure now takes into account that the probability of failure is the point where the reliability margin is less than zero. The probability of failure can therefore be determined by the cumulative probability density function of the resulting reliability margin (Φ_G, where G is defined in Equation 2.46a) at zero. Figure 2.20 shows the normal probability density function of the reliability margin, given that reliability margin variable G follows a normal distribution. The region of failure, again shaded in the figure, can now simply be computed by Equation 2.46c.

Indicated in the figure again are the statistical moment parameters for the reliability margin (μ_G and σ_g). Some simple traits from the probabilistic behaviour of the reliability margin must be mentioned at this point. An increase in standard deviation (σ_G) results directly from an increased variation and

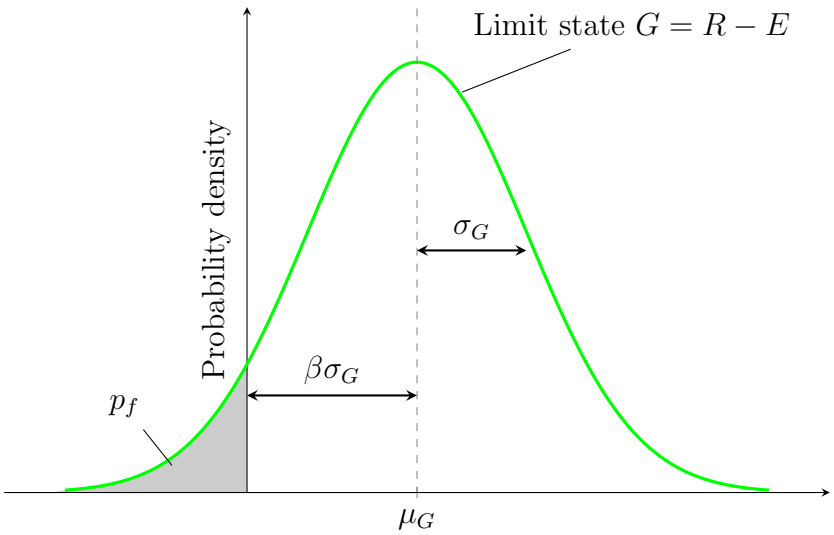

Figure 2.20: Reliability concept for the ultimate limit state

yields a larger probability of failure by making the curve wider. Furthermore a lower mean of the reliability margin (μ_G) yields a lower estimator for the reliability index as the curve shifts in the direction of the origin. Again this increases the region of failure and ultimately the probability of failure. Theses two conditions are important for the subsequent investigations of this thesis.

The alternative measure of reliability previously mentioned is now obtainable when the probability space of the reliability margin is transferred to the standardised normal space. Equation 2.47 shows this transformation procedure from normally distributed space to standardised normal space. The transformation into standardised space effectively moves the mean value of the reliability margin distribution to the origin ($\mu_G = 0$) and reduces the standard deviation to unity ($\sigma_G = 1$) (Nowak and Collins, 2012).

$$u_0 = \frac{0 - \mu_G}{\sigma_G} = -\frac{\mu_G}{\sigma_G} = -\beta \tag{2.47}$$

The now standardised variable β, also known as the reliability index, is the shortest distance between the limit state boundary and the origin in standardised space. The probability of failure condition for the standardised space is given in Equation 2.48, with Φ_U being the cumulative probability distribution function for the standardised reliability margin variable u_0 from Equation 2.47.

$$p_f = \Phi_U(u_0) = \Phi_U(-\beta) \tag{2.48}$$

From the condition that the reliability margin follows a normal probability distribution the reliability index, β, can thus be computed by Equation 2.44

and 2.45.

$$\beta = \frac{\mu_G}{\sigma_G} = \frac{\mu_R - \mu_E}{\sqrt{\sigma_R^2 + \sigma_E^2 + 2\rho_{RE}\sigma_R^2\sigma_E^2}} \tag{2.49}$$

Equation 2.48 shows the direct relation that the reliability margin has with the probability of failure and is therefore an alternative means of representation for the reliability. Even more so, the β index is a simpler and more understandable measure as it indicates improved reliability by increasing as p_f decreases.

Figure 2.21 shows how the reliability margin can be visualised in standardised space where the margin is a function of the two standardised variables of load effect and a non-linear limit state equation. Also visible in the figure is the design point (r_{0d}, e_{0d}). That is the point where the limit state is reached and β is the smallest, but the probability of failure is largest. This point is also often referred to as the most probable point (MPP) of failure (Haldar and Mahadevan, 2000). Depending on the shape of the limit state equation, multiple MPPs can exist. For the non-linear limit state equation shown in Figure 2.21 the only existing MPP produces the reliability index.

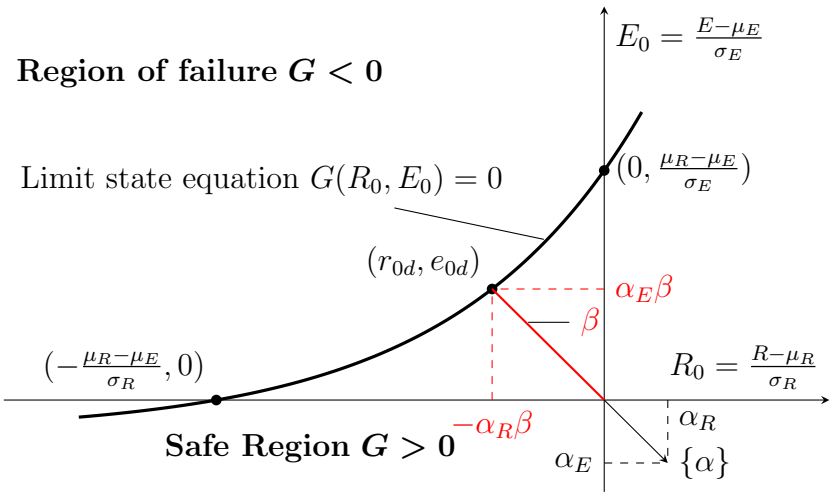

Figure 2.21: Visualisation of the reliability index and α parameters in standardised space for a non-linear limit state equation (Haldar and Mahadevan, 2000)

Another concept that is introduced from the reliability index is the direction vector of β in standardised space otherwise referred to as the sensitivity factor (α). The direction vector can be split into two components relating to the load effect $(\alpha_E\beta)$ and the resistance $(\alpha_R\beta)$ of the reliability margin problem. Equations 2.50 and 2.51 define the two components of the direction vector, which are nothing more than the direction cosines of β from the transformation to standardised space.

$$\alpha_E = -\frac{\sigma_E}{\sqrt{\sigma_E^2 + \sigma_R^2}} \tag{2.50}$$

$$\alpha_R = \frac{\sigma_R}{\sqrt{\sigma_E^2 + \sigma_R^2}} \tag{2.51}$$

The reliability index as the alternative measure of reliability has been elaborated upon in terms of the statistical parameters. However, this section only introduced a simplified measure of the reliability index by making use of the normal distribution behaviour of the reliability margin. Various approaches exist for determining the probability of failure, but methods such as direct integration of the probability distribution functions are not always possible for a n-variable reliability margin (Nowak and Collins, 2012). A procedure following the above mentioned concepts is discussed in Section 2.4.4 for a n-variable non-normal case.

2.4.3 One random variable reliability

For the purposes of design standards, reliability in the design sense is split into the two reliability components, $-\alpha_R\beta$ and $\alpha_E\beta$, elaborated upon in the previous section.Since the DSM is a resistance or strength design approach the reliability must be separately evaluated.

As was visible from Figure 2.21, the design point of resistance contributes to the overall reliability problem. Design standards approximate the design point by calibrating the limit state equation with partial factors in combination with characteristic values of the underlying variables of the limit state equation. For the load effect, the design point is approximated by upper percentiles and for the resistance, the design point is approximated by lower percentiles.

Again a safe state condition can be formulated by use of the discrete design point (r_d), also referred to as the deterministic load effect contribution, and the random variable of the resistance R (Holický, 2009). The associated probability condition is given in Equation 2.52.

$$p_f = p(r_d > R) \tag{2.52a}$$
$$p_f = p((R - r_d) < 0) \tag{2.52b}$$
$$= p(G < 0) \tag{2.52c}$$
$$= \Phi_U(-\alpha_R\beta) \tag{2.52d}$$

Figure 2.22 shows the discrete design point and the probability distribution associated with the resistance. The reliability problem is a similar condition to the one variable limit state condition G expressed in Section 2.4.2. This is similarly found by redefining the limit state function to only have one random variable, as expressed in the probability of failure condition in Equation 2.52.

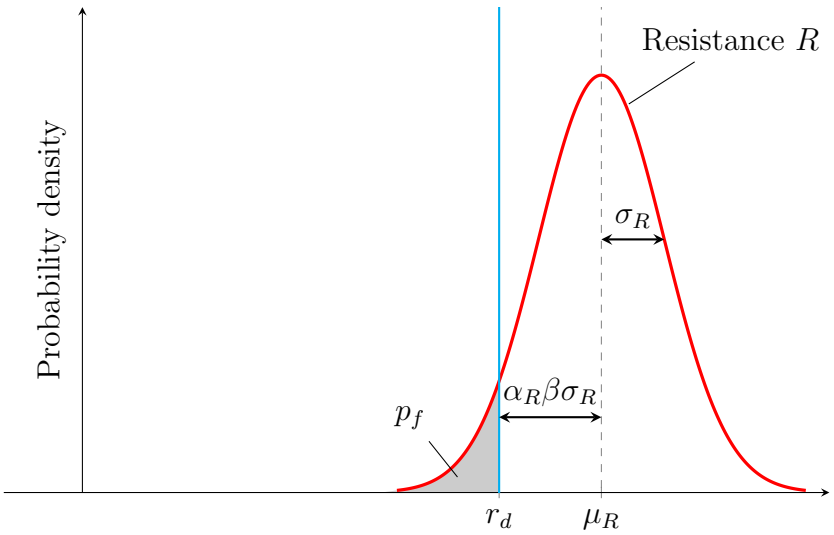

Figure 2.22: Reliability concept for the ultimate limit state

The design point on the resistance side (r_d) of the limit state equation can, looking at Figure 2.22, simply be expresses as presented in Equation 2.53. This equation is also traceable from Figure 2.21 of the previous section.

$$r_d = \mu_R - \alpha_R\beta\sigma_R \tag{2.53}$$

where α_R is the sensitivity factor mentioned in the previous section.

An important concept to remark on at this point, is that for the purposes of determining the reliability of a resistance design standard such as SANS: 10162- 2 the reliability analysed is separated to find the vector component for the resistance side, or $\beta_R = \alpha_R\beta$. This is done to attain the resistance based reliability (β_R) only, as the more intrinsic measures of a resistance specification on the reliability are therefore evaluated and since loading standards are generally not coupled to the resistance specification. The aimed at value is generally reached by calibration of partial factors to a value of target reliability which is equal to the component of accepted overall reliability (β_t), i.e. $\alpha_R\beta_t$. An investigation into the $\alpha_R\beta_t$ value for cold-formed members follows in the subsequent chapter, based on the statistical parameters specific to cold-formed steel and the DSM.

2.4.4 First Order Reliability Method

It has to this point been established how the reliability for a member may be determined using stochastic methods. The basic example was illustrated for the case when both load effect and resistance are normally distributed. Furthermore it has been shown that the reliability margin for resistance design

standards may be reduced to the reliability of only the resistance side of the limit state condition by means of some simplifications of the probability of failure. The problem that the resistance may follow an arbitrary distribution is now also considered and additionally the attribute that the resistance variable is a result of multiple underlying random variables is also addressed.

Consider again the case, previously presented in Equation 2.41, where the limit state function is a function of n-number of underlying random variables. This can be denoted by $G = g(\{X\})$, where $\{X\}$ is a vector of X_n random variables. Take note that G can be the reliability margin of the reduced reliability problem presented in the previous section or that of the full reliability problem of load effect and resistance.

The procedure that is used to solve this problem was initially developed by Hasofer and Lind (Breitung, 2015) and is the alternative measure of reliability discussed previously in Section 2.4.2. The procedure is known as the First Order Reliability Method and is from here on referred to as FORM. For variables that are not normally distributed Rackwitz and Fiessler (Breitung, 2015) developed a FORM procedure that found equivalent normal distribution parameters of mean (μ^e) and equivalent standard deviation (σ^e) to reduce the problem to the same problem as a normally distributed variable problem.

For this modified procedure to be applicable, two conditions need to be imposed in the procedure. Firstly, the cumulative distribution functions (Φ_{X_n}) and the equivalent normal variables (Φ_{U_n}) should be equal at the design point. Secondly, the probability density functions (φ_{X_n}) of the n-number of random variables should be equal to those of the equivalent normal density functions (φ_{U_n}) at the design point. The two conditions are described by equations 2.54 and 2.55 (Holický, 2009).

$$\Phi_{X_n}(x_n^*) = \Phi_U\left(\frac{x_n^* - \mu_{X_n}^e}{\sigma_{X_n}^e}\right) \tag{2.54}$$

$$\varphi_{X_n}(x_n^*) = \frac{1}{\sigma_{X_n}^e}\varphi_U\left(\frac{x_n^* - \mu_{X_n}^e}{\sigma_{X_n}^e}\right) \tag{2.55}$$

From these two equations the equivalent normal mean and equivalent normal standard deviation can be determined by rearrangement to make theses variables the subject as seen in equations 2.56 and 2.57 below.

$$\mu_{X_n}^e = x_n^* - \sigma_{X_n}^e[\Phi_U^{-1}(\Phi_{X_n}(x_n^*))] \tag{2.56}$$

$$\sigma_{X_n}^e = \frac{1}{\varphi_{X_n}(x_d^*)}\varphi_U\left(\frac{x_n^* - \mu_{X_n}^e}{\sigma_{Xn}^e}\right) = \frac{1}{\varphi_{X_n}(x_n^*)}\varphi_U[\Phi_U^{-1}(\Phi_{X_n}(x_d^*))] \tag{2.57}$$

Since solving of the limit state equation in general is a non-linear problem, the method for finding the reliability index is an iterative process. Non-linearity

of the limit state equation results even with linear limit state equations when non-normally distributed variables are used and transformed to standardised normal space (Haldar and Mahadevan, 2000). In order to solve this problem the FORM procedure approximates the higher order limit state equation by a tangent hyperplane in standardised space (Lopez and Beck, 2012). The steps necessary for the computation of the reliability index are summarised below and can be partially followed in Figure 2.23.

1. The limit state function $G(\{X\}) = 0$ is formulated and theoretical distribution models of $\{X\} = \{X_1, X_2, X_3, ..., X_n\}$ are specified.

2. An initial estimation of the design point $\{x^*\} = \{x_1^*, x_2^*, x_3^*, ..., x_n^* s\}$, which represents some realisations of the random variables, is made. Generally all $n-1$ variables are initially estimated at their means and the last variable is solved such that the limit state equation is satisfied, or $G(\{x^*\}) = 0$.

3. At the point $\{x^*\}$ equivalent normal distributions are found using equations 2.56 and 2.57.

4. The transformed standardised design point $\{u^*\} = \{u_1^*, u_2^*, u_3^*, ..., u_n^*\}$ is determined using the transformation given again in Equation 2.58 for the equivalent normal distribution case.

$$u_n^* = \frac{x_n^* - \mu_{X_n}^e}{\sigma_{X_n}^e} \tag{2.58}$$

5. Partial derivatives of all variables must be determined at the design point estimator ($\{u^*\}$) to calculate the shortest distance to the design point. The derivatives are required for their use in the mathematical procedure for obtaining function minima. This is equal to the reliability index in standardised space and the partial derivatives required are defined by Equation 2.59.

$$\{D\} = \begin{Bmatrix} D_1 = \frac{\partial G}{\partial U_1} \\ D_2 \\ . \\ . \\ . \\ D_n = \frac{\partial G}{\partial U_n} \end{Bmatrix} \tag{2.59}$$

6. From the derivatives the reliability index is estimated as the shortest distance to the origin in the transformed space resulting in Equation 2.60, where $[\rho]$ is the correlation matrix of the n number of variables.

$$\beta = -\frac{\{D\}^T\{u^*\}}{\sqrt{\{D\}^T[\rho]\{D\}}} \tag{2.60}$$

7. Sensitivity factors for each variable can be determined from Equation 2.61 which is the n-number of variables representation of Equations 2.50 and 2.51 for the two variable reliability example.

$$\{\alpha\} = \frac{[\rho]\{D\}^T}{\{D\}^T[\rho]\{D\}} \tag{2.61}$$

8. An update of the design point for $n-1$ variables is determined by the sensitivity factors using equations 2.62 and 2.63.

$$u_n^* = \alpha_n\beta \tag{2.62}$$

$$x_n^* = \mu_{X_n}^e - u_n^*\sigma_{X_n}^e \tag{2.63a}$$
$$x_n^* = \mu_{X_n}^e - \alpha_n\beta\sigma_{X_n}^e \tag{2.63b}$$

9. The limit state $G(\{x^*\}) = 0$ equation is re-solved for the n^{th} variable.

10. Steps 3 to 9 are repeated until the reliability index converges.

The convergence criterion used for this study is that the change in beta is less tau (τ), with tau equal to 0.005 ($\beta \leq \tau = 0.005$), which provides the reliability index accurate to two decimal figures. Some analysis procedures additionally require a check on the convergence of the design point as well, but this is not considered by the algorithm used in this thesis which was adopted from the original algorithm developed by Rackwitz. Haldar and Mahadevan (2000) as well as Nowak and Collins (2012) suggest a criterion of convergence of tau equal to 0.001 which generally results in five cycles of the algorithm. The difference between the τ value used and the literature-proposed value is scrutinized in Section 3.5.1.1.

The above-mentioned FORM procedure is used to perform a full probabilistic analysis for determining the reliability of cold-formed members based on a case-specific limit state condition dependant on the idealized resistance of the member. Other versions of the algorithm exist, such as the Second Order Reliability Method (SORM), that approximates the failure boundary with a quadratic surface in order to address the possibility of multiple MPPs. This let-back is however not a problem due to the nature of the limit state equation associated with the DSM and the reason for this is addressed in Chapter 3.

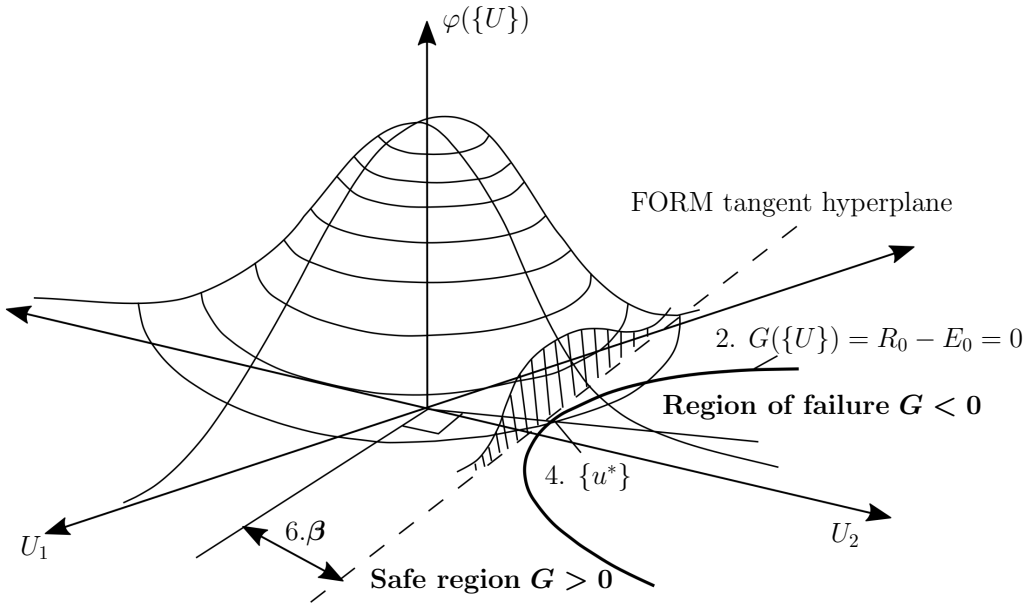

Figure 2.23: Illustration of the reliability index concept and the linearisation of the limit state function in standard normal space for a two variable case (Lopez and Beck, 2012)

2.4.5 Previous studies and basis of investigation

Basic reliability for the DSM was determined for cold-formed steel members by calibration of a partial factor. The procedure for this was done for a simple limit state condition model explained in the AISI commentary (American Iron and Steel Institute *et al.*, 2012) irrespective of an exact limit state equation from DSM or EWM.

To understand the simplified calibration approach an alteration of the safe state condition must first be explained. Consider again the unsafe state of Equation 2.64 below. Note that the limit state condition can alternatively be expressed by dividing both sides by the load effect E, as seen in Equation 2.65 Nowak and Collins (2012).

$$R < E \tag{2.64}$$

$$\frac{R}{E} < 1 \tag{2.65}$$

$$G(R, E) = \frac{R}{E} < 1 \tag{2.66}$$

$$\tag{2.67}$$

For the safe state condition of flexural steel members, which includes both compression and bending, the resistance in general can be expressed as a product of some cross-section component such as area A or section modulus, Z,

and yield strength, f_y. To incorporate the uncertainty of that model (δ_R) the probabilistic resistance variable can thus be expressed as a function of these three variables with the uncertainty of a cross section dominantly presented by the thickness of the section, t. $R = f(\delta_R, t, f_y)$.

If we now take the natural logarithm (ln) of Equation 2.66, the probability of failure can be expressed by Equation 2.68 below. This assumption does change the distributions of the underlying variables to be lognormal, but the variable $\ln(R)$ and $\ln(E)$ are now normally distributed (Haldar and Mahadevan, 2000).

$$p_f = p(\ln(\frac{R}{E}) < \{\ln(1) = 0\}) \tag{2.68}$$

Similar to the two-variable-case, the reliability index can be calculated from the definition of the standardised-space two-variable normal-distribution case as presented in Equation 2.69 (Haldar and Mahadevan, 2000; Nowak and Collins, 2012). For this simplification to hold true, coefficients of variation must be small (less than or equal to 0.39 (Haldar and Mahadevan, 2000)). Limits to this assumption however are that both the load effect and the resistance variables are lognormally distributed since they can never take negative values (Haldar and Mahadevan, 2000).

$$\beta = \frac{\mu_{ln(G)}}{\sigma_{ln(G)}} = \frac{\mu_{ln(R)} - \mu_{ln(E)}}{\sqrt{\sigma^2_{ln(R)} + \sigma^2_{ln(E)}}} \approx \frac{ln(\frac{\mu_R}{\mu_E})}{\sqrt{V_R^2 + V_E^2}} \tag{2.69}$$

The mean resistance from this assumption is assumed to be the product of mean of the bias factors (δ) for all other probabilistic variables and the nominal resistance as shown in Equation 2.70 (American Iron and Steel Institute *et al.*, 2012).

$$\mu_R = \mu_{\delta_R}\mu_{\delta_t}\mu_{\delta_{f_y}}R_{nominal} \tag{2.70}$$

In addition, by using the transformed limit state equation, a simplification of the standard deviation is made for the coefficients of variation (V, the ratio of standard deviation to the mean, from here on referred to as COV), clearly visible in Equation 2.69. If the substitution of the COV for lognormal standard deviation is considered to be true, a modification of the sensitivity factors calculation, but more importantly the influence on the sensitivity of the resistance, can be assumed as shown in Equation 2.71 below (Mori *et al.*, 2002).

$$\alpha_R = \frac{V_R}{\sqrt{V_E^2 + V_R^2}} \tag{2.71}$$

This simplification assumption is quite useful as the sensitivity factors are now expressed in terms of COVs. Also, if a COV is a function of multiple underlying random variables, that COV can be expressed as the sum of squares of the underlying variables (Haldar and Mahadevan, 2000). An example of

this is shown for the COV of the resistance (V_R) by its underling bias factor variables in Equation 2.72.

$$V_R^2 = V_{\delta_R}^2 + V_{\delta_t}^2 + V_{\delta f_y}^2 \tag{2.72}$$

From the above fundamentals, cold-formed section design using the DSM was calibrated to acceptable reliability previously achieved by the safety factor design. This was readily achieved by updating the new model factor to that obtained from the DSM equations, with other variables' moment parameters well known from past probabilistic investigations. Back-calibration of the safety factor design method yielded an overall β of 2.8 including both the load effect and the resistance (American Iron and Steel Institute *et al.*, 2012).

The overall target reliability (β_t) that the DSM equations' partial factors were calibrated for is more extensively explained at the end of Chapter 3. However, the above mentioned process is the fundamental basis for the back-calibration of the partial factor to an acceptable β_t for the DSM. The calibration resulted in the prescribed partial factor that is also currently in use in SANS 10161-2. The above-mentioned random variables (t, fy, δ_R) are thus reason or the basis for the probabilistic variables that are investigated by this research using an extensive FORM analysis for a more complex limit state prediction model. No correlation was assumed to exist between the random variables by the AISI. Although some correlation exists between yield strength and thickness (Li *et al.*, 2007), no correlation is assumed from here onwards which means that the correlation has negligible effect on the reliability.

To conclude this chapter it must be mentioned that the South African Standard for cold-formed member design at this point in time is not calibrated to the South African loading code. SANS 10162-2 clearly states that the code must be used in combination with the Austrailian/New Zealand loading code. The use of a non-South-African loading code is ultimately impractical as live loads such as wind load, which are generally the dominating design condition for cold-formed members (American Iron and Steel Institute *et al.*, 2012), are not predicted accurately by non-South-African loading standards due to topological and meteorological factors. The use of the South African loading code has two implications: Firstly, the current partial factor contains a target reliability that follows from the Australian standards, which differs from the target reliability of the South African Standard. Secondly, if design of the members is done based on loading of the South African Standard, the reliability of the member is unknown. Therefore it must first be established from a more extensive reliability analysis, what the achieved reliability of the resistance side is, in order to make conclusions that could lead to the calibration to the South African loading code in the future. This outcome of establishing the exact reliability based on previous calibration is the aim and core focus of this thesis.

Chapter 3

Reliability Analysis of Cold-formed Steel Elements

In this chapter the main contributions to the dissertation are presented. Firstly the procedure for determining the reliability margin by implementation of the FORM analysis with CUFSM is explained. Thereafter factors that influence the reliability-outcome are discussed and elaborated upon.

3.1 The limit state equation for compression or bending

The analysis algorithm used for the FORM procedure, discussed in Section 2.4.4, was implemented directly into the DSM equations given in Section 2.2.4. To better understand this procedure, the limit state as function of the most important underlying random variables, from all variables effecting the resistance mentioned in the previous chapter, can be written as in seen Equation 3.1 below:

$$G = R(\delta_R \cdot min \begin{cases} F_{nl}(f_y, t) \\ F_{nd}(f_y, t) \\ F_{ne}(f_y, t) \end{cases}) - R_d \tag{3.1}$$

This equation however generalises the procedure for both loading in compression and bending; where R is the probabilistic resistance and R_d is the deterministic design resistance. As can be seen, Equation 3.1 is only a function of the resistance based random variables and therefore only evaluates the resistance side of the reliability margin (β_R) as explained by Equation 2.52 in Section 2.4.3. The variable F_n refers to the failure mode and the subscript n refers to the failure by either: local buckling nl, distortional buckling nd and Euler or elastic global buckling ne, as explained in Section 2.2.4, respectively. At this point each mode is still dependant on the appropriate DSM equation, but is shown in Equation 3.1 as functions of only the thickness and yield

strength, as these are assumed to be the most influential random variables, which was mentioned in the previous chapter.

The deterministic resistance in the procedure followed in this dissertation, is analysed as the factored resistance (R_d) from the values used in design for the thickness (t_d) and yield strength (f_{y_d}). This approach is justified by the procedure to find only the resistance based reliability margin ($\alpha_R\beta$) motivated in Section 2.4.3. The load effect side of the design may be ignored by this assumption, since the appropriate loading code used for design should account for the simplification by making use of the coupled sensitivity factor α_E. A more extensive elaboration on the limitations of this assumption are presented in Section 3.5.2 of this chapter.

Equation 3.2 explains how the smallest mode-dependant resistance F_n is factored by the design partial factor (ϕ) to give the design resistance (R_d). The yield strength f_y and the thickness t on this side of the limit state are the values based on design of the member and are denoted by the subscript d.

$$R_d = \phi \cdot min \begin{cases} F_{nl}(f_{y_d}, t_d) \\ F_{nd}(f_{y_d}, t_d) \\ F_{ne}(f_{y_d}, t_d) \end{cases} \tag{3.2}$$

In order to determine the probabilistic part of the limit state function, R of Equation 3.1, the resistance failure mode must be obtained for a member as a function of the probabilistic random variable fy and t to account for the uncertainty that follows from these parameters. Another variable that incorporates uncertainty on the resistance side of the limit state is additionally introduced: namely the model factor of the resistance δ_R. The origin and influence of this probabilistic variable are discussed in Section 3.4 of this chapter. Important to note is that the model factor is multiplied with the relevant failure mode to produce the probabilistic resistance part of the limit state condition.

Both the deterministic resistance R_d and the probabilistic resistance are assumed for the idealized pin-pin ended boundary condition case. Although the limit state equation (3.1) does not change in the above-presented generalized form, assumptions for alternating boundary conditions affect CUFSM analysis results. These results will in turn influence the reliability analysis, since CUFSM output is subject to the member force distributions and loading that the structural component is designed to resist.

Figure 3.1 shows the idealized pin-pin ended boundary condition for compression and bending as well as the idealized loading that is assumed in this dissertation. The figure illustrates the loaded members with some arbitrary cross-section of single symmetry. Structural members are shown in this configuration, to point out that one of the fundamental assumptions in order to

make use of the DSM, is that the studied beams and columns are commonly singly symmetric. As mentioned, the loading for the beam can be about either of the major axes of the cross-section, but in this dissertation is limited to bending about the axis of symmetry. For cold-formed members designed following the DSM, the symmetry-axis is generally the strong-axis. The scope is hereby limited to this condition, since beam members are optimally used when designed to be bent about the strong axis. Reliability for cold-formed beams for this design scenario is therefore of interest.

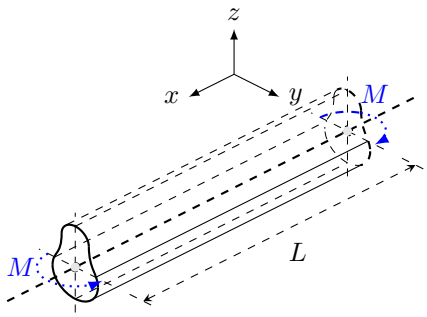

(a) Pin-pin restrained idealized laterally unrestrained beam in pure bending.

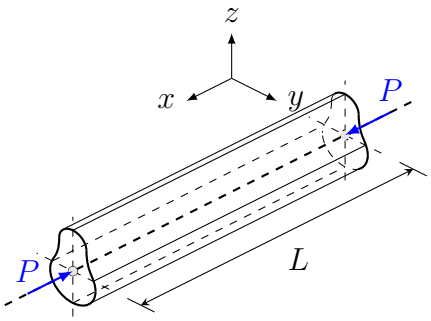

(b) Pin-pin restrained idealized column in pure compression.

Figure 3.1: Illustration of loading which structural members are analysed to resist

Figure 3.2 below shows the member force distributions that follow from the idealized loading and end conditions of Figure 3.1. Although CUFSM allows alternative end-boundary conditions to be analysed, the loading and member load distributions when using CUFSM are limited to be the ones shown in the diagrams in Figure 3.2. This comes from the fact that CUFSM only allows a linear stress distribution through the length of the member by means of tractions and they are only achieved by uniform member load distributions as

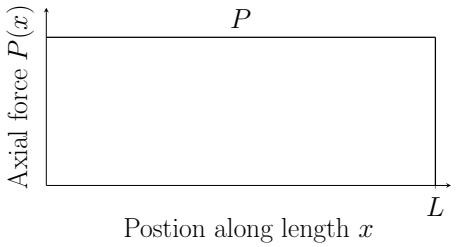

(a) Axial force diagram

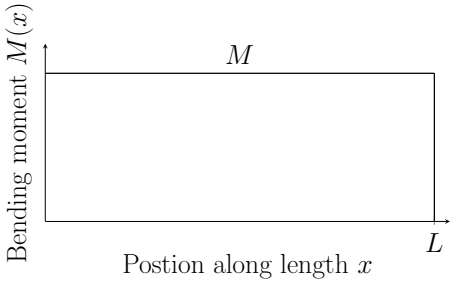

(b) Bending moment diagram

Figure 3.2: Member load distribution diagrams

shown. The tractions may however still vary linearly through the depth of a member which is achieved by an applied moment.

For the pin-ended conditions assumed, the section force diagrams are linear and thus the load maximum is consistent throughout the length. Each maximum represent the design resistance of Equation 3.1 used in the reliability analyses and adheres to the assumptions of CUFSM. Although the member load distribution from Figure 3.1 for the column has no influence on the limit state equation used in this dissertation, the beam load distribution has an effect on the flexural torsional buckling equation that is inherently included in Equation 3.1. The fact that pin-ended beams with uniform moment are considered, makes the critical torsional-flexural buckling equation by Timoshenko independent of the moment curvature and simplifies the formula considerably.

3.2 Analysis algorithm

The following section explains how the FORM procedure was combined with CUFSM to perform the reliability analysis. In order to determine the reliability of members designed according to the DSM correctly, all of the influencing factors had to be investigated. This section deals with these influencing components and presents how they impact the reliability analysis.

3.2.1 Logic

Since the failure-mode-dependant limit state can be determined by means of the DSM equations using CUFSM, the FORM algorithm was directly implemented into the CUFSM code. Each step mentioned in the FORM procedure (see Section 2.4.4) and the interrelation can be seen in the flow diagram in Figure 3.3.

The algorithm begins with the input of the profile cross-section dimensions. This mainly consist of the bending radii, overall centre lengths of elements as well as the modulus of elasticity and the Poisson ratio for the provided material. Input values of these deterministic variables are elaborated upon in Section 3.3.

At the next step in the flow, the thickness and yield strength are substituted in the CUFSM code to determine the design resistance R_d. This is achieved by determining the various critical buckling loads from a signature curve and inserting them into the DSM equations and subsequently finding the lowest mode dependant load effect F_n and factoring it. See the design resistance side of the limit state equation 3.1. The run of CUFSM for this step is important, since the buckling coefficient, as shown in the previous chapter, is dependant on both the geometrical properties as well as the yield capacity, to form the design resistance; one of the most important parameters in the limit state equation.

Once this has been completed, the algorithm re-evaluates the profile's probabilistic resistance side of the limit state equation (R) at the mean values of two of the three random variables, namely: the thickness and the yield strength. This coincides with the FORM procedure's step 1 mentioned in Section 2.4.4. As discussed, the algorithm considers each mode-dependant resistance separately, to produce one reliability index for each probabilistic resistance mode.

Now the third random variable, as mentioned in step 2 in Section 2.4.4, is solved for, to set the limit state function equal to zero. The variable for which this thesis' specific algorithm does this, is the model factor of the resistance δ_R. Choosing to solve for this variable is the simplest choice when considering Equation 3.1. Solving the limit state equation for any of the other random variables would require a non-linear solution procedure due to the nature of

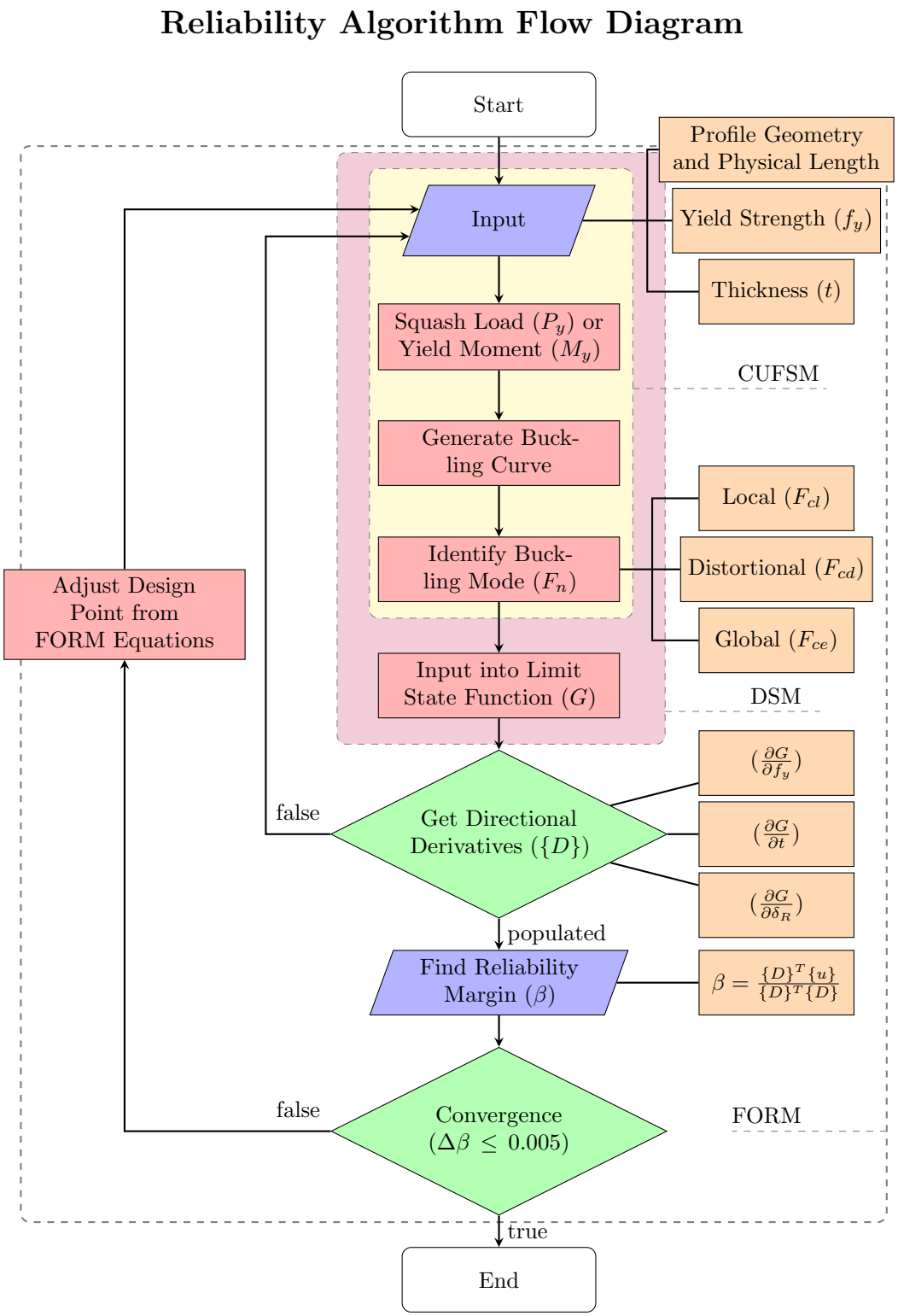

Figure 3.3: Flow diagram depicting the relationship between limit state function generation process and the FORM procedure

the DSM equations and is therefore the rational choice.

At this stage the flow diagram separates into two loops, as the procedure mentioned up to this point has to be repeated. The reason for this is that the directional derivatives necessary for the FORM procedure have to be determined numerically. This means that a numerical difference on the limit state, at the design point, has to be implemented on all variables affecting the limit state function. Finding the directional derivatives corresponds with step 4 of the FORM procedure and is a uniquely addressed by means of CUFSM.

In the visually displayed inner loop, the algorithm now takes definite forward and backward differences from the design point estimate, first of the yield strength while the thickness remains constant, then of the thickness as the yield strength remains constant. All five cases are considered for one mode of resistance and repeated for the other modes. Now a numerical field for the limit state exists and the numerical derivative of the limit state function can be obtained. This procedure is known as the central difference method for obtaining the derivative of a function and the advantages of this procedure as well as a visual explanation will be given in the following subsection.

The derivative of the limit state function has now been determined with respect to the yield strength as well the thickness. For the model factor the central difference method is also applied. Nevertheless, CUFSM does not need to be re-run as a variation in the model factor does not influence the resistance mode (F_n) results on the resistance side of the limit state function. A difference for the model factor is recorded by numerical substitution of the forward and backward difference-values only.

Finally the routine continues in the outer loop by implementing the FORM equations, as seen in step 5 to 8 in Section 2.4.4 and checking the convergence criteria (step 10). If the condition of convergence is not met, the adjustment to the design point is implemented by means of the sensitivity factors introduced in step 6 of the FORM algorithm. This ends the run of the outer loop by adjusting the input to CUFSM and re-running the inner loop until convergence in the reliability value is obtained.

3.2.2 Directional derivatives from the Central Difference Method

To better understand the procedure of using finite incremental differences in the FORM, the processes for obtaining these derivatives using CUFSM is presented next.

The partial derivative vector $\{\mathbf{D}\}$ of the limit state function G with respect to all normalised random variables $\{\mathbf{U}\}$, as was mentioned in Section 2.4.4 in the FORM procedure, is again stated in Equation 3.3 below:

$$\{\mathbf{D}\} = \frac{\partial G(\{\mathbf{X}\})}{\partial \{\mathbf{U}\}} = [\sigma_{\mathbf{X}}] \frac{\partial G(\{\mathbf{X}\})}{\partial \{\mathbf{X}\}} = [\sigma_{\mathbf{X}}] \nabla G(\{\mathbf{X}\}) \tag{3.3}$$

The matrix $[\sigma_{\mathbf{X}}]$ arises from differentiation and simplifies to a diagonal matrix due to the normalizing transformation of Equation 2.58. This directional derivative vector needs to be determined at the design point $\{\mathbf{x}\}^T = \{f_y, t, \delta_R\}$ which is the realisation of the random variable vector $\{\mathbf{X}\}$ for the variables discussed in the previous section. For the case of the limit state function (Equation 3.1), Equation 3.3 can be written as follows for the three considered random variables:

$$\begin{Bmatrix} D_{f_y} \\ D_t \\ D_{\delta_R} \end{Bmatrix} = \begin{bmatrix} \sigma_{f_y} & & \\ & \sigma_t & \\ & & \sigma_{\delta_R} \end{bmatrix} \begin{Bmatrix} \frac{\partial}{\partial f_y} \\ \frac{\partial}{\partial t} \\ \frac{\partial}{\partial \delta_R} \end{Bmatrix} G(f_y, t, \delta_R) \tag{3.4}$$

For any of the three directional derivatives a component is found using the central difference method. The central difference method allows to differentiate by a numerical procedure, which for any of the direction derivatives i simplifies to the following equation:

$$D_i = \frac{\partial G(\{\mathbf{x}\})}{\partial x_i} \sigma_{x_i} \approx \frac{G(x_1, .., x_i + h, .., x_n) - G(x_1, .., x_i - h, .., x_n)}{2h} \sigma_{x_i} \tag{3.5}$$

where h is some interval length forward and backward from the design vector component x_i under consideration. Figure 3.4 below shows a 2D section through the variable abscissa x_i of this study's specific limit state function illustrated to be that of the yield strength.

The graph shows the three points, the realisation of each variable denoted by the asterisk, necessary for the computation of Equation 3.5 where it is now visible that if h approaches 0, the true derivative is found. Hence the central difference method becomes a better approximation of the true directional derivative the smaller h is chosen. From Equation 3.5 and Figure 3.4 it appears that only two points need to be determined to numerically evaluate the directional derivative, however the central point is still key in the FORM procedure and the forward and backward difference cannot be obtained without it. It should

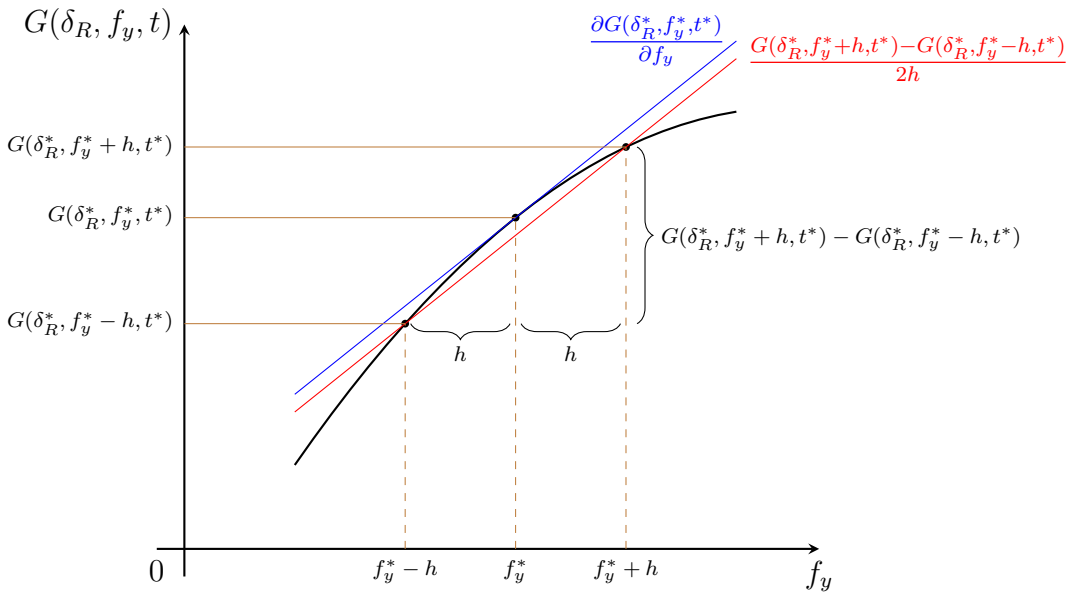

Figure 3.4: Central difference applied to the limit state function for the variable of the yield strength

now be apparent why the CUFSM algorithm must run five times to determine the partial derivative vector, since each point needs to be determined from CUFSM for the affecting variables as explained in the previous section.

Now looking at Equation 3.5 with the limit state function in Equation 3.3 substituted, it should become clear that the design resistance R_d, which is deterministic, stays constant and can thus be eliminated from the calculation procedure. This attribute was used in the implementation of the central difference method.

Lastly the advantage of using the central-difference-method over the forward- or backward-difference method can be explained. The derivative approximation from the central difference method is determined more exactly by adding only one more point to the numerical calculation procedure. This largely adds to the convergence speed of the FORM, since derivatives are determined with improved accuracy each time the design point is updated (Haldar and Mahadevan, 2000).

3.2.3 Challenges

In order for the analysis algorithm mentioned above to run flawlessly, certain DSM related challenges needed to be addressed first. DSM results are cross-section dependent, but the exact profile properties are not highly influential on the challenges presented in this section and thus the profile details will be

mentioned at a later stage in this chapter. Some challenges however influence the uncertainty introduced by using the DSM as a resistance prediction model and these are discussed here.

To identify which is the mode-dependant-resistance, F_n (see Equation 3.1), from the local, distortional and global mode, the signature curve has to be established using CUFSM, as mentioned in Section 2.2.4. This part in the algorithm requires the extraction of the buckling coefficients for the various modes from the CUFSM output and then inserting them in the DSM equations to determine the exact limit state function. All three buckling coefficients must be identified since there is interdependency between the local and global mode in the DSM equations and since the lowest mode must ultimately be determined. At this point it is important to again take note that the following procedure is only applicable to pin-supported boundary conditions. Buckling coefficients for various other boundary conditions must be found by a different process and this procedure is not covered by the implemented code for reliability assessment of this thesis.

The problem that presents itself in the pin-ended analysis procedure, is the localisation of the minima points of the buckling coefficient associated with their respective local, distortional and global buckling lengths. One option to extract these values from the signature curve is to find the numerical inflection points where the gradient of the curve changes from negative to positive, which will return a wavelength as an index to finding the associated buckling factor. For every possible profile, except angle sections without lips, there exist two minima-identifying critical wavelengths and another third critical wavelength. The third being the physical length of the profile for the pin-ended boundary condition (American Iron and Steel Institute *et al.*, 2012).

An alternative option is to obtain the minima by visual inspection of the signature curve. Classification of the mode can then be performed by reviewing the deformation of the cross-section which can indicate what minima are associated with their respective mode of buckling. This is the proposed procedure as described in Section 2.3.2, but the former process allows for implementation and is hence used. Once these points are found, the classification can be done from smallest to largest wavelength, since the local to global modes are also classified respectively. This is the process explained by the Commentary to the North American Specification's Appendix 1-Design of Cold-Formed Steel Structural Members with the Direct Strength Method (2012, p.11-13), which was motivated in the background chapter. Nevertheless, the assumption of modes should be confirmed by the procedure of modal decomposition allowed by CUFSM, which is the improved identifying method that was developed specifically to aid users in the determination process.

CUFSM allows the user to activate the modal decomposition of the signature curve in order to associate critical points with the three influential buckling modes. This procedure conditions the matrices used in the strips to the deformations of the pure modes of local, distortional and global buckling only, as mentioned in the previous chapter. The true behaviour of the member is determined by combining all modes. From this decomposition one can then identify the minima on the separated buckling curves as those of either dominating local or of distortional buckling.

Multiple problems now present themselves with the introduction of conditioning of the stiffness matrices. As mentioned in Chapter 2 (see section 2.3), the accuracy of the buckling factors is influenced by the number of elements along the length of a cross-section segment. The accuracy of the mode dependent buckling coefficients is furthermore dependent on the numerical accuracy of wavelengths provided for an analysis in the vicinity of possible minima. More influences which the accuracy has on the reliability analysis are discussed later on in this section. Still, these wavelengths, as previously stated, are key to identifying the buckling coefficient for the various true member buckling modes. The number of finite wavelengths included in the reliability procedure is also important as the wavelength may shift during the analysis as the FORM procedure adjusts the design point. Influences resulting from this are also elaborated later on in this section.

3.2.3.1 Stability of signature curve

Figure 3.5 below shows how the conditioning of the deformation space affects critical buckling coefficients in the distortional buckling half-wavelength vicinity. This effect becomes especially prevalent when a larger number of finite length terms is included in a FSM analysis and is similar for the rest of the signature curve.

With the algorithm written so that it must find points of sign-alternating tangents, as seen in Figure 3.5, the critical buckling load factor for distortional buckling is not clearly identifiable. The signature curve instability problem is known to exist with cross-sectional models that include bends (Schafer and Ádány, 2006) as mentioned in the background chapter. However, if the number of elements in the cross-section is generally increased to eight per segment, the accuracy of the solver becomes even more problematic, if model decomposition is allowed. This increase in number of elements and the resulting signature curve can be seen in Figure 3.6. When considering Figure 3.6 it is necessary to take note that the previous figure's signature curve is also included for comparison purpose. Therefore it has been demonstrated, that if modal decomposition is allowed in CUFSM and bends exist, an increase in number of elements does not imply an increased accuracy in the buckling coefficient. The reason for this can be related to the conditioning of the stiffness matrices, that

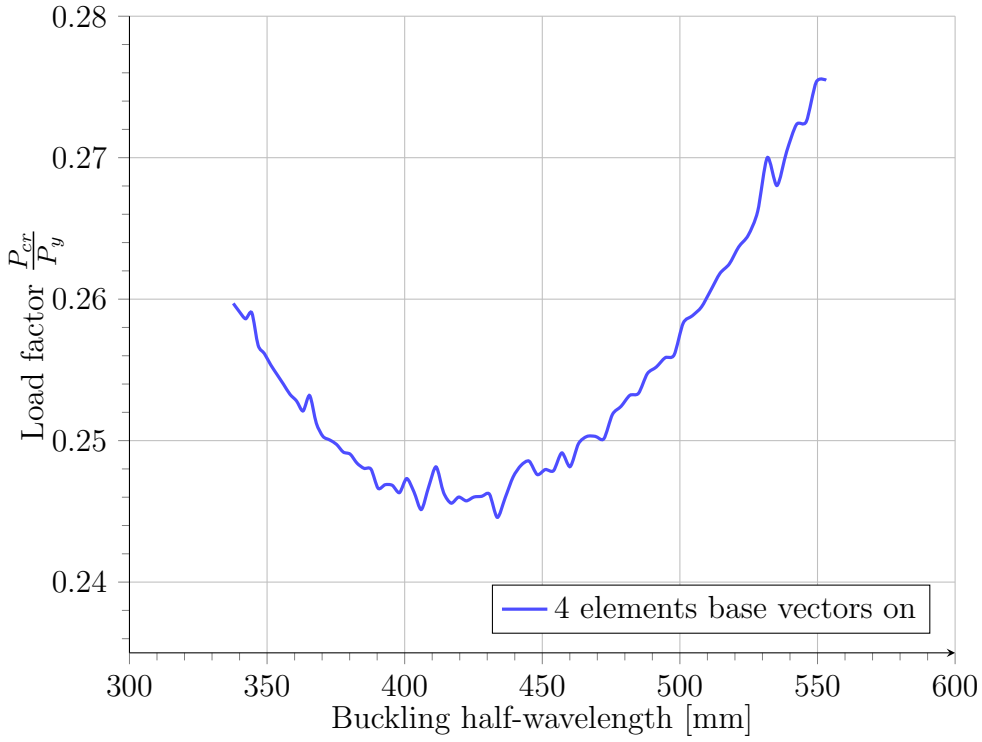

Figure 3.5: cFSM signature curve in the vicinity of the distortional buckling half-wavelength

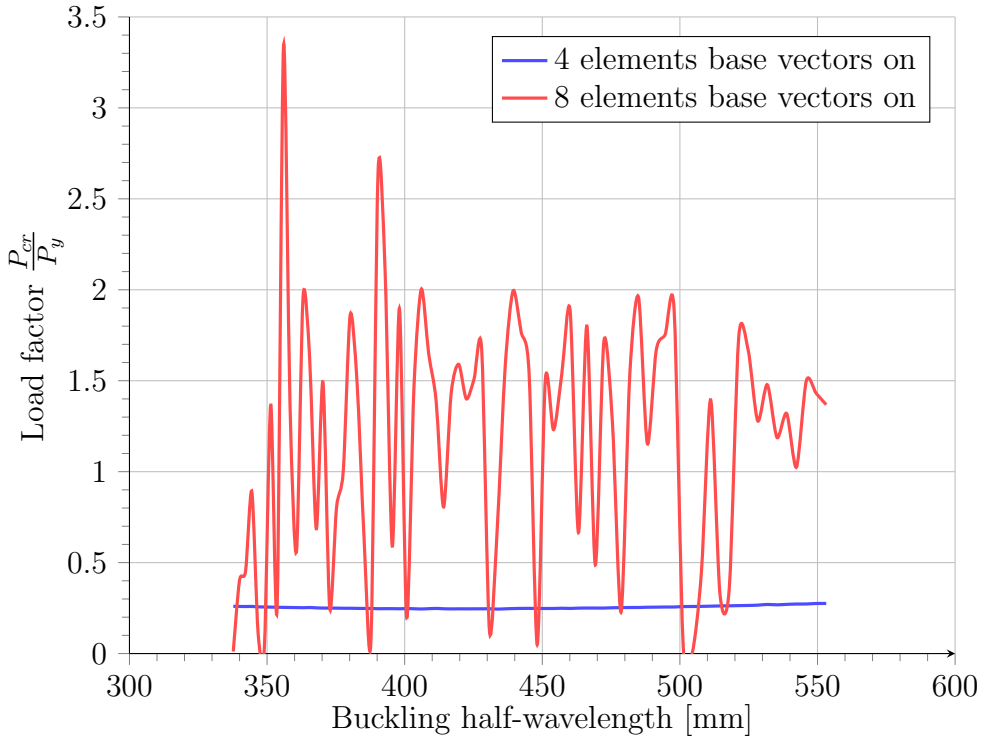

Figure 3.6: Comparison of generated signature curves in the vicinity of the distortional buckling half-wavelength

correspondingly creates instability of the eigen-value solver.

An important question must now be answered: how does one correctly identify the buckling coefficients that correspond to the respective local to global buckling modes? The solution to the identification process of the minima is as simple as turning off the model decomposition in the CUFSM procedure. Thereafter analysis can proceed by assuming that the three modes of buckling and their respective critical load factors follow a sequential relationship which can be tracked by the linked wavelengths. That is to say that the three critical wavelengths from shortest to largest correspond to the buckling modes of local to global respectively. Figure 3.7 shows how the identification of the distortional buckling coefficient is reduced to only one critical wavelength in the critical distortional buckling factor vicinity.

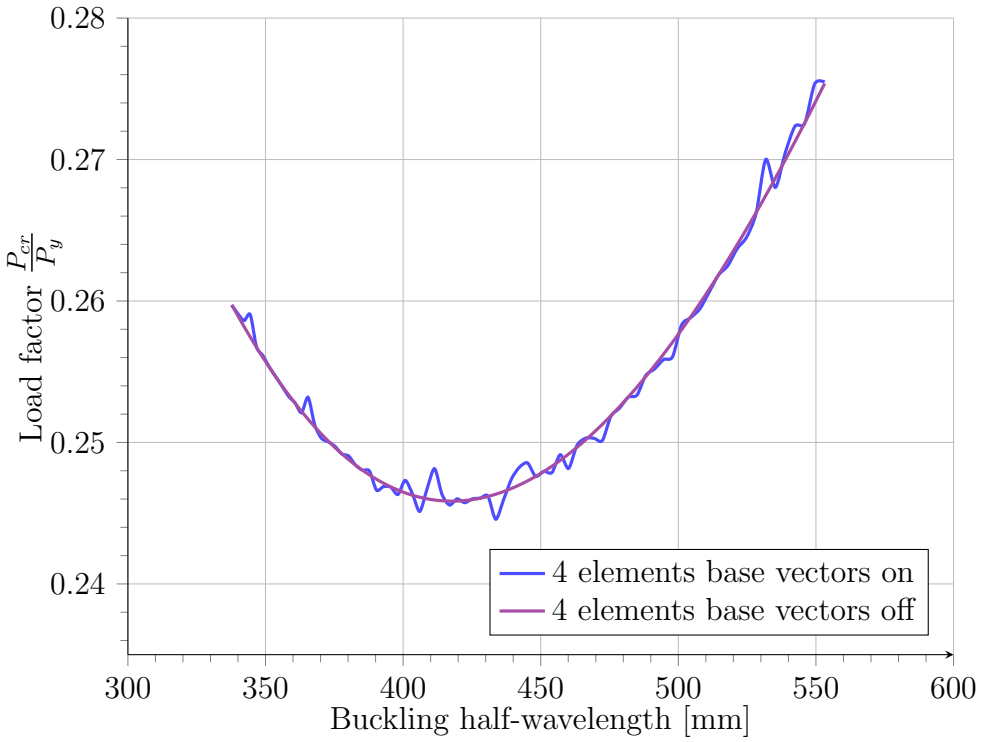

Figure 3.7: Signature curve in the vicinity of the distortional buckling half-wavelength

The assumption must then be checked by either visual inspection of the cross-section deformation at the critical wavelengths or by building an equivalent cross-section model with no corners, as is suggested by Schafer (2006*a*) and in the background chapter of this thesis. An equivalent cross-sectional profile entails that key properties such as the cross-sectional area and the warping

properties are the same as for a model without bends. The mode dependency of the wavelength that is assumed can then be confirmed.

A signature curve was also generated for a cross-section model using eight elements per segment with model decomposition off. However, the increase in accuracy on the buckling coefficient for the local buckling mode showed no improvement. The percentage difference between the distortional buckling coefficient from four to eight elements was calculated to be nil and hence had no effect on the reliability, since design point estimators would remain the same irrespective of the increase in the resolution of elements.

3.2.3.2 Accuracy of the buckling wavelength

As was discussed in the background chapter, the buckling half-wavelengths are a substantial parameter in determining the buckling coefficients used for the DSM equations. To recall, the three elastic mode dependant critical buckling coefficients are each linked to one critical buckling half-wavelength. This buckling half-wavelength must be included in the length terms used in a FSM analysis. It is however impossible to know the accurate critical-wavelength without having already performed a FSM analysis. The exception of course being the global buckling length, which is the physical length of the member.

The buckling length is treated as an analysis parameter of which the variation has an influence on the reliability margin. Half-wavelength variation is however directly coupled to other random variable variation. Therefore the critical half-wavelengths shift during the FORM procedure, since they depend on the type of loading as well as the profile's input parameters in CUFSM. Knowing that a signature curve is set up from discrete points preselected for an analysis, the more accurate the buckling lengths are chosen, the more accurate the buckling stress can be determined for the use in the DSM equations. The buckling stresses have a significant effect on the reliability, because the DSM equations directly depend on the buckling stresses. Since the half-wavelength and buckling stress are linked, an initial sensitivity analysis has to be performed on the buckling lengths, which have to be included in a FSM analysis used for the FORM procedures.

In combination with the above it must already be known what half-wavelength range is associated with which mode of failure, to know what buckling half-wavelengths to include in the analysis, in order to converge on them. This is again an interrelated problem and for explanation purposes it is assumed that the pure mode classifications are already known. Modal buckling curves are assumed to be known, to show how critical half-wavelength on the signature curve are associated with one of the three pure deformation modes in the analysis.

Figure 3.8 shows what the effect is, if the buckling-wavelengths are not sensitively incorporated in the FSM analysis. One mixed deformation behaviour signature-curve is shown with random length terms included in the FSM analysis to produce the critical buckling coefficients of interest for the DSM equations. A second curve shows the new lengths included around the vicinity of the previous curve's critical buckling coefficients. The first curve visibly skips the absolute half-wavelength of interest and creates seemingly critical minima in the signature curve. Therefore new discrete lengths in the vicinity of the false critical and inaccurate half-wavelength have to be chosen and re-analysed until the minima do not change position. The three pure mode curves are shown in order to know that the mixed mode curve, which more accurately captures the true behaviour, actually includes lengths that converge on an elastic mode dependent minimum and not some alternative inflection point resulting from inclusion of all deformation types in the FSM analysis.

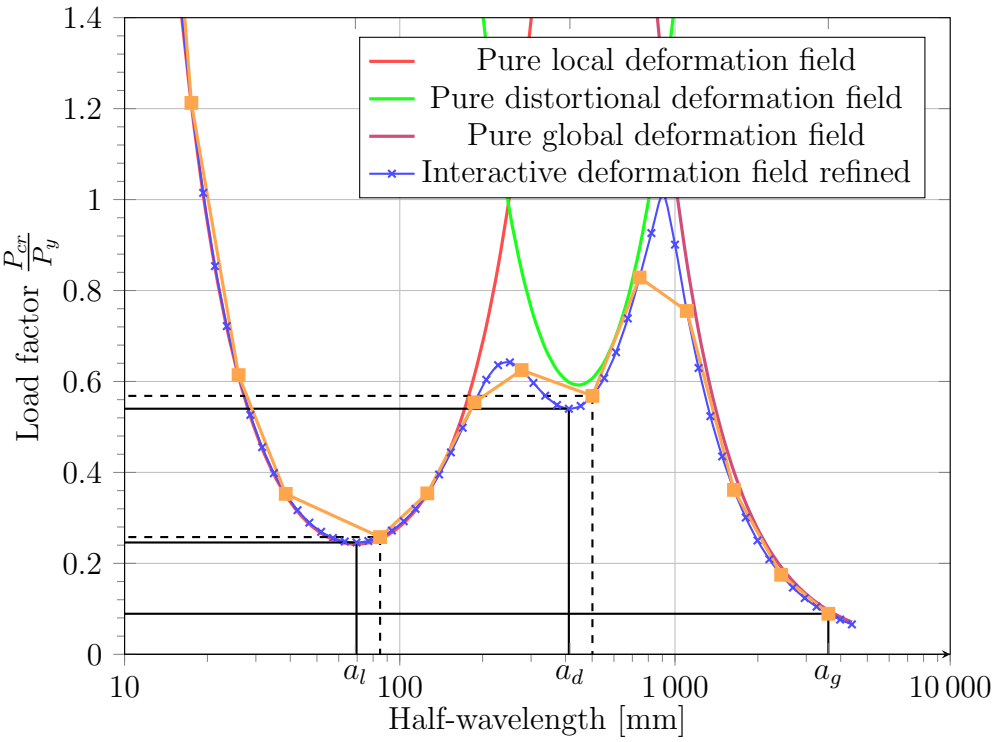

Figure 3.8: Illustration of sensitivity of half-wavelengths in signature curve

If the first curve with less accurate buckling half-wavelengths is chosen to be included in the FORM analysis, the reliability may falsely be predicted. This is due to incorrect high buckling stress being used in the DSM equations that are the foundation for the limit state equation calculations. The effect can be followed by the dashed lines in the figure above. Accurate buckling coefficients with the newly included wavelengths are visible by the solid lines. Hence including the correct length terms in the FSM analysis will affect the

correctness of the reliability obtained.

The curve presented here, is the signature curve of the cross-section used in the dissertation to show the effect of the problem and emphasise that this analysis was specifically performed. The process has to be repeated as soon as the cross-section changes, different support conditions are used or if different cross-section shapes are considered. As mentioned, the wavelength is treated as a design variable and the sensitivity analysis shown, was performed at the values used for design of the input variables. It can nevertheless not be assumed that this sensitivity covers the full spectrum of critical wavelengths in a probabilistic analysis.

3.2.3.3 Signature curve behaviour during analysis

A FORM reliability procedure may input a random range of thickness and stress values during CUFSM iterations. The critical wavelengths are expected, from FSM theory, to also be different at iterating points of the thickness and yield variables. This infers that again various discrete wavelengths have to be provided in the FSM analysis, to capture the absolute localized minima on the signature curve. To understand the half-wavelength behaviour over the possible range of the thickness and yield variables, points at larger and smaller values than the mean input of the two random variables were analysed in CUFSM. The increments were done at more than three standard deviations away from the mean value of the one input variable, while the other variable was kept at its mean value.

The influences of the variation of the input variables critical to half-wavelength behaviour was investigated for both compression and bending. Figure 3.9 shows five signature curves at different states of the input variables. The solid blue curve shows the buckling coefficients as a function of the half-wavelengths, with the thickness and yield strength at their respective mean values. Solid vertical lines point out the critical buckling half-wavelengths. From left to right, the first vertical line is associated with the critical local buckling half-wavelength and the second with the critical distortional buckling half-wavelength. Quite clearly visible from the figure is that increases and decreases of yield stress do not cause a shift in the critical wavelength for both local and distortional buckling. Minima on both signature curves for an increased or a decreased yield strength, shown in purple, coincide with the vertical lines indicating the critical buckling half-wavelengths. On the other hand, the adjustment of the thickness away from the mean has an influence on the distortional buckling critical half-wavelength. A decrease in the thickness of a profile therefore increases the distortional buckling critical half-wavelength. The converse is also true and the shift in the critical half-wavelength can be observed in Figure 3.9 by the vertical dashed lines. All of the above is similarly true for bending and can be seen in Figure 3.10.

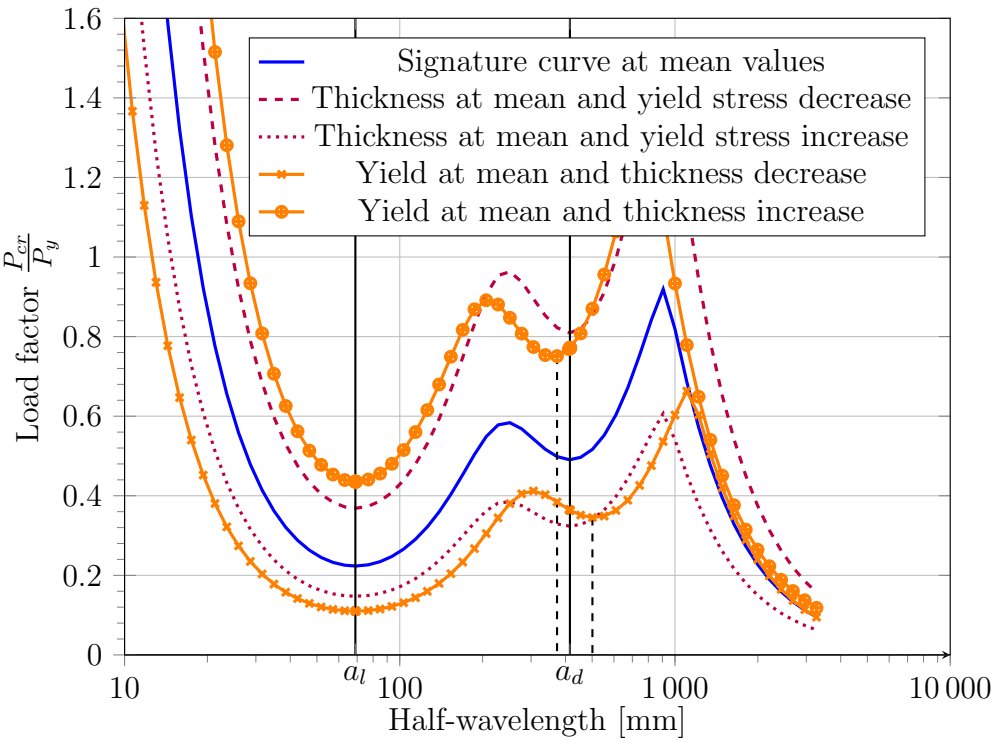

Figure 3.9: Critical half-wavelength behaviour due to random variables for compression

If the above-mentioned is now brought into context with the problem of discrete half-wavelength terms included in a CUFSM analysis, the inclusion of the important half-wavelength is deemed necessary. To insure that for reiterative runs of CUFSM, a half-wavelength-shift is possible as the FORM algorithm loops, small enough discrete half-wavelength increments must be included in the length terms available to produce a signature curve. For each iteration of the design point in the FORM analysis, the critical half-wavelength is thus available from the solution set of wavelengths and can be found using the sign-altering-tangent procedure. Only then does the set of discrete half-wavelengths hold a half-wavelength which can coincide with the absolute critical buckling coefficient used in the limit state equation evaluation. Exclusion of a possible realisation of a critical half-wavelength can thus lead to inaccuracy in the reliability margin.

From the two figures it is also convenient to point out how the variation of the variables affects the buckling coefficients associated with a specific realisation of a random variable. Especially in the larger half-wavelength region, generally associated with global buckling, variation of the thickness has less influence on the global buckling coefficient than its yield strength counterpart.

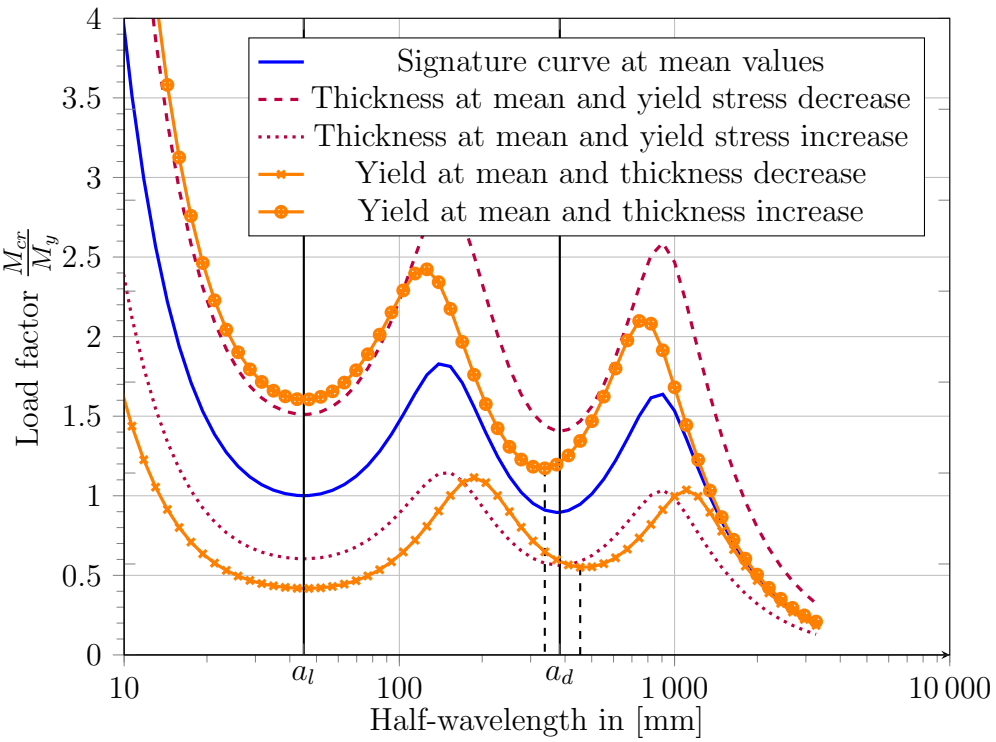

Figure 3.10: Critical half-wavelength behaviour due to random variables for bending

3.2.3.4 Global buckling from CUFSM

Up to now the fact that the critical global buckling load is calculated at the physical member length has been addressed on multiple occasions. The DSM allows the buckling coefficients for global buckling to be calculated using a FSM buckling analysis (Schafer, 2006*a*). However, if the member physical length coincides with shorter length terms used in a FSM buckling analysis, CUFSM will, if all deformation modes are allowed, produce only the lowest buckling coefficient out of all modes. This will, for shorter length terms, be a coefficient that corresponds to buckling behaviour linked to either distortional or local buckling, depending on how short the physical length is. Torsional-lateral buckling factors for columns and flexural-lateral-tortional buckling factors for beams, which represent the global buckling scenarios for those members, can be determined using analytical equations developed by Timoshenko (1945). These equations are included in SANS 10162-2 and are specific to singly-symmetric and mono-symmetric sections.

One other option to determine the global buckling coefficients is to use the result of the CFSM analysis if the buckling analysis is based on only the global buckling deformation space. However, since the analytical equation by Timoshenko (1945) is an exact solution for buckling loads (or coefficients), and

CUFSM using CFSM theory is only a numerical method to give solutions for non-geometrically-simple problems, the limits to the exactness of the FSM procedure have to be investigated. As shown in the previous subsection, a solver problem is encountered when making use of the CFSM model with round corners. The associated effect on the buckling coefficients, when using the global buckling deformation space only, must therefore also be examined if this solution was to be implemented into the reliability analysis process.

An investigation was performed for both column and beam FSM solutions for longer lengths and their accuracy at longer lengths with respect to the analytical solution. Figure 3.11 and Figure 3.12 show the classical signature curve of the study's lipped C-section for use in a column or a beam member respectively. The typical signature curves have not been plotted on a log-scale abscissa as the focus of the illustrations is on longer wavelengths, whose significance is lost on a log scale. Also shown in the figures are the buckling solutions from the analytical equations for singly-symmetric members.

In the figures it is clearly visible how CUFSM captures the buckling behaviour of the member accurately for longer lengths. This plot reaffirms that the four strip elements per cross-section-line-segment are sufficiently accurate, to numerically capture the correct buckling coefficients for longer wavelengths. At the same time the graphs confirm the correct implementation and use of the analytical equation into the reliability analysis algorithm, as the solutions from CUFSM and the analytical equation converge at longer lengths.

However, it is quite clear that an error is made when the pure global buckling curve is produced from CUFSM. This option produces a seemingly consistently-offset solution to that of the exact analytical solution. The reason for this may be related to the solution space constraints associated with the global buckling deformations (refer Table 2.1 in Section 2.3.2) and how the constraints affect the decomposition from the total deformation space for round corner models. This observation led to the implementation of the analytical exact equation in the FORM procedure, when the global buckling stress or buckling coefficient is required in the algorithm.

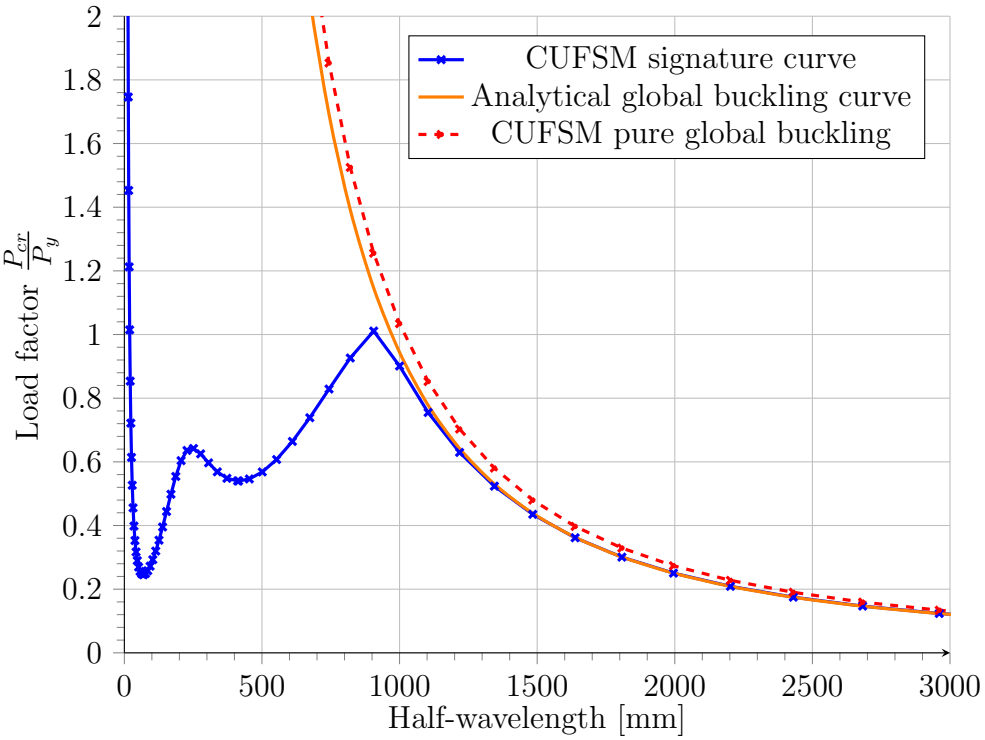

Figure 3.11: Global buckling behaviour of a lipped channel section in pure compression

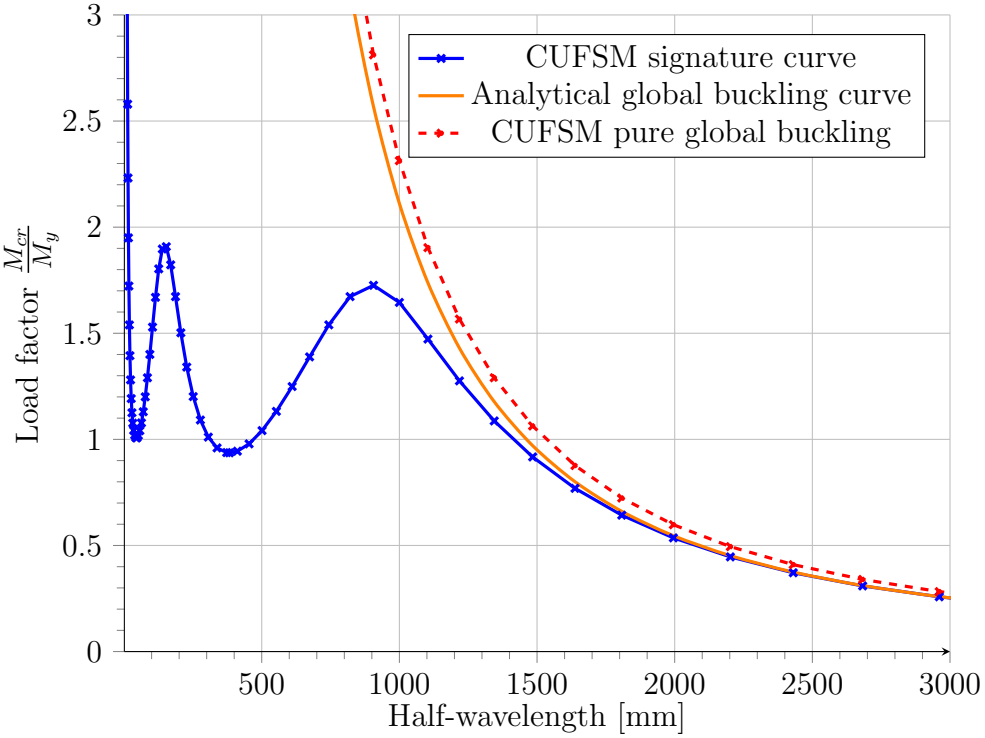

Figure 3.12: Global buckling behaviour of a lipped channel section in pure bending

3.2.3.5 Member buckling mode classification

In the background chapter the problem of buckling mode classification was introduced. There are three methods that are available to associate regions on the classical signature curve with a mode-specific deformation behaviour. The cross-section deformation as well as the half-wavelength spectrum associated with the various elastic buckling behaviours presented an initial methodology for the identification process. The third option came with the introduction of cFSM.

cFSM allows the classification by decomposition of the signature curve into its pure buckling modes using the constraint criteria of Generalised Beam Theory, as was already mentioned. Additionally to decomposing the signature curve from the GBT criteria into the pure mode dependant buckling curves, CUFSM allows a modal participation to be calculated for the signature curves based on normalisation of the deformation fields. CUFSM specifically uses the work associated with each elastic buckling deformation space as the normalisation criterion to produce a modal participation plot.

As mentioned Section 2.2.4.1 on the stability of the signature curve, a check needs to be made that the critical buckling coefficients at the start of the FORM analysis are correctly assumed to be within the same buckling mode classification as those at the end of the reliability analysis. In order to do this, the participation plots for the compression and bend plots are produced. Both of these participation graphs can be seen in Figure 3.13 and Figure 3.14, respectively.

From these plots it is visible that the first minimum, which is generally classified as local buckling from the half-wavelength criterion, is associated with a larger participation of distortional buckling. Again at this stage the Direct Strength Method Design Guide by Schafer (2006*a*) provides insight how to deal with indistinct modes, since this is contrary to the expected behaviour. The design guide addresses the problem of indistinct modes and affiliates this problem with round corner FSM models. Sharp corner models should preferably be used when the geometry (Schafer, 2006*a*) by element idealization is rather of importance and therefore should be incorporated in the buckling analysis when investigating modal participation. On the other side, the accuracy of the buckling factor solution is however provided by round corner models and improves when the number of elements in the corner increases. Figure 3.15 shows two FSM cross-section models illustrating how the geometry differs when round corner models are used compared to sharply connected geometry models.

In the reliability analysis both the initial geometry should be accurately modelled as well as an accurate buckling solution. Therefore the reliability analysis in this dissertation included round corner models, which incorporates

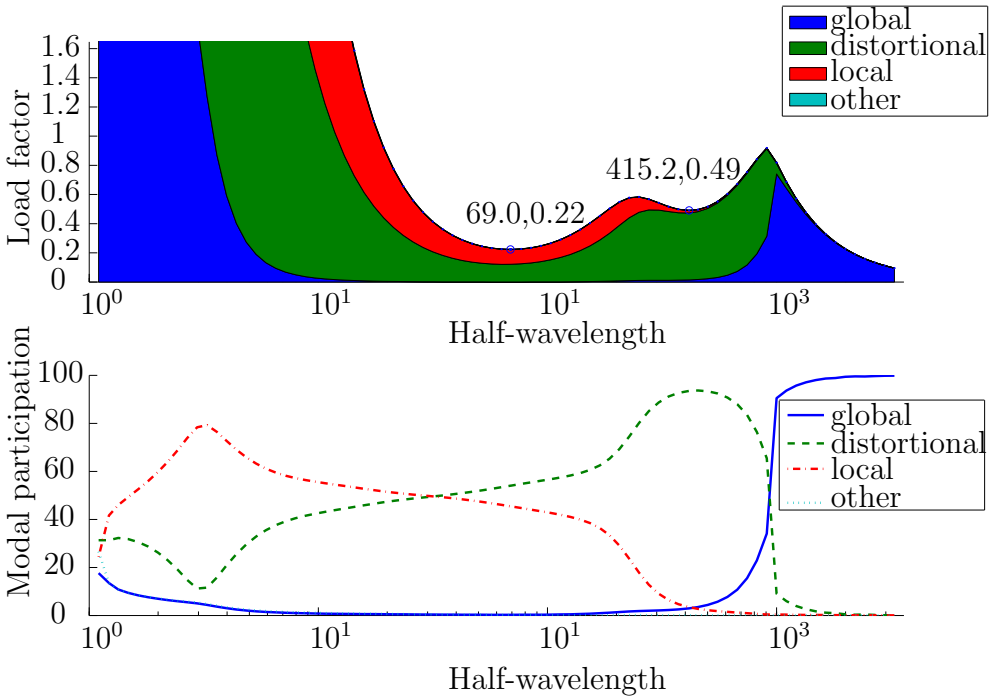

Figure 3.13: CUFSM participation plot for a lipped C-section in compression with round corners

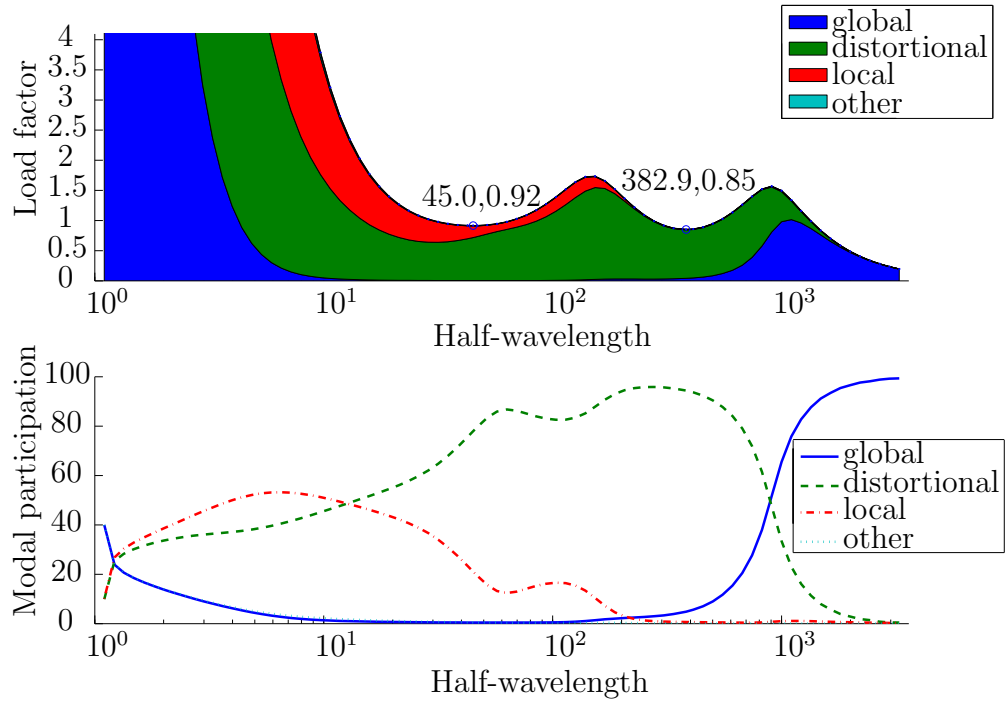

Figure 3.14: CUFSM participation plot for a lipped C-section in bending with round corners

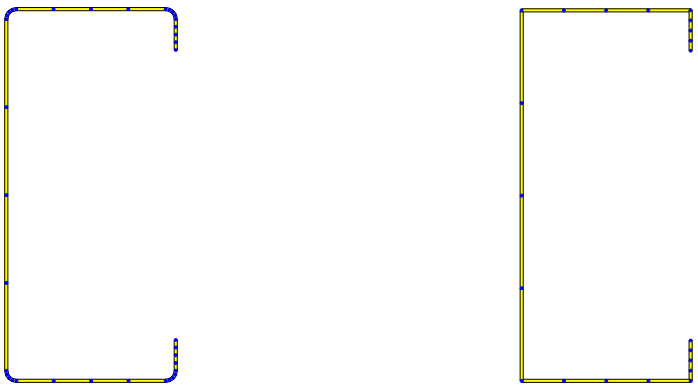

(a) Round corner model used for cFSM analysis

(b) Sharp corner model used for cFSM analysis

Figure 3.15: Cross-section corner model used for cFSM analysis

both the geometry and the accuracy problem. The design guide does however state, that when indistinct modes present themselves, as is the case in the round corner models shown in the figures above, sharp corner models with equivalent cross-section properties such as area, moment of inertia and torsional warping constant, should be used for inspection. The participation plot for the equivalent sharp corner models of compression and bending are shown in Figure 3.16 and Figure 3.17.

The participation of the elastic buckling mode at each point in the signature curve is now clear. This process was done for both compression and bending at mean values of the thickness and yield strength. It has already been established that the effect of increasing yield stress has negligible shift in the critical half-wavelength. That is why the classification of the curve can be seen as the same as for the design resistance in the reliability analysis, when the thickness and yield stress are used as characteristic values, and will have no effect on the classification as shown in the figures in this section.

From the information above it can be argued that if the participation factors at the start of the reliability analysis for round corner models are found to be the same as those found at the design point, then the modal classification can still be assumed to be the same as is predicted by the sharp corner model provided in figures 3.17 and 3.17. This check will be performed by providing participation factors for each of the critical wavelengths at the design point.

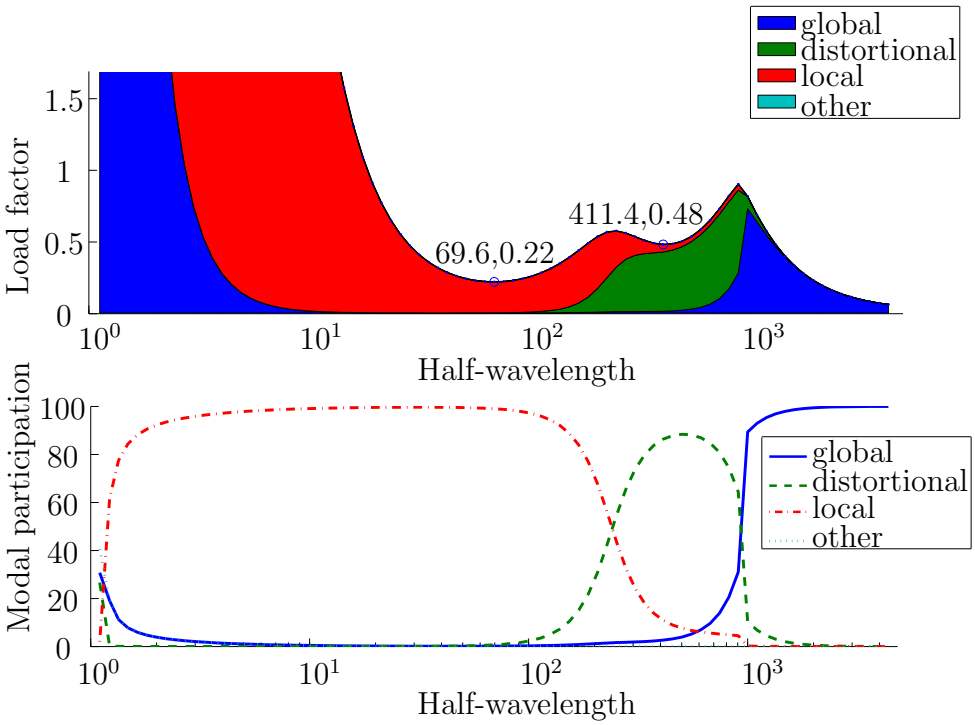

Figure 3.16: CUFSM participation plot for a lipped C-section in compression with sharp corners

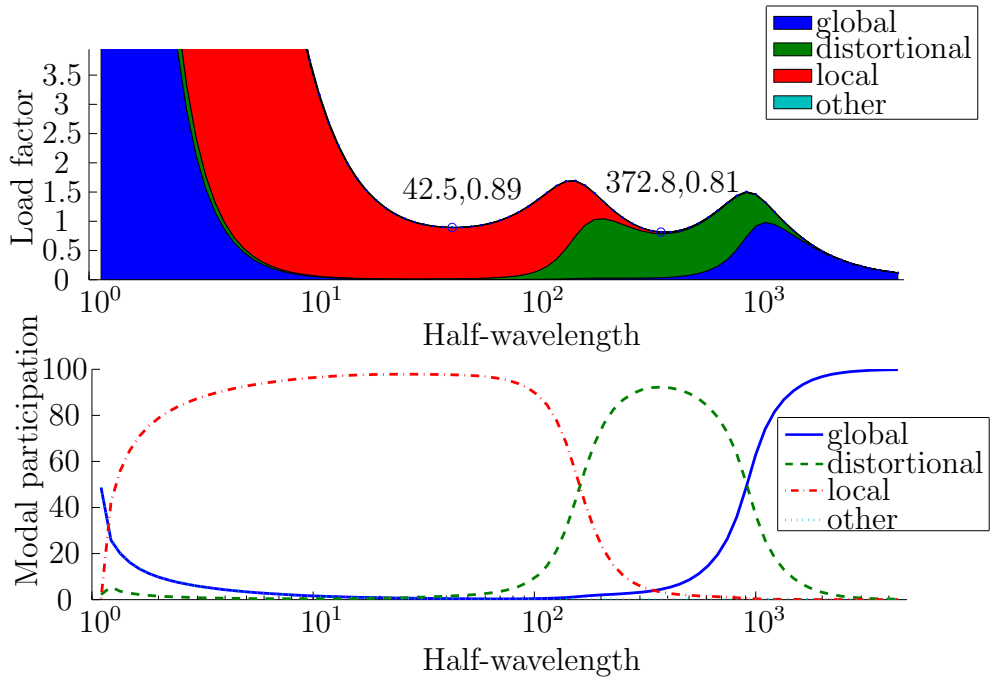

Figure 3.17: CUFSM participation plot for a lipped C-section in bending with sharp corners

3.3 Input variables of the reliability analysis

3.3.1 Member geometry and assumed distributions of random variables

Since it is a goal of this thesis to determine the reliability based on South African design practice, a cross-section was chosen with the help of John Barnard (director of the Southern African Light Steel Frame Building Association, SASFA). The profile suggested by him was a Lipped Channel or C-section which is known by the association for the fact that it is commonly supplied in Southern Africa. The suggested profile was however asymmetrical due to unequal lip lengths and for modelling purposes it was adjusted to be singly a symmetric section. A schematic of the cross-section used, is depicted in Figure 3.18 together with centreline dimensions that are required for modelling.

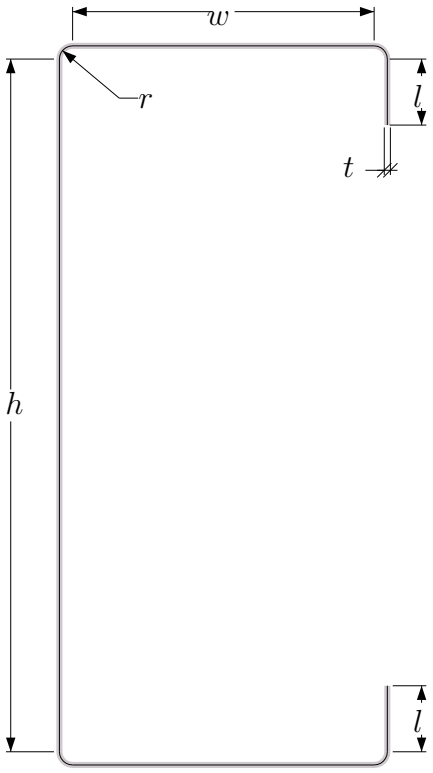

Figure 3.18: Channel Profile used in analysis

Table 3.1 captures the deterministic dimensions used in design and Table 3.2 depicts all further deterministic input variables that are used for the creation of the cross-section model in CUFSM. The Young's modulus of elasticity (E), the Poisson's ratio (υ), the shear modulus of elasticity (G), the partial factor for compression (ϕ_C), and the partial factor for bending (ϕ_B) are all from the SANS 10162-2 specifications. The characteristic design value for the yield

Table 3.1: Profile centreline dimensions

Dimension	Value [mm]
t_d	0.75
h	83.5
w	35.5
l	7.35
r	2.375

strength is also stated. As mentioned in the background chapter, various steel grades are allowed for the use with the DSM. However, the pre-qualification limits of the DSM for members subjected to bending (Clause 7.1.2) limit the yield strength to be less than 483 MPa. Grade G300 steel is the only commonly available material in South Africa which conforms to this specification and is therefore used in the investigation.

Table 3.2: Material properties used in the model for design

Input Variable	Value	Unit
f_{y_d}	300	MPa
E	200	GPa
v	0.3	
G	80	GPa
ϕ_C	0.85	
ϕ_B	0.9	

To determine the reliability of members designed according to the DSM design procedure, the distributions of the three probabilistic variables need to be defined.

The probability density function assumed for the yield strength is a lognormal distribution. A lognormal distribution for the steel yield strength is suggested by Holický (2009) and Vrouwenvelder *et al.* (2001). The major benefit of the assumed lognormal distribution over a normal distribution for steel strength is that the assumed lognormal distribution has a lower limit of zero strength. This is a highly plausible assumption as no realisations exist below zero for a steel strength. The property that the lognormal distribution has a zero lower limit, implies a positive skewness for the distribution. This in turn means that the distribution has no tail at the lower end and is therefore narrower than a normal distribution. From the reliability concepts in the first chapter, this leads to a lower probability of failure.

Figure 3.19 shows the lognormal distribution for the yield strength of G300 steel. The commentary on the AISI (2012) standard states that the mean bias factor of the yield strength for cold-formed steel is equal to 1.1 ($\mu_{\delta_{f_y}} = 1.1$). This value is based on data by Rang, Yu and Galambos (1979). From this the mean yield strength for grade G300 steel can simply be calculated to be the product of the mean bias factor and the yield strength used in design ($f_{yd} = 300\,\text{MPa}$). The resulting mean yield strength from this can be found in Table 3.3 as 330 MPa ($\mu_{f_y} = 330\,\text{MPa}$). This compares well to the bias factor of the yield strength of 1.147 ($\mu_{\delta_{f_y}} = 1.147$) determined by Li *et al.* (2007) for the use in a reliability analysis of axially compressed high-strength thin-walled cold-formed steel members. The bias factor by Li *et al.* (2007) was determined for a thickness range from less than 0.6 mm to 1.6 mm of grade G550 steel with a design yield strength of 550 MPa ($f_{yd} = 550\,\text{MPa}$) based on 8364 samples. Since the data by Rang *et al.* (1979) covers a more applicable characteristic yield strength range of cold-formed steel from 159 MPa to 379 MPa (converted from imperial units) and because the value was used in the calibration process, the bias of the yield strength referred to by the AISI (2012) was ultimately used in this dissertation.

According to the commentary of the AISI the variation of the bias factor for the yield strength is equal to 0.10 ($V_{\delta_{f_y}} = 0.10$) (American Iron and Steel Institute *et al.*, 2012; Rang *et al.*, 1979). Haldar and Mahadevan (2000) states that the COV of the bias factor may be treated equal to the COV of the variable whose bias is considered. From this property, the variation of the yield strength for this dissertation is also assumed to be 0.10 ($V_{f_y} = 0.10$). A COV of 10% is considered high when compared to the bias factor of steel yield strength determined by Li *et al.* (2007). Nevertheless, the mentioned yield strength data by Rang *et al.* (1979) includes the G300 yield strength that is used in this dissertation and is therefore rather utilised. From the COV the standard deviation of the steel yield strength may be calculated to be 33 MPa (σ_{f_y}=33 MPa), which compares well when matched with the value obtained, based on the COV range of 0.07 to 0.1 estimation provided by Holický (2009).

The uncertainty in thickness is assumed to follow a normal distribution as suggested by Holický (2009) and Vrouwenvelder *et al.* (2001) for steel geometry. A normal distribution is also suggested for cold-formed steel thickness by Schafer *et al.* (1998). Since the thickness value used in design is not a characteristic value, the mean thickness is assumed to be the thickness value provided by the geometry of the cross-section ($\mu_t = 0.75\,\text{mm}$) in this reliability analysis and follows the same assumption made by Schafer *et al.* (1998).

The variation of the bias factor of thickness suggested by the AISI is equal to 5% ($V_{\delta_t} = 0.05$). Again the variation of bias factor can be assumed to be equal to the variation of the variable considered, as was done by Schafer *et al.*

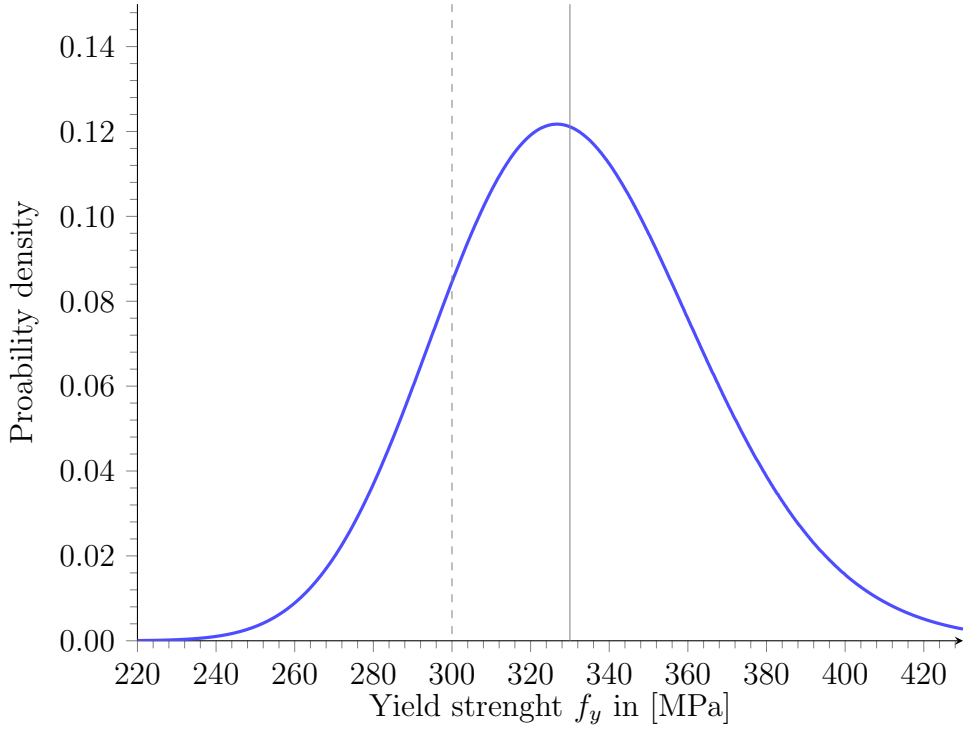

Figure 3.19: Log-normal probability density function for the yield strength, f_y

(1998) for the AISI value. However, when comparing the 5% COV to the value of 1.28% obtained by Li *et al.* in 2007, this variation seems considerably higher. Thus additional literature was examined to determine a COV that corresponds to the seemingly improved manufacturing processes of today as found by Li *et al.* (2007), when compared to the one stated by the AISI obtained by Galambos in 1979 (American Iron and Steel Institute *et al.*, 2012). One alternative was presented in a reliability investigation performed by Van Wyk (2014) at the University of Stellenbosch. Van Wyk determined a sheet steel thickness COV of 1% based on 21 specimen from 7 different steel coils. An additional state of the art COV was obtained by a study performed on cold-formed steel by Rogers and Hancock (1997). An uncoated sheet steel thickness COV of 1.6% based on 135 specimen from 15 sampled coils was determined (Rogers and Hancock, 1997). This COV was rather chosen to be used in the reliability analysis for this dissertation, since Rogers and Hancock's COV represents a range motivated by more than one reference with a significantly large number of coils in the sample. The number of coils being more significant than the number of samples, as a larger number of coils ensures more randomness in the sampling process, inherently making the sample data less biased. In addition to this the COV of 1.6% is slightly higher, but still significantly close to the values obtained by Li *et al.* (2007) and Van Wyk (2014).

Making use of Rogers and Hancock's COV for the thickness implies a lower scatter of realisations away from the mean thickness value. Since the 1.6% COV is used, a higher reliability index is expected, than the one originally aimed to be achieved in the calibration process by the AISI. An increased β results from the lower scatter, which is directly linked to a lower probability of failure when considering the concepts of sections 2.4.5 and 2.4.1. The extent of the increase in reliability nevertheless still depends on the sensitivity of the thickness variable. Based on these assumptions the probability density function for the thickness of the C-section is presented by Figure 3.20.

Table 3.3 below summarizes the statistical parameters used for the physical probabilistic variables of the member.

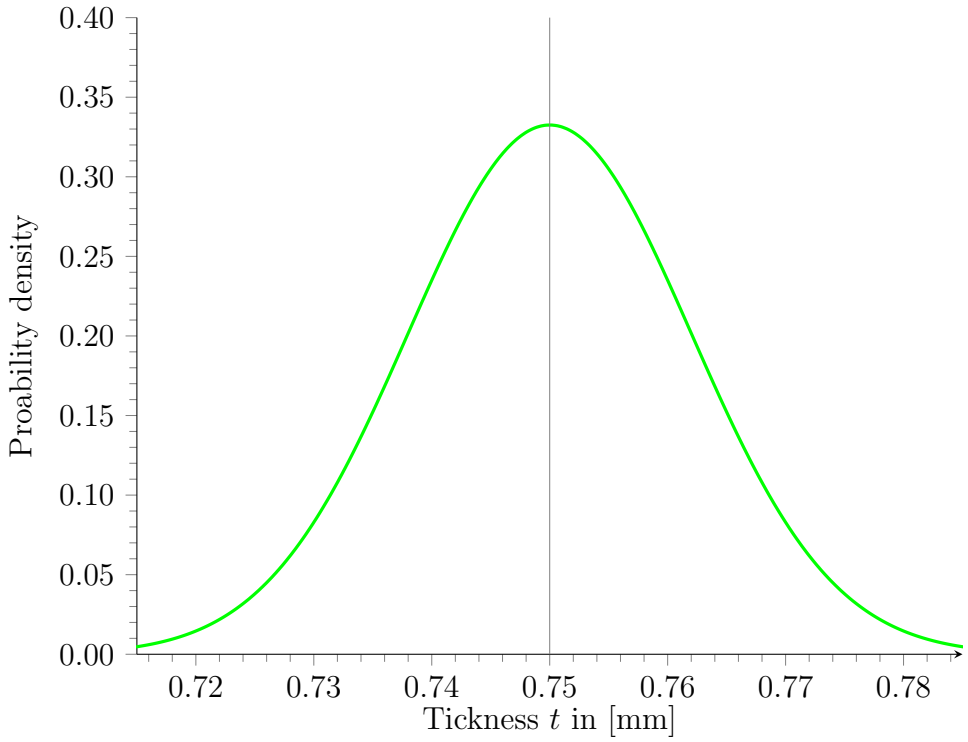

Figure 3.20: Normal probability density function for the thickness of the member, t

Table 3.3: Statistical parameters of assumed random variables

Variable	Symbol	μ	σ	a	COV	Distr
Yield stress	f_y	330 MPa	33 MPa	0.301	10%	LN
Thickness	t	0.75 mm	0.012 mm	-	1.6%	N

3.3.2 Sensitivity of assumed random variables

The basis for investigating the reliability based only on the physical random variables of yield strength and thickness was motivated in Section 2.4.5.

For both scenarios of compression and bending an initial resistance model factor is based on information from Holický (2009). The probability density function of the model factor is assumed to be that of a normal-distribution (Holický, 2009). Figure 3.21 shows the distribution function for the parameters based on the information from Holický found in Table 3.4.

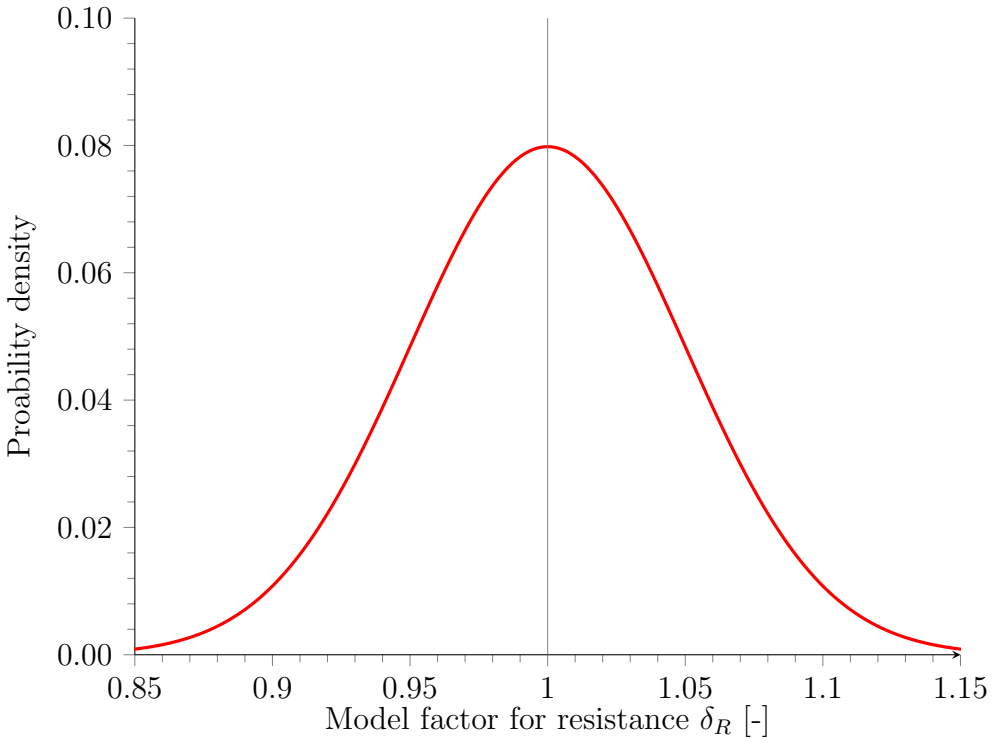

Figure 3.21: Normal probability density function of model factor for resistance based on initial investigation

Table 3.4: Statistical parameters of the model factor for the resistance

Variable	Symbol	μ	σ	a	COV	Distr.
Model factor	δ_R	1	0.05	-	5%	N

From this initial assumption the dominating random variable contributing to the resistance based reliability could be determined. The initial investigation using the statistical parameters from Table 3.3 and from Table 3.4 for the model factor, showed that for both the case of compression and bending the

model factor has the dominating sensitivity for the critical beta value from the three failure types. Figure 3.22 shows the sensitivity factor for all three random variables as the FORM algorithm from Section 3.2 converges. Indicated by the top most lines in the figure, one can clearly see that the sensitivity of the model factor dominates for both design cases.

Based on this initial result an in-depth investigation into the model factor specific to the DSM design equations was conducted and is presented next.

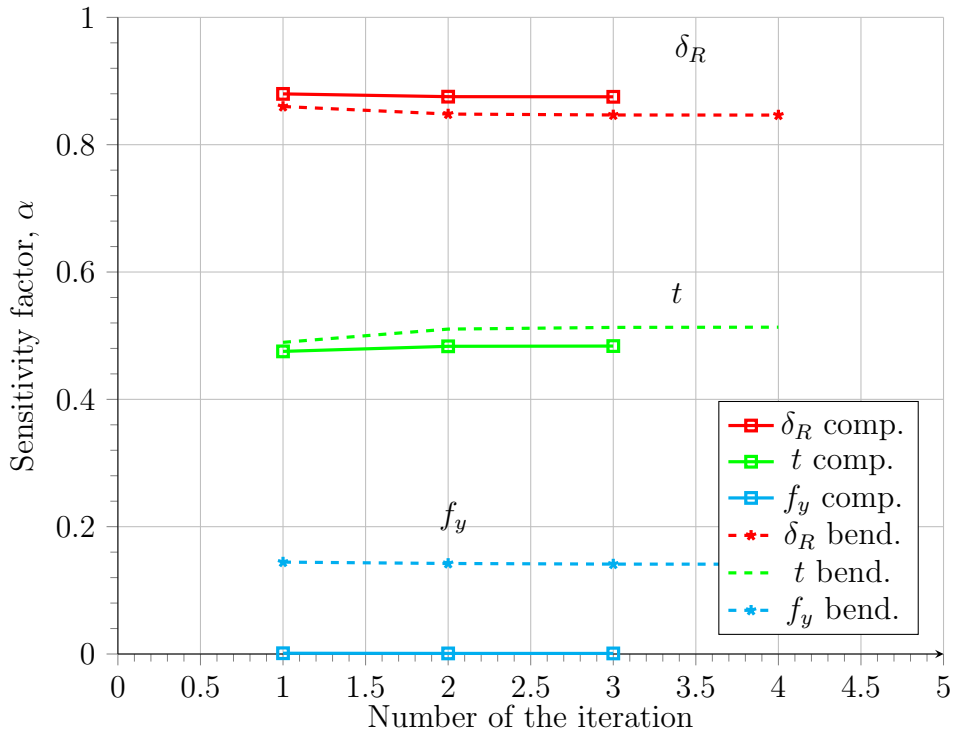

Figure 3.22: Sensitivity factors from assumed random variables for initial investigation based on the governing reliability mode

3.4 The model factor

The model factor is part of the limit state function's variables, to cover uncertainty and incompleteness of the applied theoretical model's design equations (Holický *et al.*, 2015).

Generally a design equation is based on a theoretical or an empirical model. As explained in Chapter 2, the DSM equations are semi-empirically based prediction models. When a model is exact and the input parameters are determined from experimental data, then the predicted solution will be found without an error (Holický *et al.*, 2015). This is almost never the case though. Hence the model factor for the resistance can be found using the fundamental relationship expressed in Equation 3.6:

$$\delta_R = \frac{F_{test}}{F_{model}} \tag{3.6}$$

Where F_{test} is the tested capacity excluding uncertainty arising from the method of sampling and F_{model} is the capacity resulting from an unbiased realisation of the prediction model. For the capacity model value to be unbiased, all underlying variables in the model must be evaluated at the measured value and therefore cannot contain only favourable data from testing.

Inaccuracy in the model occurs from either random effects that are neglected by the model (lack of data) or deliberate oversimplification of the model. The latter is done to ease the design process (Holický *et al.*, 2015). The model factor can also be denoted as a modifier on the model to predict experimental values and is often referred to as such in literature.

With the above mentioned in mind, one can now follow the argument that for each mode of failure mentioned in Equation 3.1 (see Section 3.1) there exists a separate model factor. A separate model factor needs to be considered for both design for members in compression and members subject to bending, since the design equations (the model), differ significantly. Since the reliability margin that is investigated by this work should cover the design procedure for all possible modes of failure within one design model, a model factor is used for each design scenario covered by the code. Thus, as the design procedure specifies a different partial factor for each load condition, the model factor must reflect the uncertainty accordingly. As mentioned, the model factor used for analysing reliability may only be chosen when the capacity from the prediction model, from equation 3.6, is based solely on unbiased prediction by the DSM equations. Unbiased in this instance means that recorded rather then characteristic values in the calculation of the prediction value must be used (Holický *et al.*, 2015).

After more in depth investigation into the model factor it was found that the design specification commentary to the DSM presents statistical data necessary for the use for an assumption of the distribution of the model factor for both columns (compression) and beams (bending) (American Iron and Steel Institute *et al.*, 2012). The commentary on the data confirms that the data conforms to the criteria mentioned in Equation 3.6. What is more, is that the data is based on specific work by all research mentioned in Chapter 2, which was used to develop the DSM equations. However, the mean value recorded for compression is smaller than unity, which implies over-prediction for compression loading of the DSM equations compared to tested data. For design purposes this is generally not a favourable condition as the largest amount of the reliability in design is then incorporated only by the partial factor.

The poor performance of the model factor from the AISI commentary results largely from tested data from research produced by Thomasson (American Iron and Steel Institute *et al.*, 2012; Schafer, 2008) and implies inadequacy of the DSM equations to predict a conservative capacity, if un-factored. Since the development of the equations more research has been conducted on the predictability of the design method for columns. The state of the art research has been reviewed by Ganesan and Moen (2012) and a more updated model factor for column design is presented. Ganesan and Moen (2012) state that their data were calculated specifically for the newly developed DSM for the use in their own reliability analysis. The statistics for the model factor adopted from Ganesan and Moen (2012) are selected from data that fall within the pre-qualification limits of the DSM only. The new mean model factor from this data-set shows better prediction by the DSM equations and is found in Table 3.5. The data still include the results by Thomasson (Ganesan and Moen, 2012), however the increased conservative results found by multiple researchers which are not included in AISI statistics, decrease the effects of the results by Thomasson. The data from Ganesan and Moen (2012) does not include angle sections, as this design is not covered by the DSM pre-qualification limits for compression. No comment on the distribution behaviour could be found. Thus a normal distribution behaviour was further assumed.

No state of the art investigation could be found on the predictability of the DSM for bending, other than the statistical parameters from the AISI commentary of the design specification and these statistics were therefore used. It is nonetheless noteworthy, that the mean model factor is shown to be larger than unity, implying that the un-factored DSM equations are a conservative estimator for the true bending resistance. A graph of the model factor probability density function for both bending and compression are seen in Figure 3.23. The relevant statistical parameters for the bending model factor are given in Table 3.5.

The work by Ganesan and Moen (2012) also presents model factors depending on the mode of failure. This information allows for the determination of the reliability of sections known to fail in certain modes of buckling. As it remains the aim of this research to find the reliability dependant on the prediction method and not the reliability of individual cross-sections, this influence on the reliability is neglected for the outcomes of this research.

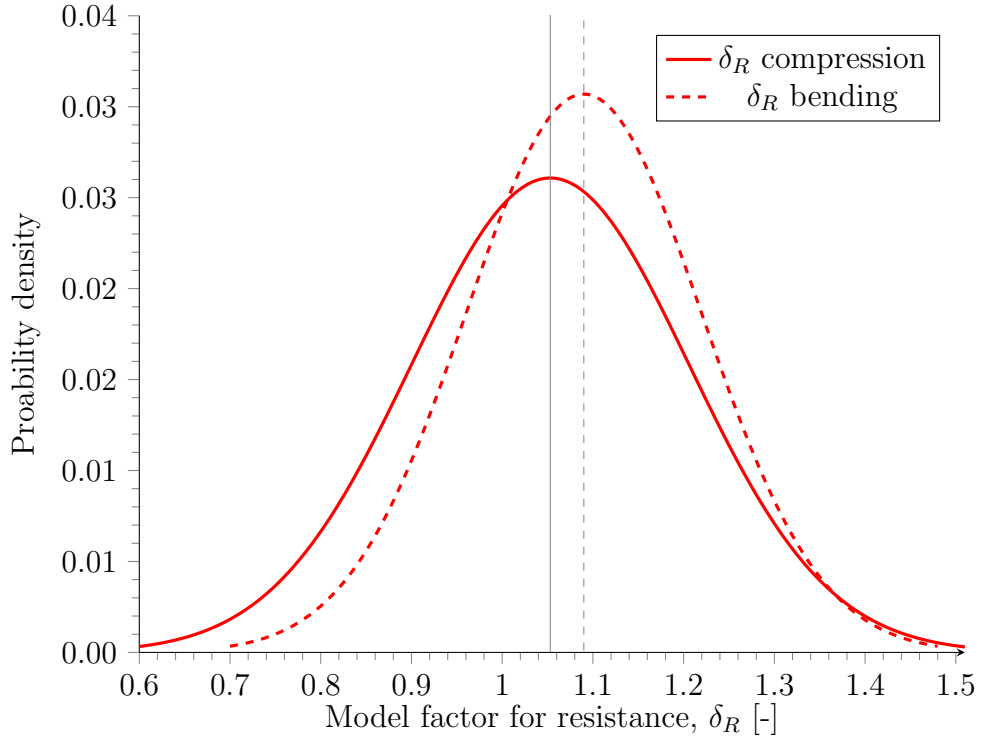

Figure 3.23: Normal probability density function of model factor for resistance used in the reliability analysis

Table 3.5: Model factor statistics for the various resistance models

Variable	Symbol	μ	σ	a	COV	Distr
Model factor for compression	δ_{Rc}	1.053	0.153	-	14.5%	N
Model factor for bending	δ_{R_b}	1.090	0.131	-	12%	N

It must furthermore be mentioned that the model factor for the DSM takes account of the uncertainty in the numerical error of the FSM. However, it does not take into account the error of input by the user, which cannot be incorporated in the assessed reliability of the design following the specification.

For both bending and compression no probability distribution behaviour for the DSM was found. Although Holický (2009) suggests model factors for the resistance to generally follow a normal distribution, resistance based model factors for hot-rolled members in bending as well as hot-rolled members in compression are recommended to follow a zero origin lognormal distribution. Nevertheless a normal distribution was further assumed for the purposes of this dissertation. A motivation for this assumption is presented in the subsequent section.

3.5 Reliability margin

3.5.1 Reliability and limit state verification

After completing the implementation of the routine for determining the reliability index as mentioned in section 3.2, a verification of the programmed procedure was undertaken for a 1 m column and beam member of the lipped C-section considered. The correctness of the implemented FORM analysis came into question due to initial reliability results from the algorithm producing unexpectedly low reliability indices.

A well established program that implements the FORM algorithm is VaP, developed at ETH Zurich (Swiss Federal Institute of Technology) by Markus Petchacher, which is distributed by Petchacher Software and Development (Petschacher, 1997). The program allows for the definition of the distributions of various probabilistic variables as well as the implicit limit state equation as a function of these variables. In Section 3.2 it was however explained that when using the DSM, the limit state function cannot be easily expressed without the use of the program CUFSM. VaP is from its implementation also not able to call the CUFSM program during the FORM iterations. Therefore a process needed to be considered that could replace CUFSM for the evaluation of the limit state equation in VaP.

From the definition of the limit state equation, the generation of an implicit surface function for the mode dependant resistance F_n, mentioned in Equation 3.1, as a function of the two underlying random variables was required. Generation of such a function was managed by fitting a polynomial or a different higher order regression function to the profile specific DSM capacity curves generated with the help of CUFSM. Since three probabilistic modes of failure exist, the process was repeated for all three modes. The limit state equation can then be discretely generated as it depends on the three assumed random variables only. VaP is then able to confirm the algorithm of this thesis by comparing the resulting reliability index β, the sensitivity factors and ultimately the design point.

As the limit state function depends on the mode-dependent resistance F_n, which can only be determined by means of the DSM equations with input resulting from a CUFSM analysis, an incremental scatter was created around the mean values of the random variables of thickness (t) and yield strength (f_y). Each variable was investigated up to approximately three standard deviations from its mean. The procedure had to be performed for the load case of concentric compression and for the case of pure bending separately for the cross-section specific to this study. A confirmation was only performed for the physical section length of 1 m and the simply supported boundary condition.

In order to produce an implicit surface function for mode dependant resistance (F_n), the following process was repeated for both loading conditions:

Firstly buckling loads using CUFSM were generated for yield strengths ranging from 210 MPa to 450 MPa with an increment size of 2 MPa, while the thickness was kept constant at the mean value. This implies that for each increment, three buckling loads for each of the three elastic failure modes were obtained. The mode dependent resistances (un-factored DSM capacities) were then computed by inserting the CUFSM buckling loads into the Direct Strength equations (see Section 2.2.4.3 and 2.2.4.4). This procedure now produced a scatter of resistance versus yield strength for the three modes of failure for both bending and compression.

Secondly the procedure of generating a discrete field of the DSM predicted capacity was repeated with the incremental variable replaced by the thickness, while the yield strength was kept at the mean value. The range of investigation for the thickness was from 0.715 mm to 0.785 mm with increments of 5 µm.

Finally trend-line fits were produced for each failure mode as they depend on either of the two variables of yield strength and thickness.

Thereafter, for each mode separately, the yield strength and thickness prediction curves were established as found in the simplified form of equations 3.7 and 3.8.

$$F_n(f_y, t = \{\mu_t = 0.75\,\text{mm}\}) = k(f_y) \tag{3.7}$$

$$F_n(f_y = \{\mu_{f_y} = 330\,\text{MPa}\}, t) = g(t) \tag{3.8}$$

Where k is a function only of f_y and g is only a function of t. However some function must exist in the form of Equation 3.9 that predicts the behaviour of the capacity as it depends on both variables.

$$F_n(f_y, t) = a \cdot g(t) \cdot f_y \cdot k(f_y) \cdot t \tag{3.9}$$

The Unknown constant a from Equation 3.9 is found by the shared point of Equations 3.7 and 3.8. The shared point is found by substitution of the known realisations of the mean value for both variables f_y and t. This is shown conceptually in equation 3.10.

$$a = \frac{F_n(f_y = 330\,\text{MPa}, t = 0.75\,\text{mm})}{330\,\text{MPa} \cdot g(t = 0.75\,\text{mm}) \cdot k(f_y = 330\,\text{MPa}) \cdot 0.75\,\text{mm}} \tag{3.10}$$

From this substitution, Equation 3.9 is now a predictor surface-function for the capacity, also referred to as a performance surface. To validate the accuracy of the surface-function, four more two-dimensional plots were generated with CUFSM and the DSM on the boundaries of the variables' distributions. In other words: points at approximately more and less than three standard deviations away from the mean value were considered as the constant for either

variable. The accuracy of the prediction surface was then investigated. The 1 m specific capacity prediction plot for the concentric compression and pure bending loading scenario are presented in the following subsection. The error of the prediction plots and the exact functions are also presented.

3.5.1.1 Concentric uniform compression

The three graphs pertaining to Equation 3.7 for each of the three failure modes are seen in Figure 3.24 and are made up from discrete points, not the regression equation. All prediction equations of these curves were obtained using sixth-order polynomial functions and it can be denoted that the r-squared values (a statistical measure of error for regression purposes with lowest error when unity) for all three equations are unity. Also indicated in the figure, are the capacity points where both variables are at their means. Furthermore the unfactored design capacity is shown and can only be presented on this set of curves. This follows from the attribute that the thickness used in design is the same as the mean value, a constant in these curves.

Similarly the graphs for the discrete points following the DSM output as a function of thickness, following the concept of Equation 3.9, can bee seen in Figure 3.25 for all three modes of failure. For these graphs power trend-lines

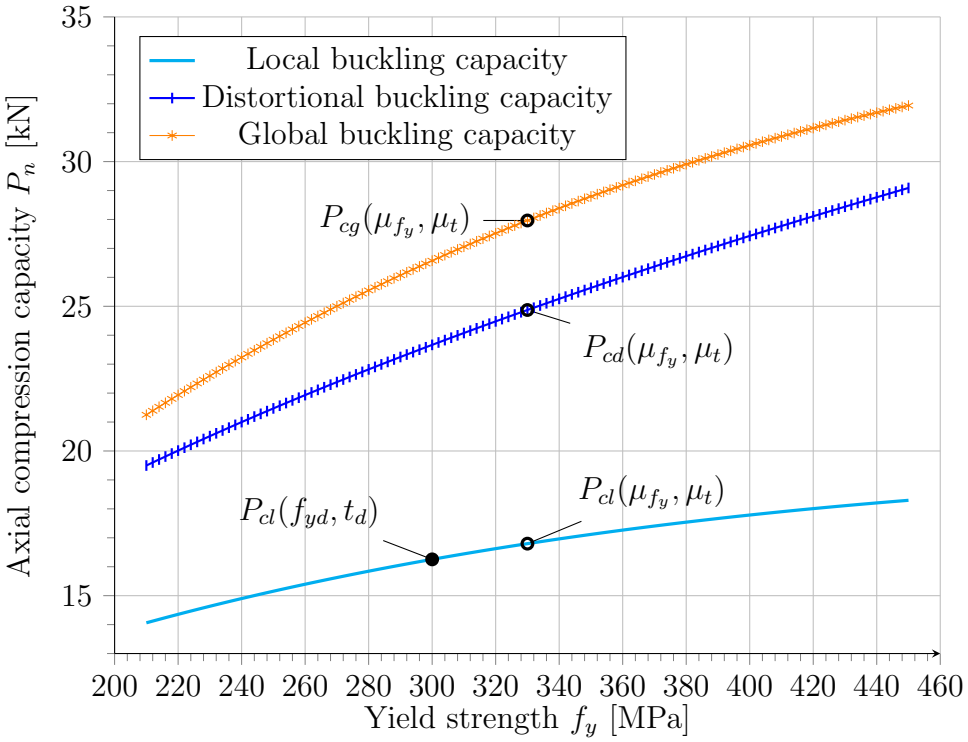

Figure 3.24: DSM generated mode-dependant capacity as a function of yield strength (f_y) at the mean thickness (μ_t)

were used and the r-squared values were also found to be unity. Again points of mode dependent capacity evaluated at the means of the physical variables are seen and show the intersection with the previous curves. From the graphs it is clear that the lowest capacity mode is in the form of local buckling. Although the reliability index presented next was obtained from combinations of lowest design resistance and all three probabilistic modes of failure, since it is assumed that all three modes have similar level of uncertainty attributed to them, the procedure that makes use of Equation 3.9 is only presented for the case of local buckling. The probabilistic design capacity following from local buckling produced the lowest reliability margin and is therefore explained more here.

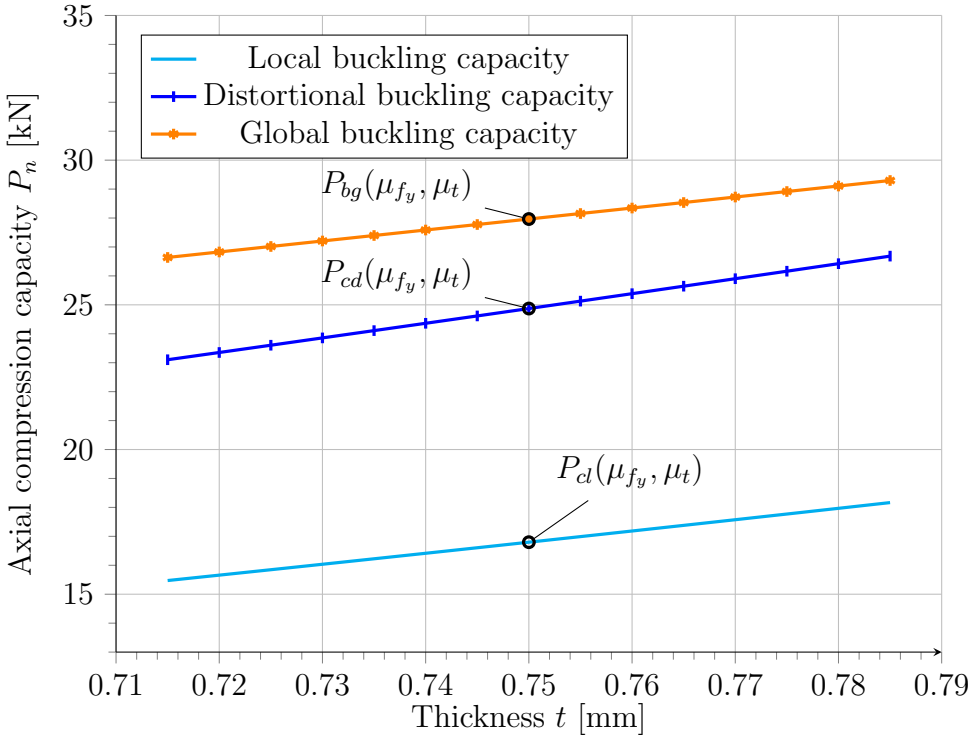

Figure 3.25: DSM generated mode dependant capacity as a function of thickness (t) at the mean yield strength (μ_{f_y})

A plot of the explicit function formulated in terms of both the yield strength and the thickness can be seen in Figure 3.26. Once more indicated in the figure is the design resistance. The numerical values substituted for the random variables to determine this point are the values used for design, presented in tables 3.1 and 3.2 of Section 3.3. One must however take note, that this capacity is not yet multiplied by the partial factor. Another point of interest that is depicted in the figure, is the capacity at the mean value of both variables showing the intersection of the direction dependant functions.

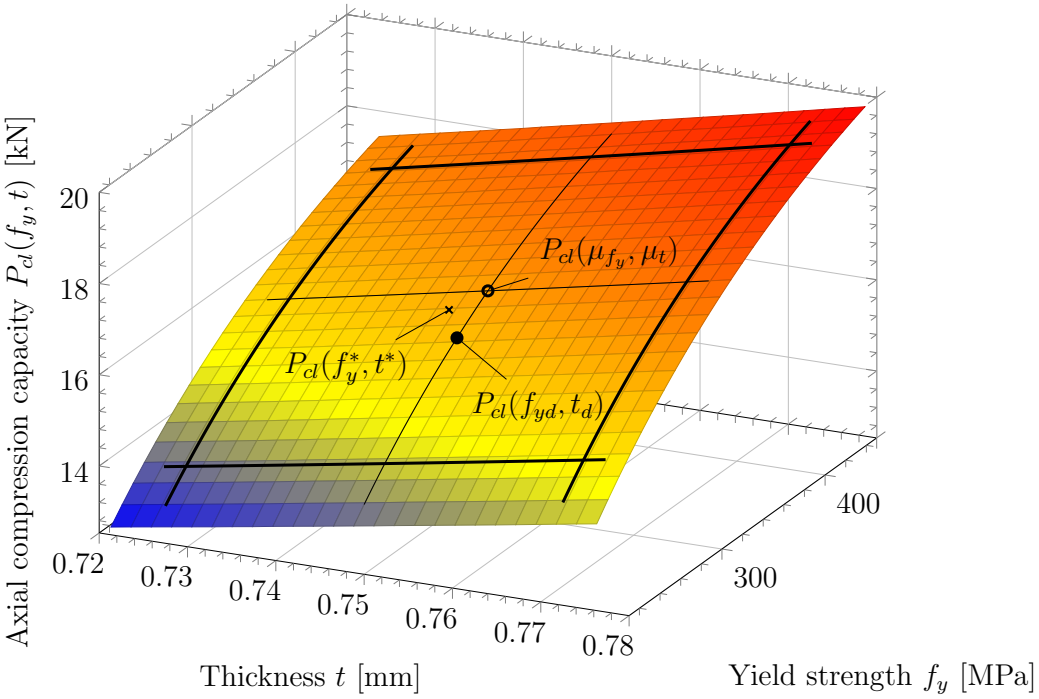

Figure 3.26: Performance surface of the cross-section in compression used in reliability analysis

As mentioned, the accuracy of the performance surface was checked on boundary values of the two dependant variables. The capacity boundaries that were checked are also shown on the performance surface of Figure 3.26. The maximum error of the performance surface with respect to the capacity at boundary lines is presented in Table 3.6. From the table it is clear that the error of the performance-predicting surface function is small within the boundary considered.

Table 3.6: Maximum error of performance function

Error in %	$P_{cl}(f_y, t)$			
	$f_y = 230$, t	$f_y = 430$, t	f_y, $t = 0.7225$	f_y, $t = 0.7725$
Min	-0.05	-0.03	-0.03	-0.05
Max	0.06	0.04	0.05	0.03
Absolute	0.06	0.04	0.05	0.05

The surface function now represents the member local buckling capacity as a function of the yield strength and the thickness with negligible error. Since an explicit equation exists, it was substituted in the limit state equation from Section 3.1. The limit state function is hence defined in terms of all variables

and was therefore inserted in VaP, with the design resistance being an evaluated constant. From the random variable behaviour assumed in sections 3.3 and 3.4 the reliability index was then determined. The resulting reliability index from VaP is found in Table 3.7. To compare to this result, the self-implemented algorithm elaborated in Section 3.2 was also run. Keeping in mind that this algorithm considers all capacity dependent failure modes and that the lowest reliability margin is computed, the reliability index found from the analysis matched the one obtained utilizing VaP.

Two properties resulted from the production of the performance surface. First, the analysis FORM algorithm that was implemented in combination (linked) with the DSM is confirmed to be correct. Secondly, the performance surface in combination with VaP allows for an easy tool to investigate how the distribution assumptions of the random variables affects the reliability. An additional reliability analysis was run with the VaP program to determine the reliability index, if the model factor was assumed to follow a lognormal distribution with a zero lower bound as is suggested by Holický *et al.* (2015). The result can be seen tabulated in the right most column of Table 3.7 with the two matching reliability indices results and the slightly higher obtained reliability index of 1.67. Also shown with the reliability index are the sensitivity

Table 3.7: Reliability index due to local buckling capacity for 1 m member in compression using the FORM

Random Variable	Symbol	Linked		VaP		VaP	
		Distr	α	Distr	α	Distr	α
Yield strength	f_y	LN	0.214	LN	0.180	LN	0.274
Thickness	t	N	0.173	N	0.147	N	0.219
Model factor	δ_R	N	0.961	N	0.973	LN	0.936
Reliability index β_R		1.46		1.46		1.67	

factors, which indicate the contributions to the reliability from each variable. From the table is clear that the model factor remains the dominating variable irrespective of the assumption of its probability distribution and the increase in reliably is largely attributed to a shift in sensitivity to the other random variables. Comments about the assumption for model factor distribution follow in the subsequent section.

3.5.1.2 Unrestrained strong axis bending

Once more the performance surface methodology was used for determining the member bending capacity of the three failure modes. The nominal capacity curves as a function of yield strength can repeatedly be associated with the conceptual Equation 3.7 and are presented in Figure 3.27. Again the graphs show the discrete set of data points produced from iterations of the DSM, including FSM analyses. All r-squared values were also found to be unity for the sixth-order polynomial regression equations used, once more indicating the prediction-error of the equations is none. The capacity for the 1 m member and the mean value for all failure modes, as well as the nominal capacity used for design, are additionally visible on the graph.

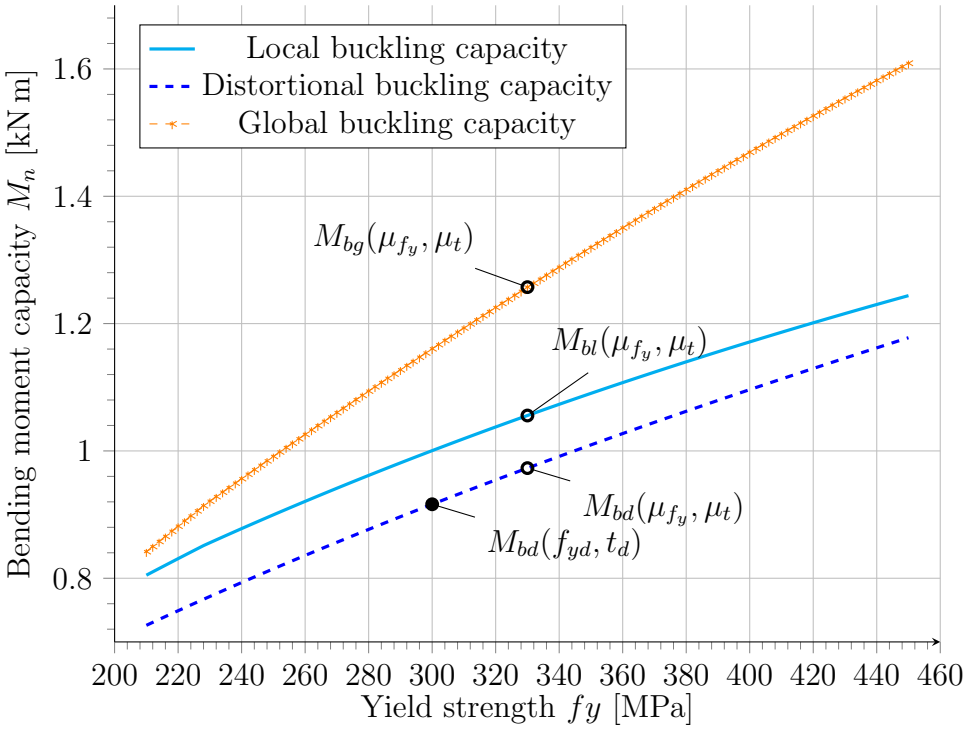

Figure 3.27: DSM generated mode dependant capacity as a function of thickness (t) at the mean yield strength (μ_{f_y})

The bending capacity behaviour for the member as a function of the thickness, for all three failure modes, is depicted in Figure 3.28. Intersection-points with the curves of Figure 3.27 are also visible. All three of the indicated capacity-points are produced with the yield strength likewise at its mean value. The limiting capacity can be seen in the figure to be the product of distortional buckling. The same can be said for the capacity as a function of yield strength. Once more all modes of failure were considered, but the lowest reliability was again achieved when both the probabilistic resistance and the design resistance were in the same mode of failure. Therefore the generalized

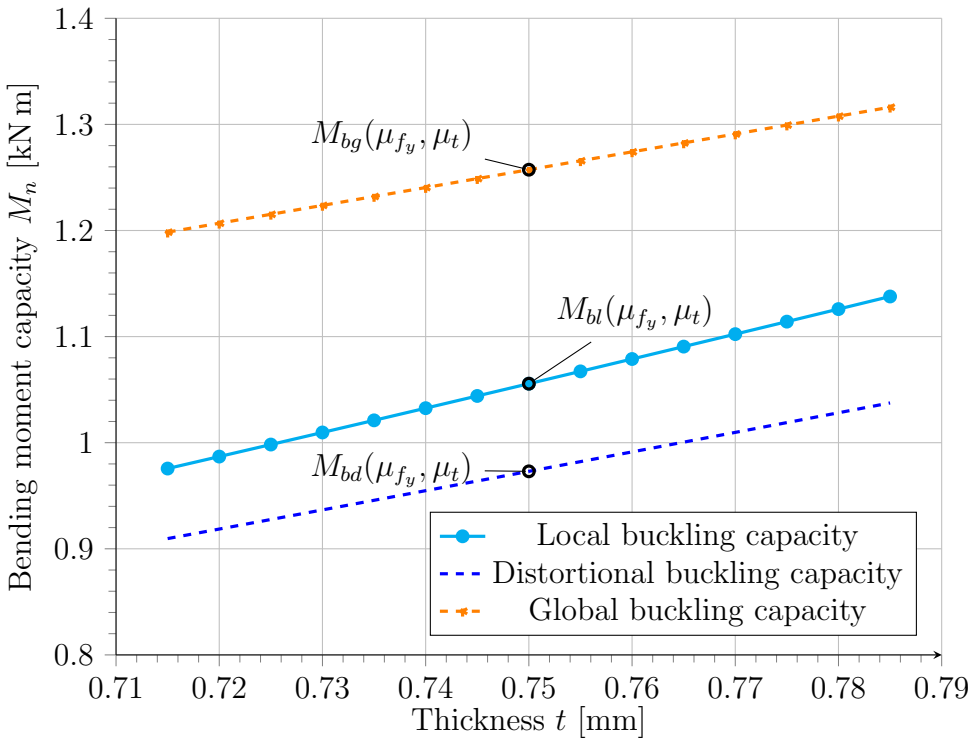

Figure 3.28: DSM generated mode dependant capacity as a function of yield strength, f_y, at the mean thickness, μ_t.

procedure of Equation 3.9 for determining the performance surface function is only presented for the distortional capacity mode.

A plot of the three dimensional behaviour of the resulting performance surface is displayed in Figure 3.29 together with capacity points of interest. Additionally indicated on the performance surface plot are the discrete boundary capacities generated to determine the error of the performance surface. Maximum errors for the variable boundaries were again calculated and are found in Table 3.8. Once more the prediction equation of the performance surface shows low error in comparison to the definite DSM-FSM predictions and was again used as input in the reliability analysis program VaP.

Table 3.8: Maximum error of performance function

Error in %	$M_{bd}(f_y, t)$			
	$f_y = 230$, t	$f_y = 430$, t	f_y, $t = 0.7225$	f_y, $t = 0.7725$
Min	-0.16	-0.09	-0.14	-0.07
Max	0.18	0.11	0.14	0.15
Absolute	0.18	0.11	0.14	0.15

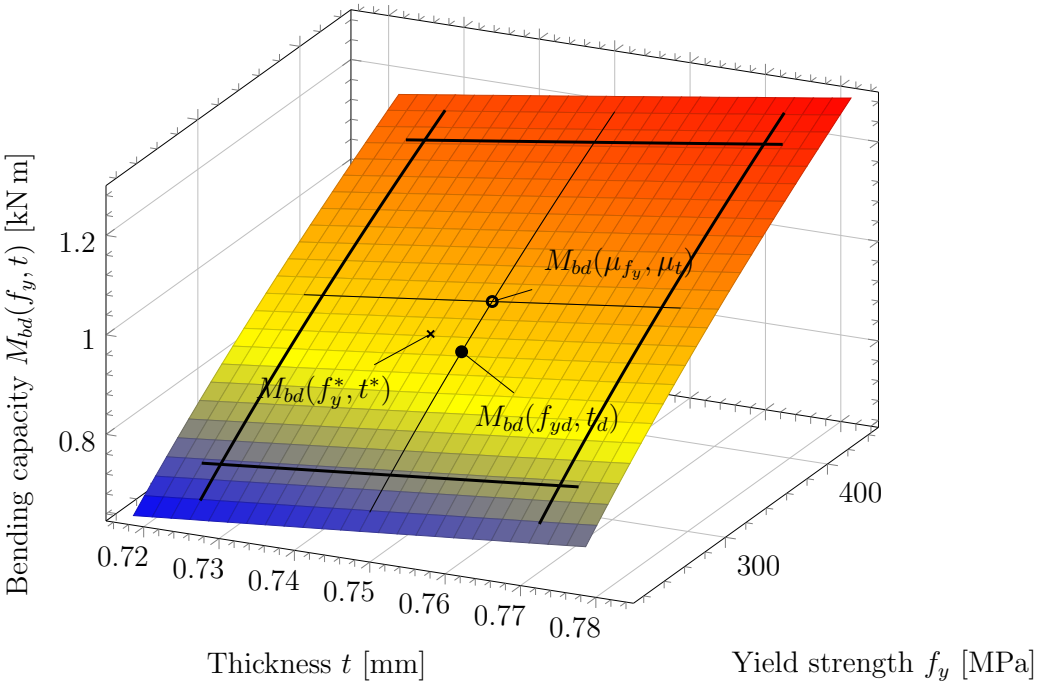

Figure 3.29: Performance surface of cross-section in bending used in reliability analysis

Now that an explicit equation for the capacity of members subject to bending was defined, the design resistance was computed and the associated limit state, Equation 3.1, was set out. The reliability index was again calculated using the VaP program to determine the reliability for the distortional buckling failure mode for member bending-resistance. The results are presented in Table 3.9. Again the reliability was obtained by the author's implemented algorithm and compared with the results from the performance curve. When considering the stated β result, it must be pointed out that the reliability index shown in Table 3.9 is found from the probabilistic distortional buckling capacity as assumed for the VaP performance surface analysis. The author's linked CUFSM-FORM result was determined from the same failure mode. However, it was obtained as the lowest value considering all probabilistic resistance modes separately. Although not shown in the body of this document, all three failure mode performance surfaces were developed and checked. The lowest reliability attributed to distortional buckling failure as is presented here. The reliability index from a lognormal distribution assumption for the model factor was additionally checked, which produced a higher value of 1.81, again found in the right most column of the table.

A slight difference in reliability is visible between the author's algorithm and VaP when a normal distribution is assumed for the model factor, but generally the same reliability index is achieved. The difference in sensitivity

and reliability indices may be explained due to the different convergence criteria used by the two analyses. The convergence criteria for VaP consisting of both convergence of the reliability index as well as the design point. More specifically convergence is achieved with respect to the limit of the double-precision floating-point computer number accuracy (Petschacher, 1997). From the fact that the error is shown to be small (less than 1%) the VaP calculation for the reliability index is deemed more accurate. This may indicate insufficient accuracy in the interactive algorithm presented in this dissertation, however when increasing the required convergence accuracy, it was found that the algorithm converged within the same number of iterations as well as to the same accuracy.

Table 3.9: Reliability index due to distortional buckling capacity for 1 m member in bending using the FORM

Random Variable	Symbol	Linked		VaP		VaP	
		Distr	α	Distr	α	Distr	α
Yield strength	f_y	LN	0.432	LN	0.391	LN	0.500
Thickness	t	N	0.186	N	0.140	N	0.179
Model factor	δ_R	N	0.882	N	0.910	LN	0.847
Reliability index β_R		1.69		1.67		1.81	

Therefore the central difference increment or h was scrutinized. A forward and backward difference for the dissertation-specific variables as shown in Table 3.10 were used for the reliability results of tables 3.7 and 3.9. The magnitude of h is determined as a percentage of each design-point-iteration of the FORM algorithm. Investigation showed that a decrease in the increment-percentages did not achieve additional accuracy in the β value, nor the sensitivity factors, nor did it ultimately affect the design point. Increment decrease, as shown in Section 3.2.2, increases the accuracy of the numerical derivative closer to that of the true derivative which is directly linked to decreased number of iterations required for the FORM.

Table 3.10: Forward and backward difference increment

Variable	Symbol	Difference h in %
Yield strength	f_y	0.1
Thickness	t	0.1
Model factor	δ_R	0.5

Lastly, the assumption of the model factor following a normal distribution was re-evaluated. As mentioned Holický (2009) suggests that resistance model

factors in general can be assumed to follow a normal distribution. When looking at model factors for bending and compression of hot-rolled steel members, the model factor can generally be assumed to follow a lognormal distribution with zero lower bound as is suggested by Holický (2009) and Vrouwenvelder *et al.* (2001). However, the model factors specific to the DSM method as presented by the American Iron and Steel Institute *et al.* (2012), Schafer (2008), and Ganesan and Moen (2012) do not mention any behavioural assumption or provisions of the distribution of the model factor specific to the DSM. Using VaP it could easily be shown that the original assumption of a normal distribution achieved conservative results and is therefore the suggested assumption by Holický, Retief and Sỳkora (2015). Since the FORM results of this section are only based on the resistance side of the reliability margin, the results should now be compared to the aimed reliability that the DSM's partial factor was calibrated for. Therefore a discussion on what the reliability of the resistance side for cold-formed steel members that was targeted, is presented next.

3.5.2 Sensitivity of the resistance and the target reliability

In Chapter 2 the relation between the probability of failure and the reliability index was introduced. The target overall reliability (β_t) that a structure or structural member should achieve from the design method used, may differ by expert opinion, which is shown in the course of this section. Since the target reliability covered by a resistance design code such as SANS 10162-2 depends on the sensitivity of the resistance (α_R) and the aimed overall reliability, as was shown in Section 2.4.3, an investigation into these two parameters was necessary. As soon as the resistance based sensitivity used in the calibration of the partial factor is known, insight may be found as to why the preliminary β_R values of the previous section are much lower than expected.

As was mentioned in Section 2.4.5, the reliability that was achieved by designing cold-formed steel beams according to the former Safety Factor (a ratio based solely on the nominal strength with respect to design strength) was back-calibrated to give a reliability index of $\beta = 2.8$ (Ellingwood and Galambos, 1983). After establishment of the reliability from a Safety Factor point of design and a specific assumption of loading (dead load to imposed load ratio was 1 to 5), a partial factor based design procedure was introduced to the existing method of design for cold-formed members of the AISI. Overall reliability of $\beta_t = 3.0$ for gravity loading, $\beta_t = 2.5$ for wind loading and $\beta_t = 4.5$ for connections was suggested by Ellingwood and Galambos (1983). In order to allow for more consistency of reliability when incorporating various arrangements of loading as well as different types of construction and most importantly different types of members, this arrangement of reliability was suggested (Ellingwood and Galambos, 1983). Limiting values of $\beta_t = 2.5$ and

$\beta_t = 3.5$ were lastly chosen for cold-formed steel members and connections respectively, in order to allow for the same level of safety as achieved with the previous design procedure (American Iron and Steel Institute *et al.*, 2012). Depending on the sensitivity of the resistance, the reliability index of 2.5 is therefore the overall level of target reliability that appears in the partial factors for the United States of America (USA) used with the DSM presented by American Iron and Steel Institute *et al.* (2012) and corresponds with the partial factors (see Table 3.2) currently stated in SANS 10162-2.

A different target reliability index is aimed at by Canada (CAN) for member design, with a value of $\beta_t = 3.0$ (American Iron and Steel Institute *et al.*, 2012). Partial factors for this target are also presented in the North American Specification, as the standard allows for design to accommodate for both countries' aimed at levels of reliability.

However, one of the most fundamental points when considering the reliability of a structure or a structural member is the lifetime expected from it. Therefore a structure is generally designed to resist collapse for a specific design lifetime, which reflects to some extent the cost of erection of the structure as well as the feasibility of the consequence of collapse. These influences are commonly referred to as the durability aspects of structures. Structural members generally require lower reliability when used in structural systems due to their redundancy and redistribution of load after component failure. Redundancy is generally ignored when member resistance calibrations are considered. Since the load effect, together with the design lifetime, represent large contributing factors to the target reliability or level of safety, these two parameters generally dominate the choice of what level of safety is accepted for a structure.

Cold-formed systems may be highly redundant when used for light-frame steel buildings and failure of members results in low consequence. However, cold-formed steel may be used for key structural components such as floor-beams or base-columns in slender multi-story structures. Very low redundancy may be associated with these systems and failure may be of high consequence. The same is true if cold-formed steel members are used for storage racks or critical members in warehouses. SANS 10162-2 does not limit the specific use of members designed according to the DSM (Section 1 SANS). Thus the level of reliability required for structural elements depends on the use of the member and the dominating load case in its design lifetime. Conservatively it should be assumed that members are used in non redundant systems.

ISO 2394: 1998, an international standard for structural reliability, specifies the reliability associated with a notional design lifetime of 50 years as $\beta_t = 3.8$ for the ultimate limit state. General buildings and non-temporary structures

are associated with this design lifetime, which coincides with a durability of Class 1. This level of reliability is associated with various combinations of moderate to low costs for the targeted measures of safety, together with variations of some, up to great consequence of failure (ISO, 1998).

Incidentally the same reliability index is presented for structures designed according to EN 1990: 2002, the European basis for structural design. The same reference period for the design lifetime as in ISO 2394 is presumed when design is evaluated at ultimate limit state (BSI, 2002). An accepted lethal accident rate of 10^{-6} per year is associated with the standard's reference period according to Holický (2009). In EN 1990 durability is related with consequence classes that are directly related to reliability classes. General structures such as warehouses and office buildings are associated with Reliability Class 2. The same reliability class, according to section D 8.3 of the standard, is suggested to be incorporated by structural members designed at ultimate limit state. Hence the reference reliability index for cold-formed steel member design would also fall in the category of $\beta_t = 3.8$ (BSI, 2002).

The reliability required by SANS 10160-2011, the South African standard for the basis of structural design, is set out with a reliability classification system closely linked to that of ISO 2394 and EN 1990 (Retief and Dunaiski, 2009). The normative reliability associated with the South African basis of structural design is for medium economic and medium social level of consequence from collapse of the structure. Furthermore the normative reliability is, as is the case with ISO and EN 1190, associated with a 50 year lifetime design and moderate economic consequence due to collapse (Retief and Dunaiski, 2009). However, a considerable environmental consequence is introduced with this level of reliability in SANS 10160. The normative reliability index from all of these factors results in $\beta_t = 3.0$. Based on earlier versions of the South African basis of design (SABS), reliability was classified according to the mode of failure. A reliability index of structural components associated with brittle failure was $\beta_t = 4.0$ and with ductile failure $\beta_t = 3.0$ (Retief and Dunaiski, 2009). The scope of SANS cold-formed member resistance design clearly states that methods covered in it do not cover design according to brittle fracture. Hence, the expected reliability margin by European standards as well as South African is quite well defined when assumed to follow a normal distribution.

Table 3.11 summarises the reliability of the above-mentioned literature for both random variables of resistance and load effect. It must be pointed out that the South African level of reliability associated with member design is $\beta_t = 3$, as presented in the basis of structural design, SANS 10160 (SABS, 2011). The partial factor currently in SANS 10162-2 is associated with an expected reliability index $\beta_t = 2.5$ as based on AS/NSZ standard and already it can be said that the reliability does not meet South African requirements.

Table 3.11: Reliability index for cold-formed steel members according to various specifications

Standard	**Overall β_t**	**p_f ($\approx$)**
ISO/EN 1990	3.8	0.0001
SANS 10160-1:2011/ AISI (CAN)	3.0	0.001
AISI (USA)/ AS/NZS 4600	2.5	0.006

Now that the overall reliability indices have been defined according to various standards and specifically the partial factor calibrator AISI, the sensitivity of the resistance side of the limit state function must be considered to allow for comparison with the reliability indices of Section 3.5.1. To recapture, these results should then be compared to the target reliability of the resistance $\beta_{t_R} = \alpha_R \beta_t$ only (see Section 2.52). Table 3.12 shows the target reliability of the resistance side of the reliability margin based on the conservative sensitivity factor $\alpha_R = 0.8$ suggested in EN 1990 and the target reliability from SANS 10160 is calculated for the same sensitivity. The reason for the earlier statement that reliability results were considered low should now be clear. Nevertheless, a sensitivity suggested by the AISI calibration must differ significantly when looking at the obtained β_R results and was therefore investigated next.

Table 3.12: Target reliability for ISO and SANS

		SANS	**EN/ISO**
Sens. of resist.	α_R	0.8	0.8
Reli. index	β_t	3.0	3.8
Target index	$\alpha_R \beta_t$	2.40	3.04

By assuming a lognormal distribution of the limit state function, as was done by the American Iron and Steel Institute *et al.* (2012) for calibration, a simplification of the sensitivity associated with the resistance side (α_R) of the reliability margin could be made by Equation 2.51 repeated in Equation 3.11:

$$\alpha_R = \frac{V_R}{\sqrt{V_E^2 + V_R^2}} \tag{3.11}$$

where V_E and V_R are the COV of the resistance and load effect variables respectively.

The COV of the resistance, as was shown in section 2.4.5, can be determined as the sum of squares of the COV's of the thickness, yield strength and model

factor variables. A recap of this is shown Equation 3.12, a repeat of Equation 2.71 from Section 2.4.5.

$$V_R = \sqrt{V_t^2 + V_{f_y}^2 + V_{\delta_R}^2} \tag{3.12}$$

In order to determine the COV of the load effect (V_E), the calculation of load combinations must be considered. Equation 3.13 shows how the mean load effect is calculated from the combination of various mean values of loads (μ_{E_i}), where each different load is denoted by i. These can hence be rearranged to the product of various nominal loads (E_{ni}) and the bias factors of each load effect (δ_{E_i}). The constant c replaces the combination of load factors that are summed to find a mean load effect.

$$\mu_E = c \sum \mu_{E_i} = c \sum \delta_{E_i} E_{ni} \tag{3.13}$$

A similar summation is present in the denominator of the calculation for the COV of the load effects (V_E) as found in Equation 3.14. The nominator of the equation is found as a function of the bias factor for each load effect (δ_{E_i}), the nominal value of that load (E_{n_i}) and the COV of each load effect (V_{Ei})

$$V_E = \frac{\sqrt{\sum (\mu_{E_i} V_{E_i})^2}}{\sum \mu_{E_i}} = \frac{\sqrt{\sum (\delta_{E_i} E_{ni} V_{E_i})^2}}{\sum \delta_{E_i} E_{ni}} \tag{3.14}$$

For design of cold-form steel according to the American Iron and Steel Institute *et al.* (2012), the COV of the load effect which was used in calibration was obtained from a combination of imposed load (I) and dead load (D) as shown in Equation 3.15. This was done for a specific nominal dead load to nominal live load ratio of 1 to 5.

$$V_E = \frac{\sqrt{(\delta_D D_n V_D)^2 + (\delta_I I_n V_I)^2}}{\delta_D D_n + \delta_I I_n} \tag{3.15}$$

Thus all required information for the determination of the sensitivity used in calibration is available. Table 3.13 summarizes each of the parameters required for determining the sensitivity factor of resistance wich were used in calibration (American Iron and Steel Institute *et al.*, 2012). The original variance associated with the model factor (Schafer, 2008; American Iron and Steel Institute *et al.*, 2012) used for members in compression and members in bending were used for a sensitivity factor calculation using Equation 3.12 and 3.15. Other resistance COVs for the use in Equation 3.12 are stated by American Iron and Steel Institute *et al.* (2012) to be the ones that were used in calibration. The statistical parameters in Table 3.13 are given for the imposed load that was assumed by AISI for the calibration process (Ellingwood and Galambos, 1983). An assumption on the load ratio of 1 to 5 dead load to imposed load was however assumed and strongly contributes to the low α_R values calculated. No significant justification for this assumption could be

Table 3.13: Probabilistic variable information from AISI to calculate α_R

			Compression		Bending	
Variable	**Sym**	$\frac{D}{E_n}$	$\boldsymbol{\mu}$	$\boldsymbol{V}$	$\boldsymbol{\mu}$	$\boldsymbol{V}$
Yield strength	f_y		330 MPa	0.1	330 MPa	0.1
Thickness	t		0.75 mm	0.05	0.75 mm	0.05
Model factor	δ_R		0.98	0.14	1.09	0.12
Resistance	R		-	0.179	-	0.164
Dead load	D_n	1	$1.05D_n$	0.1	$1.05D_n$	0.1
Imposed load	I_n	5	$1.0I_n$	0.25	$1.0I_n$	0.25
Load effect	E		-	0.207	-	0.207
Sens. of resis.	α_R		0.654		0.620	

found in literature, but it is clear that the imposed load in the relevant load case, dominates the sensitivity.

Now that α_Rs used for calibration of the resistance partial factors for the DSM equations have been calculated, the target resistance reliability contribution from calibration can be determined. This is done in Table 3.14 for both bending and compression based on the reliability targeted (β_t) by the partial factors currently in place in SANS 10162-2. This is marked out as the USA AISI target beta. Also, the $\alpha_R\beta_t$ from Table 3.12 based on ISO/EN and SANS 10160 β_t are included as references for comparison.

Table 3.14: Target reliability from various standards based on the sensitivity of the resistance

		Compression		Bending			
		AISI		AISI			
		USA	CAN	USA	CAN	SANS	EN
Sens. load	α_E	-0.756	-0.756	-0.785	-0.785	-0.7	-0.7
Sens. resist.	α_R	0.654	0.654	0.620	0.620	0.8	0.8
Reli. index	β_t	2.5	3.0	2.5	3.0	3.0	3.8
Target index	$\alpha_R\beta_t$	1.635	1.961	1.551	1.861	2.40	3.04

A reference value for a resistance side reliability target index ($\alpha_R\beta_t$) intended during calibration has now been established. When comparing the calculations of Table 3.14 with the results of sections 3.5.1.1 and 3.5.1.2, it can be stated that the assessed reliability for the 1 m member in compression is only 11% lower than the resistance side target (AISI USA). The same can be said for the 1 m member subject to pure bending where results are 9% higher than the resistance side target from calibration (AISI USA). These differences are much lower when compared to the average discrepancy of 31% from the

SANS 10160 accepted reliability level.

Figure 3.30 shows how the sensitivity factor of the resistance (α_R), based on Equation 3.11, behaves if the assumed dead load to live load ratio changes. Two curves are depicted in the figure that present the behaviour based on AISI calibration data given in Table 3.13. The sensitivity factors of the resistance for both limit states of compression (α_{Rc}) and bending (α_{Rb}) are indicated in the figure for the case that the dead load to live load ratio is 1 to 5 (0.2). From these, the target reliability of the resistance for the DSM method were calculated.

Retief and Dunaiski (2009) give statistics for various types of loads that were used in the establishment of reliability-based load combination factors currently in place in the South African basis of structural design. They are summarised in Table 3.15 as well as the mean and COV for an assumed wind load (W). Noteworthy is that the dead load and imposed load statistical mean and COV are the same as those used for the calibration of the partial factors presented in Table 3.13. Thus, if plots of the sensitivity of resistance based on these statistics and the COV of resistance (V_R) assumed by the author are graphed following the same procedure as above, additional points of interest on Figure 3.30 can be established.

Table 3.15: Probabilistic variables used for graphing of Figure 3.30

			Compression		Bending	
Variable	**Sym**	$\frac{D}{E_n}$	$\boldsymbol{\mu}$	$\boldsymbol{V}$	$\boldsymbol{\mu}$	$\boldsymbol{V}$
Yield strength	f_y		330 MPa	0.1	330 MPa	0.1
Thickness	t		0.75 mm	0.016	0.75 mm	0.016
Model factor	δ_R		1.05	0.145	1.09	0.12
Resistance	R		-	0.177	-	0.157
Dead load	D	-	$1.05D$	0.1	$1.05D$	0.1
Imposed load	I	-	$1.0I$	0.25	$1.0I$	0.25
Wind load	W	-	$0.41W$	0.52	$0.41W$	0.52
Load effect	E	-	-	-	-	-

Using Equation 3.11 with the parameters from Table 3.15, when a load combination of a dead load (D) and a wind load (W) or a load combination of dead (D) load and imposed load (I) are studied, four additional curves are produced in Figure 3.30. These load combinations were of interest as they are important when considering the South African basis of structural design for cold-formed steel members. When re-examining Figure 3.30, the fact that the V_R used in this dissertation slightly differs from the original V_R of the AISI can be seen to have negligible influence on the sensitivity of the resistance (α_R). Comparison of the red lines with the green lines shows this,

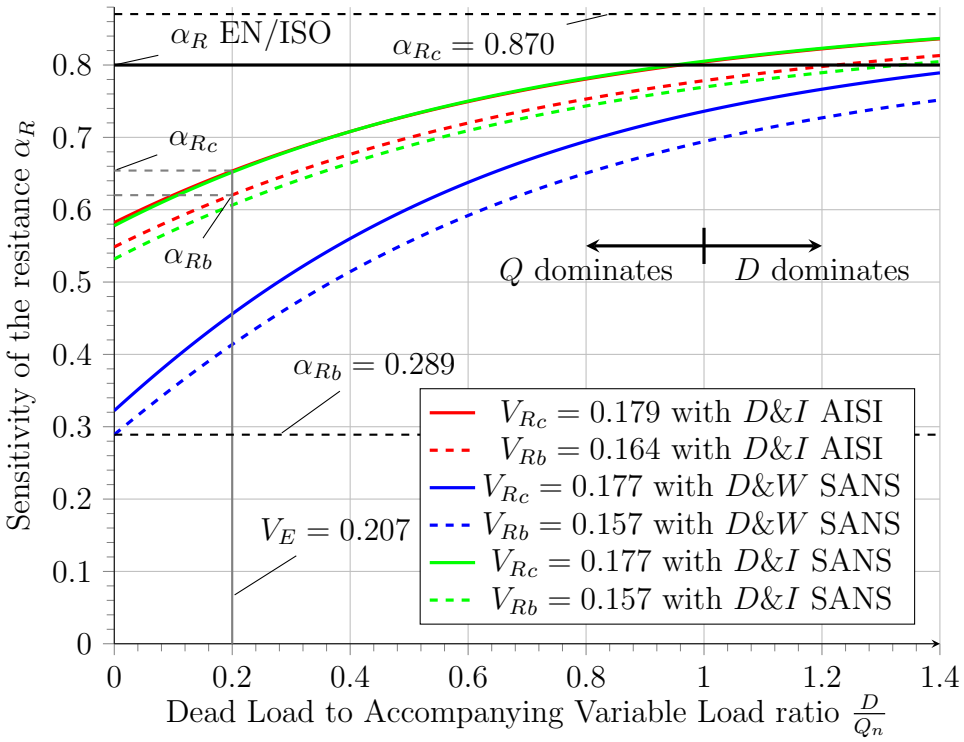

Figure 3.30: Behavioural spectrum for the sensitivity of the resistance based on literature

since the load COVs used to produce α_R are the same. One horizontal line can be added to the figure to show the lower limit of α_r, when the dead load contribution becomes negligible in its combination with a wind load. The line is indicated in Figure 3.30 as $\alpha_{Rb} = 0.289$. Subscript b is used to indicate that COVs of the bending resistance variable were used in the calculation of the value. An upper limit for the sensitivity based on the COVs from Table 3.15 is also shown as $\alpha_{Rc} = 0.870$, and is a result of only the COV of the dead load being considered. Finally Figure 3.30 depicts the conservative resistance sensitivity limit that is suggested by EN 1990 and ISO 2394 with a value of $\alpha_R = 0.8$.

From Figure 3.30 and the above explanations, insight into the sensitivity of the resistance and ultimately the target reliability index for cold-formed steel resistance based on the AISI calibrations was presented. In contrast to this, limits of the sensitivity of the resistance were calculated to be located between $\alpha_R = 0.289$ and $\alpha_R = 0.870$ within the South African reliability context, covered in SANS 10160-Basis of structural design. What Figure 3.30 shows even more, is that if the variable load contribution increases, the resistance based reliability ($\alpha_R\beta$) reduces because α_R also decreases. The EN and ISO suggested value of $\alpha_R = 0.8$ covers the ranges when variable load and dead load are equal and therefore have an even influence on the overall reliability of structural members.

Sensitivity inherently used with the SANS 10162-2 partial factor, considers the design load combination to be highly influenced by an imposed load. For the example that wind loads are the dominating design case, the sensitivity of resistance may be accepted at a much lower value than that used by the AISI. The targeted reliability on the resistance side by the AISI on the other hand is clearly based on the assumption that the variable load, specifically the imposed load, is largely significant in the design process. This assumption is warranted, if the load factors used in the loading code are calibrated to a reliability with a higher load effect sensitivity (α_E). This is currently not the case when SANS 10160 is used for determining the load effect during SANS 10162-2 DSM member resistance design. To assume a lower sensitivity of resistance and a coupled higher α_E for loading codes is after all not prudent, since the loading code covers various member-material-types for design and not only cold-formed steel. Additional reliability may still be achieved as the α_E values intended by the calibration process on the loading side (see Table 3.14), are lower than the conventional -0.7 value recommended by EN 1990 and ISO 2394. Therefore, sufficient reliability may be integrated by the currently specified SANS 10160 load factors to achieve an acceptable overall reliability margin. This however cannot be assessed by outcomes of this thesis.

However, the β_R analyses presented in sections 3.5.1.1 and 3.5.1.2 that should be compared to any target, only cover a specific buckling failure mode. One for either the column or the beam design process. From the nature of the DSM, members may experience different failure modes when different critical stresses are induced. To fully establish the reliability of DSM member design, multiple failure modes must first be considered. This can only be achieved by changing the slenderness of the members and is effectively accomplished by adjusting the length of the members. Therefore the next chapter presents the reliability based on analyses for a larger spectrum of member lengths.

Chapter 4

Results and Discussion of Slenderness Range Analysis

The following chapter focuses on the reliability indices obtained from increased member lengths. To interpret results from the investigation, important realisations due to the input variables for the FORM are discussed to show their impact on the reliability outcome.

4.1 Signature Curve

In order to explain upcoming reliability index results, the signatures curve of the lipped C-section designed for compression or bending needs to be reconsidered. Re-generations of the signature curves that are required in the reliability analysis for the two respective design cases, are independent of the member length at exactly two stages in the FORM iterations. These stages are when both f_y and t are evaluated at the values used for design, and when both f_y and t are evaluated at their mean values. Figures 4.1 and 4.2 both show theses two curves of the different variable-realisation cases for the respective member designs.

Signature curves for compression and bending capacities at f_y and t values used in design are associated with step 1 of the FORM procedure. For this step both column and beam signature curves are shown as solid curves and are necessary to formulate R_d of the limit state equation. The two dotted curves in figures 4.1 and 4.2 represent step 2 of the FORM procedure and occur when two of the three random variables have to be evaluated at the mean value.

The critical buckling coefficients that actually are the CUFSM related crucial output used for the DSM equations, are indicated in Figure 4.1 and Figure 4.2 for both steps. It is once more important to point out that the buckling coefficient that is required for global buckling is not obtained from the signature curve and shifts during a varied member length analysis. Thus, it is

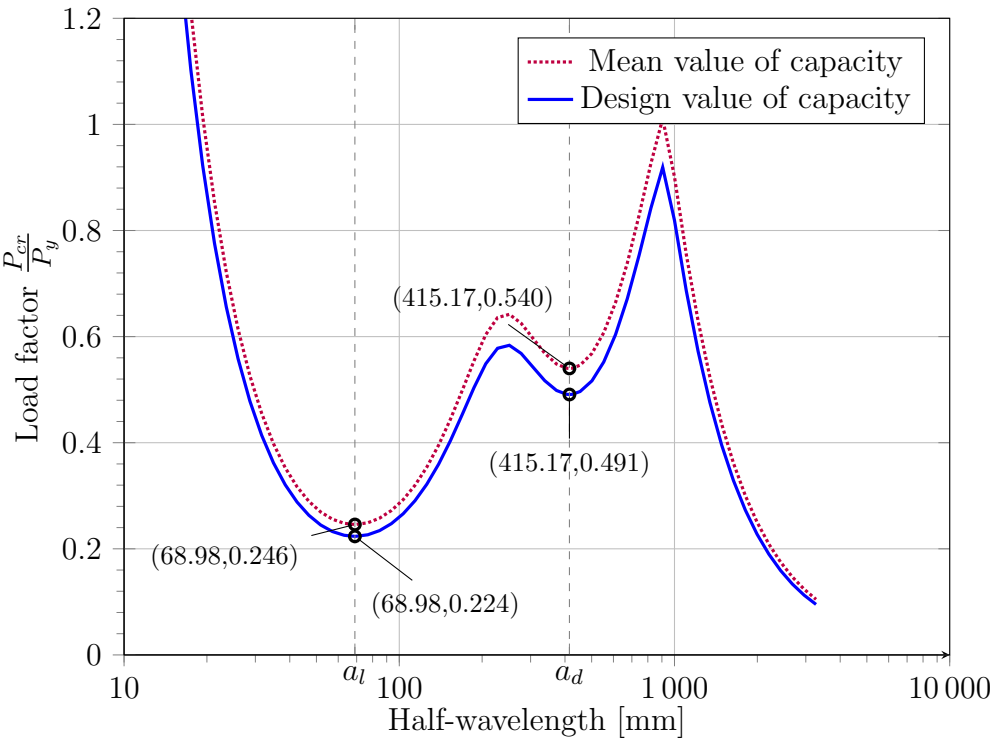

Figure 4.1: Signature curve of lipped C-section for member in pure axial compression

not indicated. The buckling coefficients that are marked do not change for the FORM steps 1 and 2 during an altering member length analysis. As this thesis deals with a lipped C-section, the critical buckling coefficients associated with local and distortional buckling are easily identified as the first and second local minima on the curves respectively. This was confirmed using the sharp corner model. However, the check of modal participation at the associated critical wavelengths (a) still needs to be performed at the converged design point of the reliability analysis to ensure each coefficient is still correctly associated with the right DSM equation.

For the next section multiple final design points, one for each analysed length, were determined, but the participation check is only shown here for the 1 m member as remarks can be extrapolated from the presented modal-participations. Tables 4.1 and 4.2 show the participation proportions for the three important FORM analysis design points for both compression and bending respectively. The points are shown in the order they are required for the FORM analysis. From the tables it is quite clear that meagre change in the participation occurs during the iterations of the FORM. This is true for final design points of longer compression or bending members as well, since the modal participations are not directly influenced by member length. Low participation change is also proven by the procedures performed in Section 3.2.3.3.

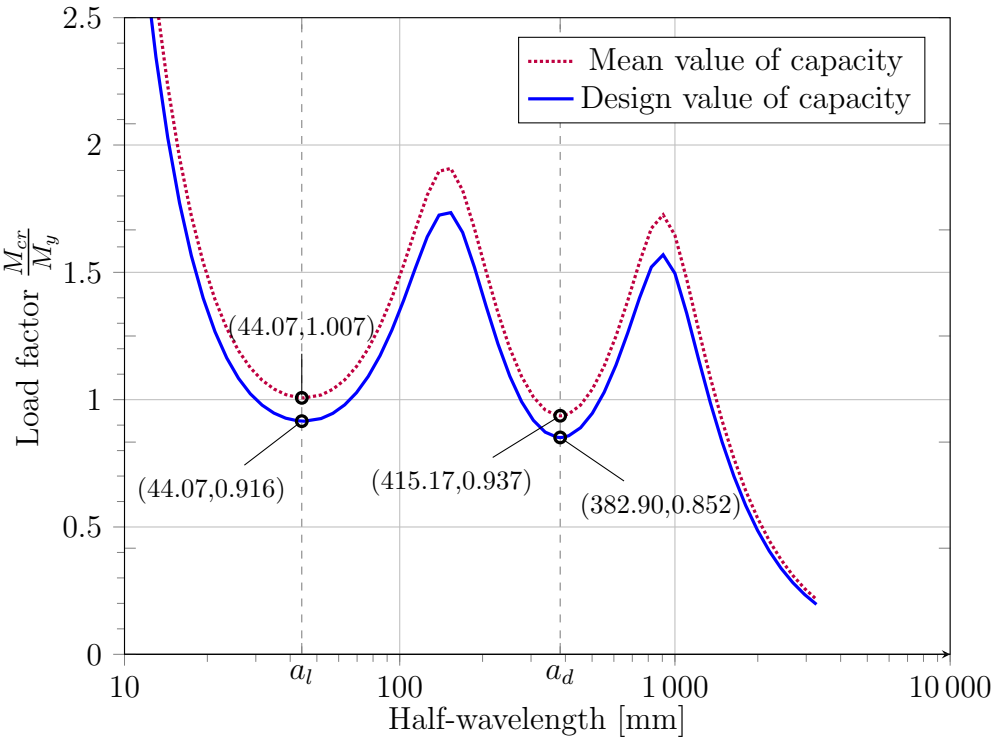

Figure 4.2: Signature curve of lipped C-section for member in unrestrained pure bending

Table 4.1: Modal participation during FORM of 1 m column member

			Participation in %			
Realisation of $\{X\}$	**Mode**	***a* in** [mm]	**L**	**D**	**G**	**O**
$\{x_d\}$	L	68.98	45.5	54.0	0.3	0.2
	D	415.17	3.5	93.5	3.0	0.1
$\{x_\mu\}$	L	68.98	45.5	54.0	0.3	0.2
	D	415.17	3.5	93.5	3.0	0.1
$\{x^*\}$	L	68.98	45.4	54.1	0.3	0.2
	D	416.32	3.5	93.5	2.9	0.1

Table 4.2: Modal participation during FORM of 1 m beam member

			Participation in %			
Realisation of $\{X\}$	**Mode**	***a* in** [mm]	**L**	**D**	**G**	**O**
$\{x_d\}$	L	45.97	21.1	77.9	0.5	0.5
	D	382.90	0.7	94.4	4.8	0.1
$\{x_\mu\}$	L	45.97	21.1	77.9	0.5	0.5
	D	382.90	0.7	94.4	4.8	0.1
$\{x^*\}$	L	45.97	21.0	78.0	0.5	0.5
	D	383.81	0.7	94.4	4.8	0.1

4.2 Reliability margin of lipped C-section in uniform axial compression

4.2.1 Resistance behaviour discussion

As the DSM equations are key components of the limit state equation in the reliability analysis, the DSM based capacities give insight into the reliability behaviour. Figure 4.3 shows the capacity of the column member for all three DSM failure modes as the length increases. Each failure mode is evaluated for the FORM steps mentioned in Section 4.1.

It is already clear from Figure 4.3 that the member capacity due to distortional buckling does not change with the length. This is true for distortional behaviour for the value used in design ($\phi P_{nd}(\{x_d\})$) and the capacity evaluated at the means of all random variables ($P_{nd}(\{x_\mu\})$). Distortional buckling capacity is independent of member length when looking at Equation 2.14 (see Section 2.2.4.3) and thus member capacity stays constant. Due to the distortional slenderness ratio of the chosen cross-section, the member distortional buckling capacity is never the limiting member capacity.

The local and global buckling capacities shown in Figure 4.3 are however a

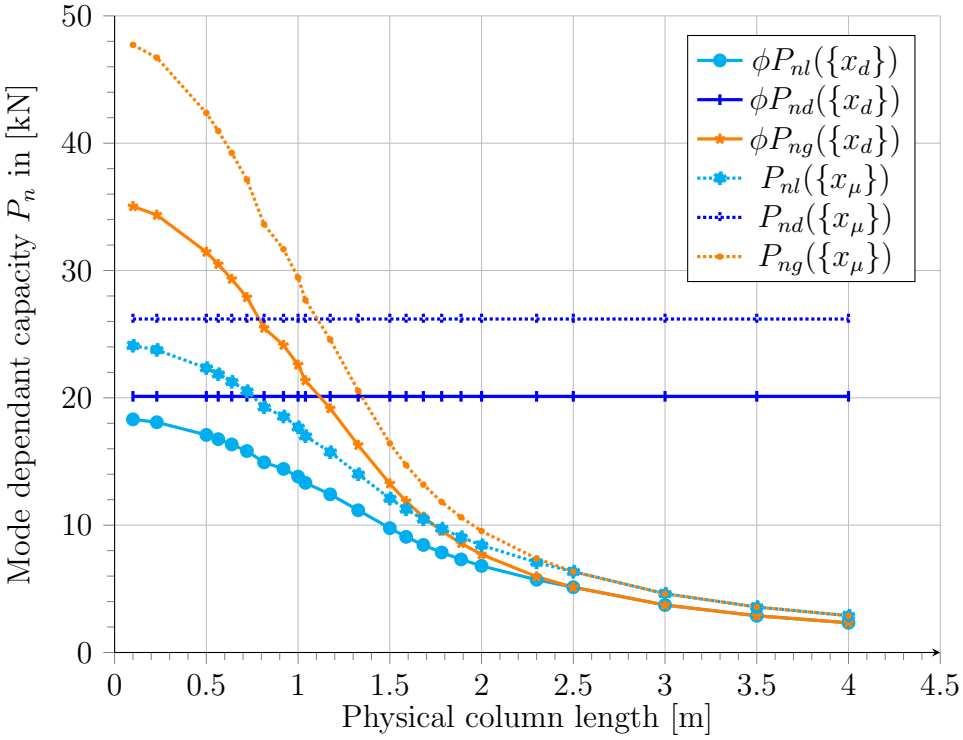

Figure 4.3: Axial compression capacity at the mean value and at value used in design for all possible failure modes

function of the member length. Local buckling is a function of the member length due to its interaction with the global buckling capacity. However, at a length of 2.5 m the local buckling slenderness (see Equation 2.11 in section 2.2.4.3) forces the local buckling capacity to equal the global buckling capacity. This is true for both the factored capacity ($\phi P_{nl}(\{x_d\})$) as well as the capacity evaluated at mean values of all random variables ($P_{nl}(\{x_\mu\})$) and is specifically related to the cross-section considered.

Also visible in Figure 4.3 is that design capacity from short lengths up to 2.5 m is dominated by local buckling ($\phi P_{nl}(\{x_d\})$), the lowest of the solid lines shown. From the 2.5 m length and longer, the capacity is limited by the global buckling capacity. From the procedural aspect of the DSM that the lowest mode dependent capacity determines member capacity this curve always represents the design resistance during the FORM algorithm of this thesis. Figure 4.4 shows the same graphs as in the former figure. However, only the limiting design resistance based on the factored local buckling capacity ($\phi P_{nl}(\{x_d\})$) is shown together with the mean capacities from all modes of failure.

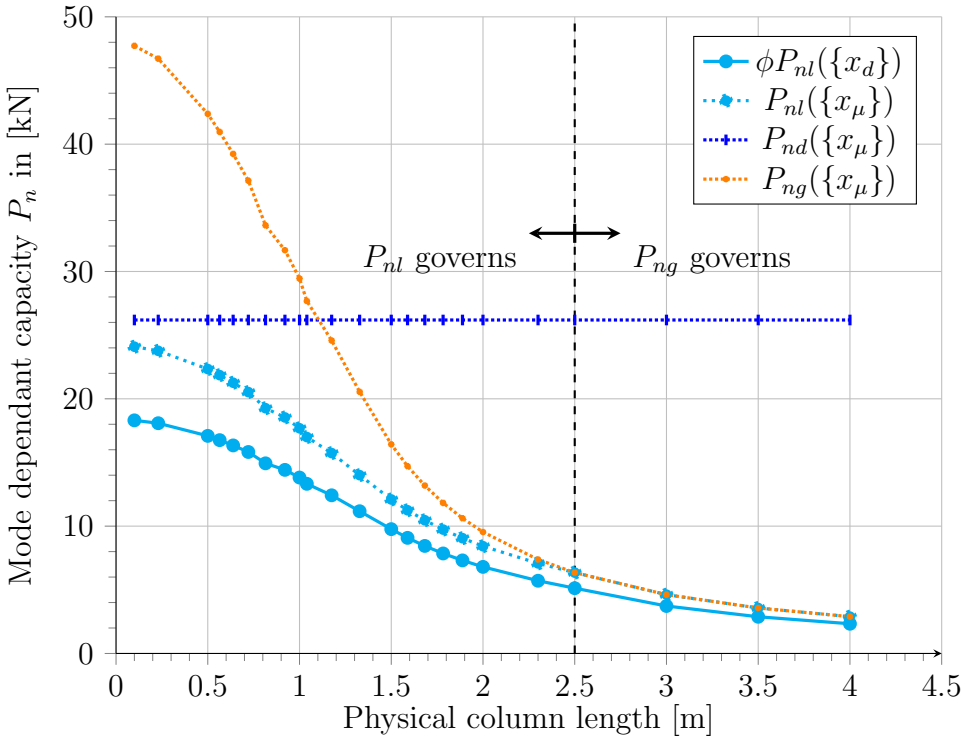

Figure 4.4: Design capacity versus mean capacity for all modes

The most important contribution to the safety included in the DSM is deducible from Figure 4.4, by considering the difference between each of the mean capacities and the design resistance ($P_n(\{x\}_\mu) - \phi P_{nl}(\{x\}_d)$). This

indicator is a direct result of the limit state equation being of the form of $G = R - r_d$ and the associated reliability index being a function of the difference of the means of these two variables ($\beta_R = f(\mu_R - r_d)$, see Section 2.4.3).

An analogous major contributor to the safety of DSM design is observable when each of the mode dependent mean capacities are normalised by the limiting design capacity ($P_n(\{x_\mu\})/\phi P_{nl}(\{x_d\})$). This is a similar notion that is captured by a safety factor. A visualisation of these ratios is seen in Figure 4.5. The lowest normalised capacity is found when the mean local buckling capacity is divided by its design value counterpart. Although the result is not strongly pronounced due to the scale of the abscissa, the lowest and limiting ratio drops from a value of 1.32 for 0.1 m to 1.24 for the 1.5 m length. The stagnation to the value of 1.24 can be explained by the change of the global buckling slenderness ratio that is inherent in the local buckling equation (see Equation 2.17a, section 2.2.4.3). For lengths shorter than approximately 1.5 m the global buckling slenderness (λ_c) is less than 1.5 and the converse is true for larger lengths. This means that the level of safety provided by global buckling capacity predictor Equation 2.8b is more consistent than by its counterpart, Equation 2.8a (see Section 2.2.4.3). An explanation for this is presented in the next section.

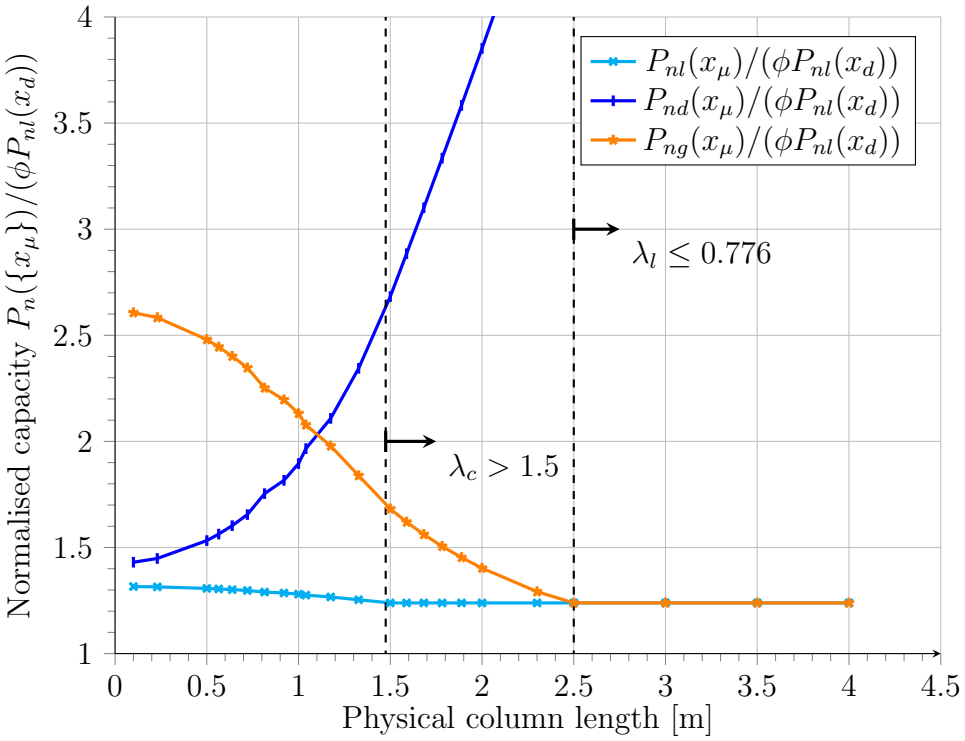

Figure 4.5: Axial compression capacity of the column normalised by the local buckling capacity

4.2.2 Reliability index

Influences on reliability that stem from the difference of the mean and design capacities is now clear. Figure 4.6 shows the reliability index across a larger member length spectrum associated with each of the three possible failure modes. Three different levels of reliability are obtained for each length. The magnitude of the reliability index depends on the mode of failure that the probabilistic resistance falls in. In this case, the lowest deterministic mode of failure falls in the local buckling mode. However, as was explained, from approximately 2.5 m onwards the local buckling capacity is equal to the global buckling capacity.

It is important to realise that trends of the reliability indices shown in Figure 4.6 correlate to the normalised capacity ratio of Figure 4.5. However the reliability index from the FORM analysis includes the probabilistic influences of the random variables.

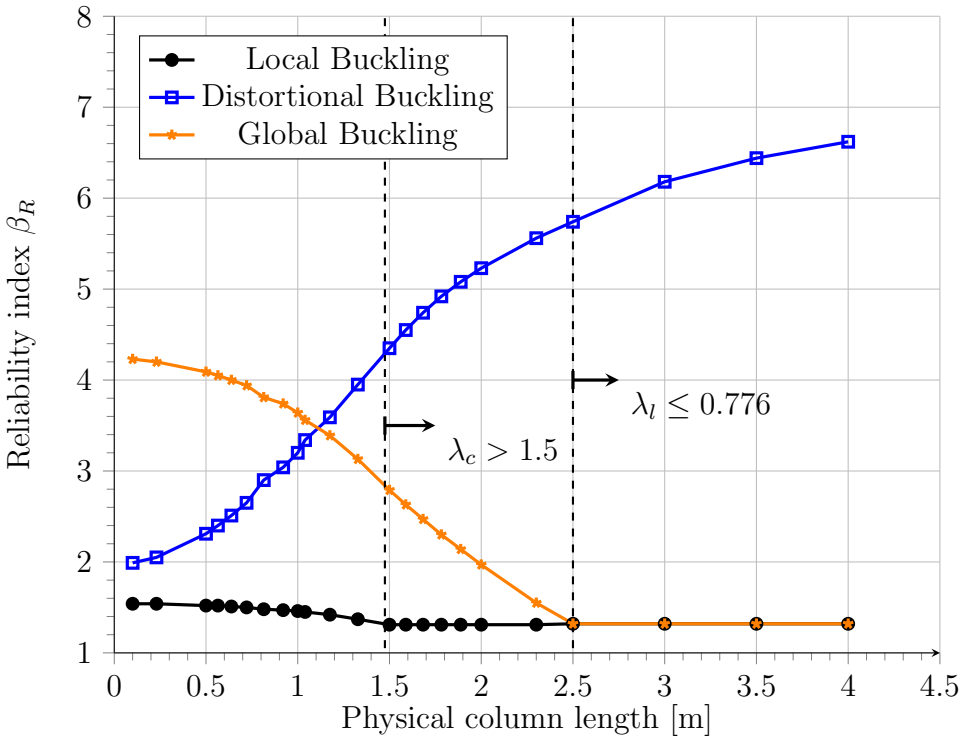

Figure 4.6: Reliability index for the various design modes versus the physical column length for the pure compression design

The limiting reliability index, seen in Figure 4.6, follows from the probabilistic local buckling resistance. More specifically this applies for lengths ranging from 0.1 m up to 2.5 m. Thereafter the limiting reliability index is the result of the global buckling behaviour. The drop in reliability is experienced

from a shift in the capacity prediction equation due to a change in slenderness. Figure 4.7 shows the influence which the global buckling prediction model has due to interaction with local buckling and the effect is visibly emphasised due to the localised and stretched abscissa.

The governing reliability index starts of at 1.45 for a 0.1 m long member, with a minimum of 1.31 at lengths larger than approximately 1.5 m. This relatively stagnant reliability index of 1.31 coincides once more with a global bucking capacity discontinuity (refer to Equation 2.8) that inherently affects the local buckling capacity predictor and has a decreasing tendency. A small increase in the reliability index is visible due to another discontinuity in the local buckling capacity prediction equation (2.11) when global buckling turns into the limiting strength predictor. The normalised capacity ratios of the previous section have been added to Figure 4.7 to show the correlated effect of the transitions between the capacity prediction equations.

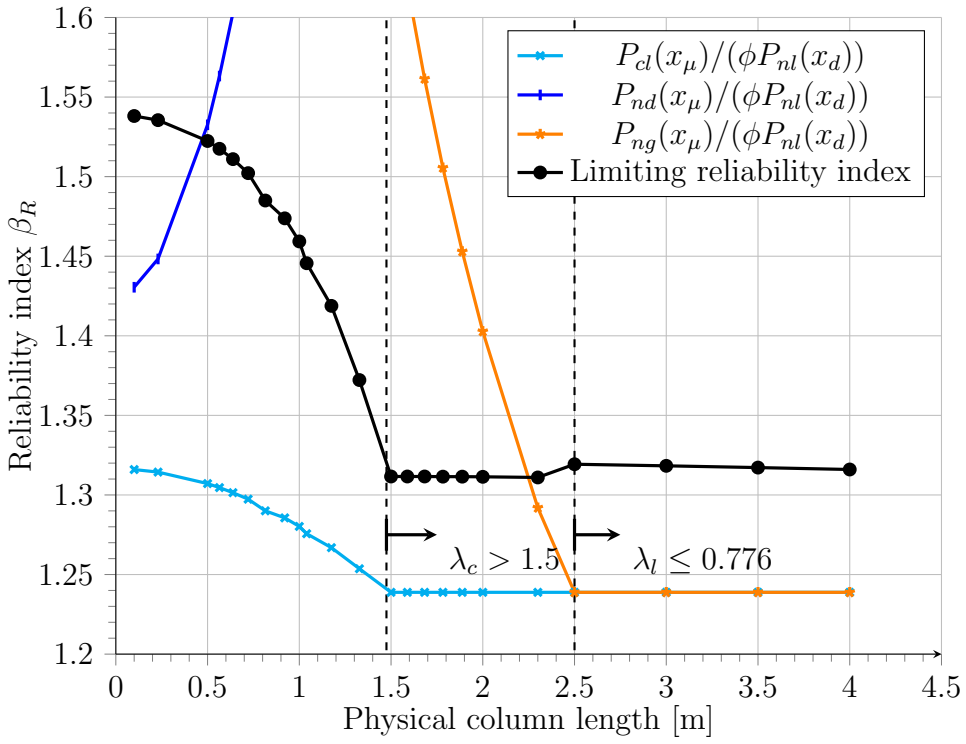

Figure 4.7: Reliability index for the various design modes versus the physical column length for the pure compression design

The real explanation for the drop in the reliability index is however found when considering the sensitivity factors of the random variables of the limit state model. Sensitivity factors and their behaviour are shown in Figure 4.8. Quite a significant drop in yield strength sensitivity is observed at a length close to 1.5 m. This once more corresponds to the discontinuity in the global

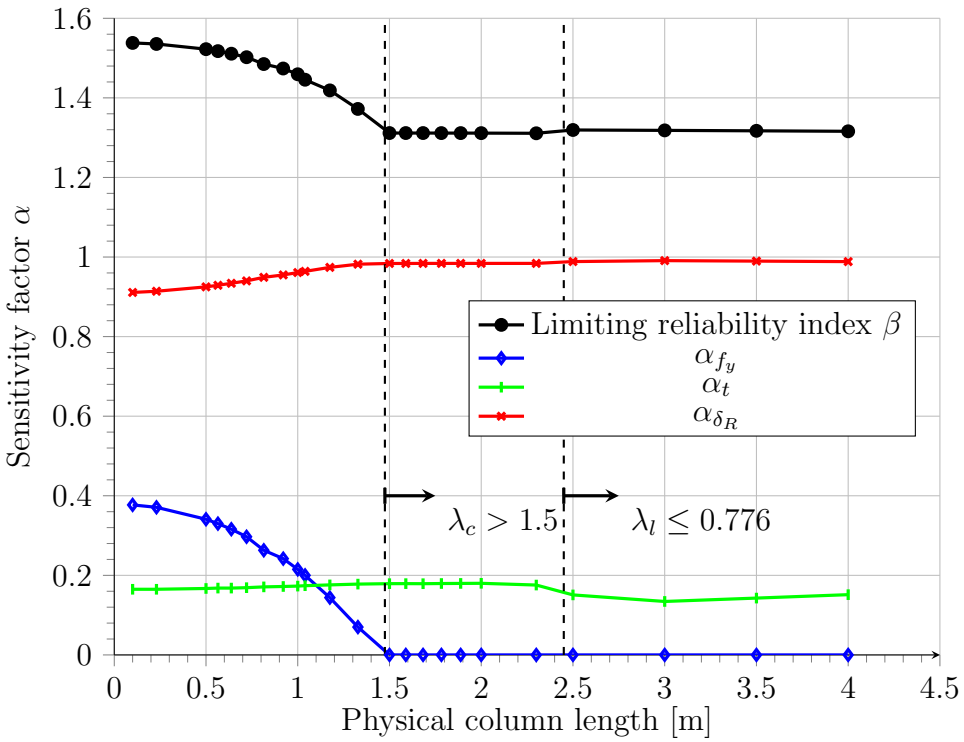

Figure 4.8: Sensitivity factors of random variables versus the physical column length for the pure compression design

buckling prediction equation.

Sensitivity drop for the yield strength can be explained from looking at Equation 2.8b repeated in Equation 4.2 below. The global buckling slenderness is also redefined in Equation 4.1. At lengths larger than approximately 1.5 m the cross-section fails due to torsional-flexural buckling ($P_{cr,e}$). The global buckling slenderness ratio from Equation 4.1 is squared in Equation 4.2, cancelling the yield stress variable out of the equation. Therefore the capacity predictor is no longer a function of yield stress as the torsional flexural buckling predictor is completely independent from this variable. The torsional flexural buckling capacity is only dependant on geometrical parameters. This causes the directional derivatives for the yield strength variable to be zero during the FORM analysis, resulting in a zero sensitivity factor.

$$\lambda_c = \sqrt{\frac{P_y}{P_{cr,e}}} \tag{4.1}$$

$$P_{ne} = \left(\frac{0.877}{\lambda_c^2}\right) P_y = \frac{0.877}{\left(\sqrt{\frac{\cancel{P_y}}{P_{cr,e}}}\right)^2 \cancel{P_y}} = 0.877 P_{cr,e} \tag{4.2}$$

This effect is carried over into the local buckling predictor equation. A slight

increase in reliability is however still seen when Equation 4.2 completely dominates the capacity prediction. This indicates that the model factor for this capacity predictor contributes more significantly to the reliability .

Now that it is established that the reliability is largely attributed to the global buckling prediction equation at lengths where the global buckling slenderness exceeds 1.5, the influence on the overall DSM reliability is better understood. From the results it is apparent that the reliability index is significantly lower than the target $\beta_{t_R} = 1.64$ as presented in Section 3.5.2. For the limit state model of this thesis, the model factor is chosen to cover the entire spectrum of the DSM equations and multiplied in with the prediction equation. The limit state model used for calibration by the AISI (see Section 2.4.5) on the other hand, does not cover the DSM specific limit state equation captured by the analysis presented in this thesis and may explain the cause for the low reliability index results presented here. The calibration model by the AISI also does not include the negligible sensitivity effect of the yield stress. To update reliability index results obtained by this dissertation, model factors may even be separately considered for each of the separate failure mode capacity prediction equations. However, since the reliability index is attributed to the partial factor which is the same for the full spectrum of DSM equations, the model factor in this thesis' limit state model was chosen to analyse the reliability from a similar approach.

When considering the reliability attributed to the global buckling capacity prediction model, an improvement in the reliability index may be expected due to the statistical attributes associated with the global buckling model factor. Ganesan and Moen (2012) provide such a model factor with an increased mean value, compared to the value currently used. This implies an increased reliability for global buckling slenderness and a potential bias of the current model factor when used for global buckling. However, the CoV of the model factor by Ganesan and Moen (2012) for global buckling also increases significantly more than the mean value. This in turn may have a more negating effect on the reliability index and should produce even lower reliability results than expected here. This influence would not have been conceivable, if the slenderness spectrum had not been investigated.

4.3 Reliability margin of lipped C-section in pure unrestrained bending

4.3.1 Resistance behaviour discussion

The capacity behaviour for unrestrained beam members considering all three possible failure modes again provides insight into the reliability behaviour for a range of beam lengths. Figure 4.9 shows the bending capacity of all three failure modes evaluated for values used in design ($\{x_d\}$) as well as the state when all random variables are at their respective mean values ($\{x_\mu\}$). For the local and distortional buckling failure modes the signature curves of Section 4.1 provide the required load factor input for these capacities.

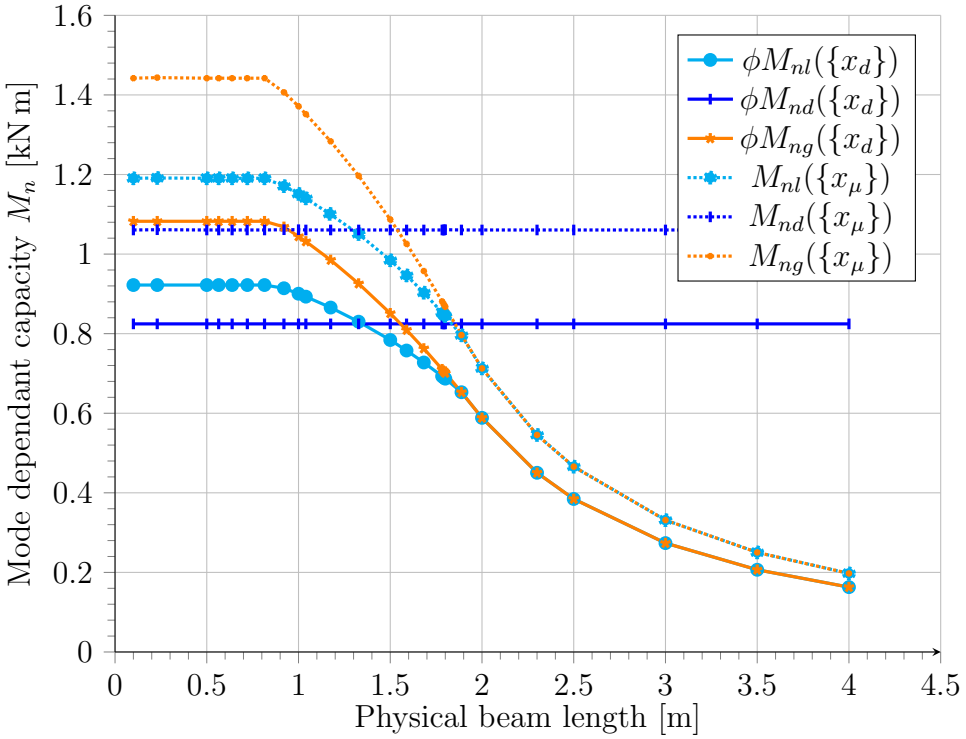

Figure 4.9: Bending moment capacity at mean value and at values used in design for all possible failure modes

As mentioned, the distortional buckling capacity is independent of the length and is constant over the range lengths. However, distortional buckling only dominates the design capacity for member lengths from 0.1 m up to approximately 1.32 m and is visible by the lowest solid line. This is an attribute that is directly related to the lipped C-section and the length geometry of the beam. From these properties the moment capacity predictions from distortional buckling failure are never a result of the section moment due to

the first yield in the top fibre.

Member capacity is governed by distortional buckling from member lengths up to 1.32 m, by local buckling for lengths between 1.32 m and 1.88 m, and by gloabl buckling for lengths longer than 1.88 m, as can be seen in Figure 4.10. Due to the global buckling interaction included in the local buckling capacity DSM predictor, the capacity reduces as a function of the length. At lengths larger than about 1.88 m the local buckling strength prediction model is equal to the global buckling strength prediction model. This is true for both the capacity determined from variables used for design as well as when capacities are evaluated at the mean value of all random variables.

The limiting member capacity is consequently a result of all three failure modes of the DSM, depending on the length of the beam. Figure 4.10 shows the design capacity of the lipped C-section from the limiting failure modes as a function of the length. The design capacity curve follows the same behaviour associated with the example lipped C-section in the DSM Design Guide (Schafer, 2006*a*).

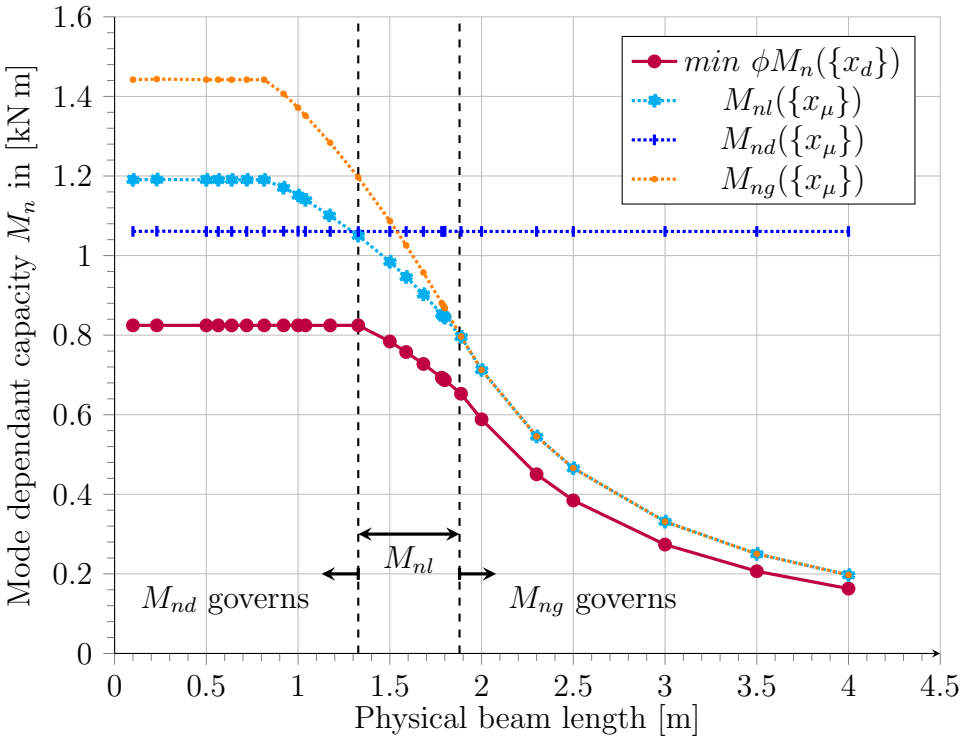

Figure 4.10: Deterministic load effect (design capacity) versus mean capacity for all modes

Clearly deducible from the Figure 4.10 is that the lowest probabilistic capacity evaluated at the mean value for each length is predicted by the same

design resistance failure mode. This implies that the limiting reliability index found at each discrete length results from the same failure mode. Failure predictor deviation for the design value and the probabilistic mode of failure are an unfavourable aspect when using the DSM in design. The above results nevertheless imply that the DSM is a sound strength prediction model when considering equal randomness of the mode of failure.

The most significant contribution to the reliability of design following the DSM for beam members can be captured by the ratio of the mean predicted capacity to the limiting design bending capacity. A plot of the normalised capacities with respect to the lowest factored resistance is shown in Figure 4.11. A relative noticeable drop occurs for the limiting ratio at around 0.89 m when the capacity limit changes from distortional buckling to local buckling. The lowest proportion capacity occurs from a length of approximately larger than 1.88 m from whereon the ratio is relatively constant. Stabilisation of the ratio coincides with the capacity prediction curve changing to the lateral-torsional buckling capacity predictor (see Equation 2.17a in Section 2.2.4.4).

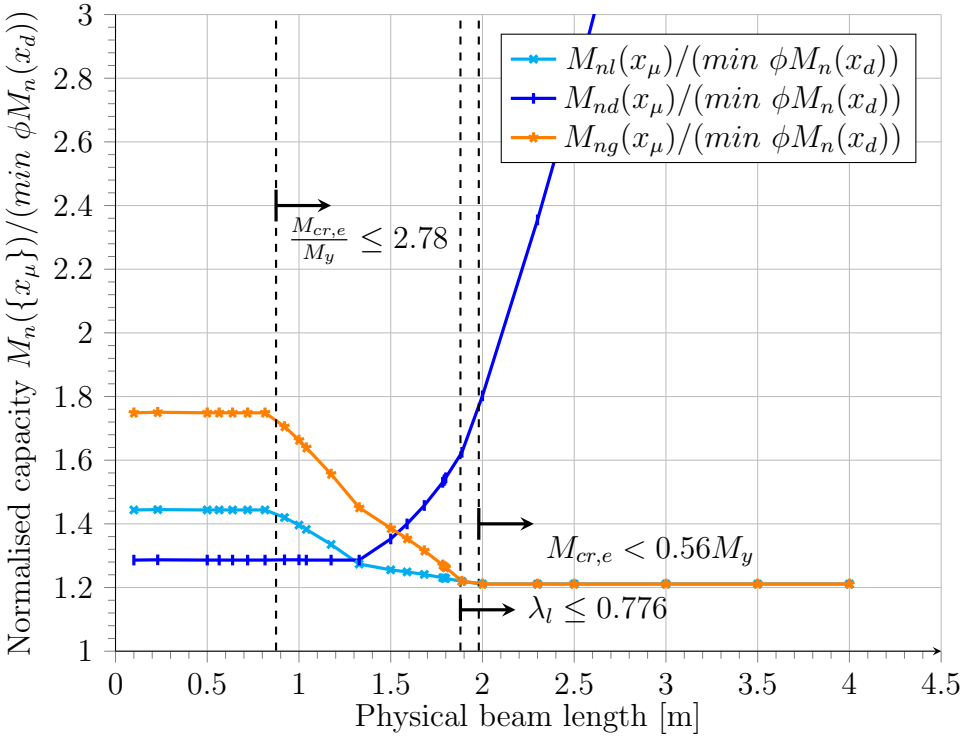

Figure 4.11: Bending moment capacity of the beam normalised by the local buckling capacity

4.3.2 Reliability index

The ratio of the mean capacity to the design capacity partially indicates the main contributing factor of the reliability. Full probabilistic influences are only given by the reliability index resulting from the FORM procedure. Figure 4.12 shows how the reliability index for beam members designed according to all failure modes covered by the DSM behaves. The governing reliability index for each discrete length analysed results from the design point falling in the same failure mode as the design capacity. Limiting reliability index behaviour is seen to drop as the DSM prediction equations shift and member design is determined by the local buckling capacity in the limit state equation. This can be seen in the figure at the diverging blue line, which represents the reliability margin being the result of probabilistic distortional buckling and design local buckling capacity. The reliability index trend as a function of length seen in Figure 4.12 correlates to the safety ratios indicated in Figure 4.11 on the previous page.

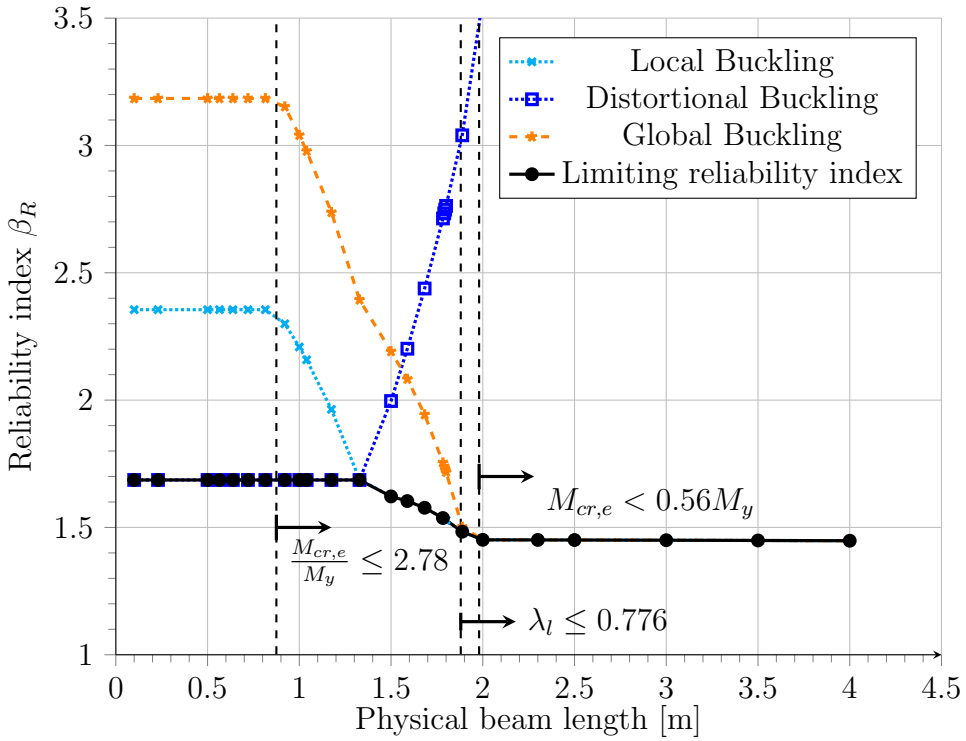

Figure 4.12: Reliability index for the various design modes versus the physical beam length for the pure bending design

Figure 4.13 shows more clearly the limiting reliability index behaviour over the range of member lengths analysed. Also shown in the figure are the ratios of mean and design capacity for each failure mode. The reliability index associated with the distortional capacity prediction region is 1.69 and applies

for member lengths from 0.1 m to lengths of 0.815 m. A strong correlation between the limiting normalised capacities and the limiting reliability indices is naturally identified. As soon as the global buckling prediction bending capacity prediction equation (2.17) takes influence on the local buckling capacity prediction equation, the reliability drops to a relatively consistent value of 1.45. A decreasing trend is sill visible. The reliability index of 1.45 is the result of the critical elastic later-torsional buckling moment that governs which can be strongly related to the normalised bending capacity behaviour of Section 4.3.1. A dropping reliability influence from global buckling is already included from member lengths of approximately 1.3 m up to 1.88 m

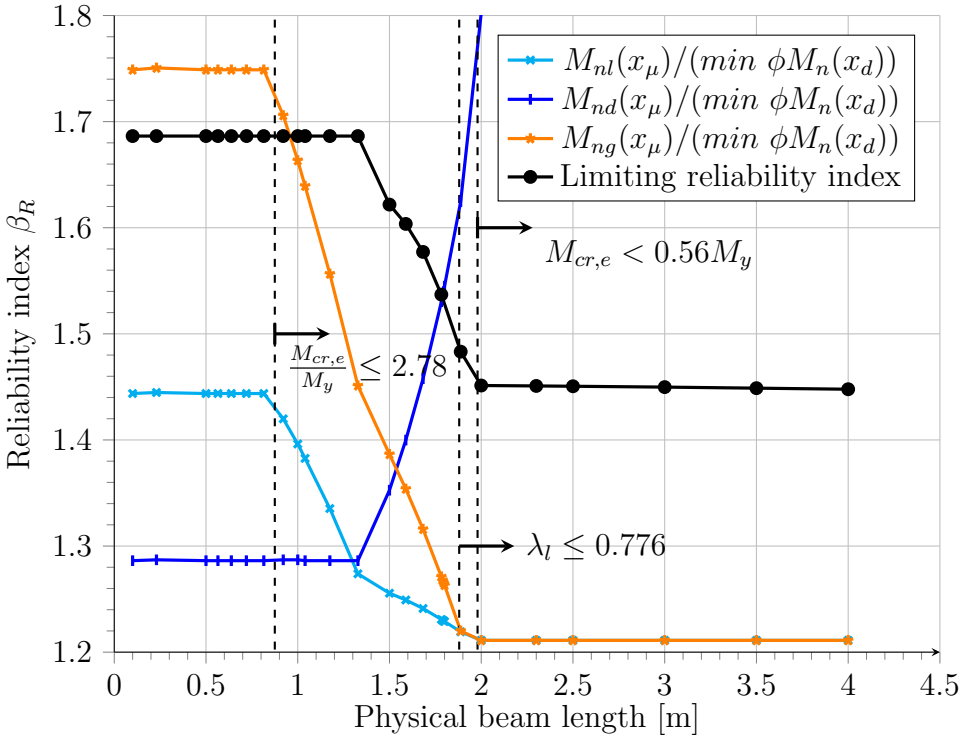

Figure 4.13: Reliability index versus the physical beam length for the pure bending design

From inspection of Figure 4.14, the decrease in reliability is once more a result of the decreased sensitivity of the yield strength and the corresponding increase of the model factor sensitivity for member lengths larger than about 1.3 m. In other words the reliability index decreases due to higher uncertainty of the model factor. When considering the prediction equation that governs at these lengths, it is quite clear that the yield stress variable has no influence in the predictor equation (see Appendix A.1). The design capacity at larger lengths is directly determined from the critical elastic buckling moment where the use of a characteristic yield strength has no influence on the reliability. Consequentially reliability for larger lengths is more a function of the slen-

derness parameters such as the moments of inertia of the section, the area of the section and the warping torsion constant which are all affected by the thickness variable.

The model factor however still dominates the influence on the reliability for all lengths and the statistics used for it, momentarily cover all ranges of slenderness and are applicable to all direct strength equations. The current statistics for the model factor of members subject to bending have a mean of 1.09. This already suggests conservatism of the prediction equations. For longer members a similar mean model factor is to be expected since the critical elastic flexural-torsional buckling moment is an exact solution of a differential equation. Nonetheless, improved reliability could be expected for longer members if separate model factors for all three failure modes are used, but only if the uncertainty of the updated global buckling model factor is lower than the current overall average model factor used. No such statistics database was found in current literature and will take significant research to be developed.

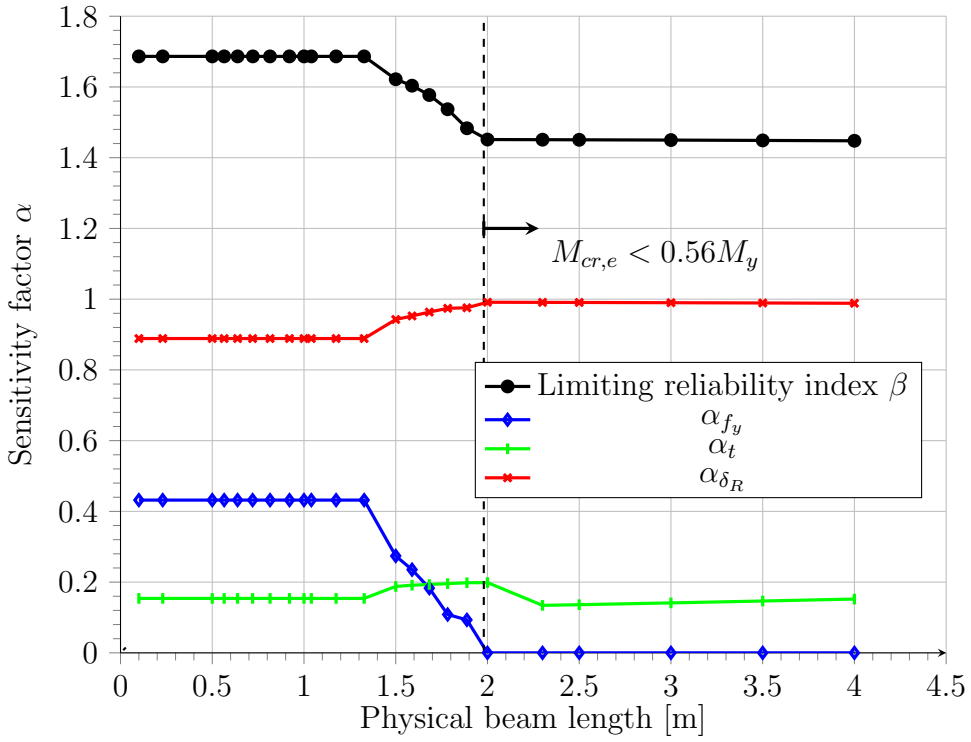

Figure 4.14: Sensitivity factor of random variables versus the physical beam length for the pure bending design

4.4 Partial factor behaviour

Up to this stage the reliability margin has been explained from the behavioural point of view of the probabilistic variables. However, the partial factor has the largest influence on the achieved reliability from the design standard's perspective and must therefore also be discussed. This section deals with the behaviour of the reliability index from the influence of the partial factor and importantly brings it into context with the suggested target β_{t_R}.

4.4.1 Reliability margin of lipped C-section in uniform axial compression

For the length analysis it was shown that the lowest reliability index results from the local buckling-strength prediction equation of the DSM. A minimum reliability index of $\beta_R = 1.31$ was calculated based on the procedure followed by this thesis. Although the interaction of global buckling and local buckling being the largest contributor to this result, the reliability for the local buckling mode was still less than that of the pure global buckling capacity prediction equations.

It was already established that the reliability indices based on the normal distribution assumption of the model factor produced conservative reliability results. Nevertheless the reliability index still needs to be put into perspective to the targeted reliability.

Figure 4.15 shows the reliability index based on the distribution assumptions explained in Chapter 3 for a discrete member length of 2.3 m. At this length the compressed member still falls in the prediction behaviour of the DSM local buckling capacity prediction equation. Thus the model factor that was assumed for the analysis is highly applicable. Figure 4.15 shows that the reliability index behaves linearly increasing when the partial factor decreases. This is the aimed influence of the partial factor on the reliability. Highly important is that when looking at the reliability index achieved by the current SANS 10162-2 partial factor, the target reliability of the resistance side based on the AISI calibration is not achieved. A reduction in the partial factor is thus required.

Additionally visible from the graph based on the conservative assumptions in this dissertation is that a reduction in the partial factor from the current value of $\phi = 0.85$ to the Canadian specified value of $\phi = 0.8$ would not achieve the the resistance component reliability of $\beta_t = 1.961$, associated with that partial factor, either. Freitas *et al.* (2013) found the same to be true based on their investigation into a resistance factor which is the inverse definition of the partial factor. The calibrated partial factor according to Freitas *et al.* (2013) is based on the same dead load to live load ratio of 1 to 5 as was assumed

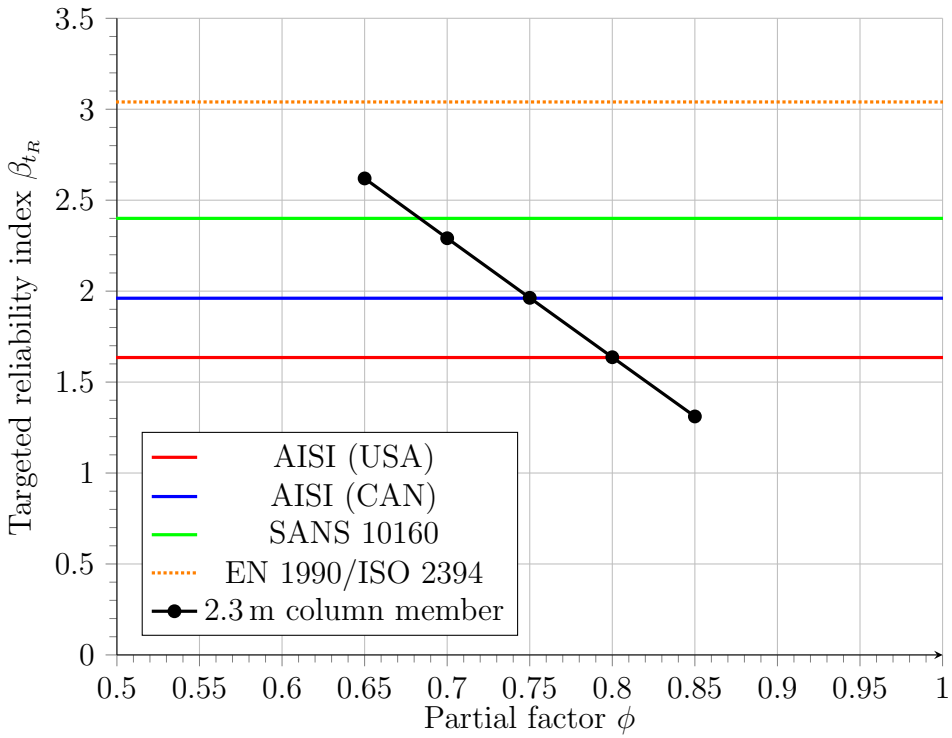

Figure 4.15: Reliability index as a function of the partial factor in comparison to the resistance side target reliability for a column member

in the AISI calibration and stands at a value of 0.88. This corresponds with a targeted overall reliability of 2.5. From Figure 4.15 a partial factor for an overall reliability index of $\beta_t = 3.0$ (CAN) is proposed as $\phi = 0.77$ given the α_R presented by the AISI.

Based on the distribution assumptions of the random values used for this thesis, a predicted partial factor of $\phi = 0.67$ would achieve the target reliability of $\beta_t \alpha_R = 3.0 \cdot 0.8 = 2.4$ based on the conservative sensitivity factor of EN 1990 and the accepted overall reliability index for member design according to SANS 10160-Basis of structural design. This value is not a newly calibrated value of the partial factor, but it is a partial factor associated with DSM capacity prediction that achieves the overall reliability index associated with member design based on SANS 10160 for all modes of failure. Furthermore $\phi = 0.67$ shows the significant reduction in the partial factor required to achieve the South African accepted target reliability index.

4.4.2 Reliability margin of lipped C-section subject to unrestrained bending

From the beam member length reliability index results it was found that the lowest reliability index was associated with long beams failing due to global

buckling. The reliability index for members failing from global buckling is a relatively consistent value of $\beta_R = 1.45$. Even thought this reliability is based on the lateral-flexural buckling mode of failure, the reliability is still a direct result of the prescribed partial factor. Therefore the influence on the reliability at a member length of 2.3 m falling in the lateral-torsional buckling predictor equation and the partial factor influence was inspected.

Again all reliability results presented here are based on the partial factor and the probabilistic distribution of variables has been shown to produce conservative β_R results (see Section 3.5.1.2). However, the influence of the partial factor on reliability needs to be compared to suggested target values from literature.

Figure 4.16 shows once more that a reduced partial factor has a linearly increasing effect on the reliability for the range of partial factors considered. Once again the highly important fact that the target reliability index is not achieved by both the current partial factor (AISI (USA)) and the Canadian partial factor (AISI), is visible.

Based on the fact that reliability results are conservative when considering a normal distribution of the model factor, the performance of the prescribed

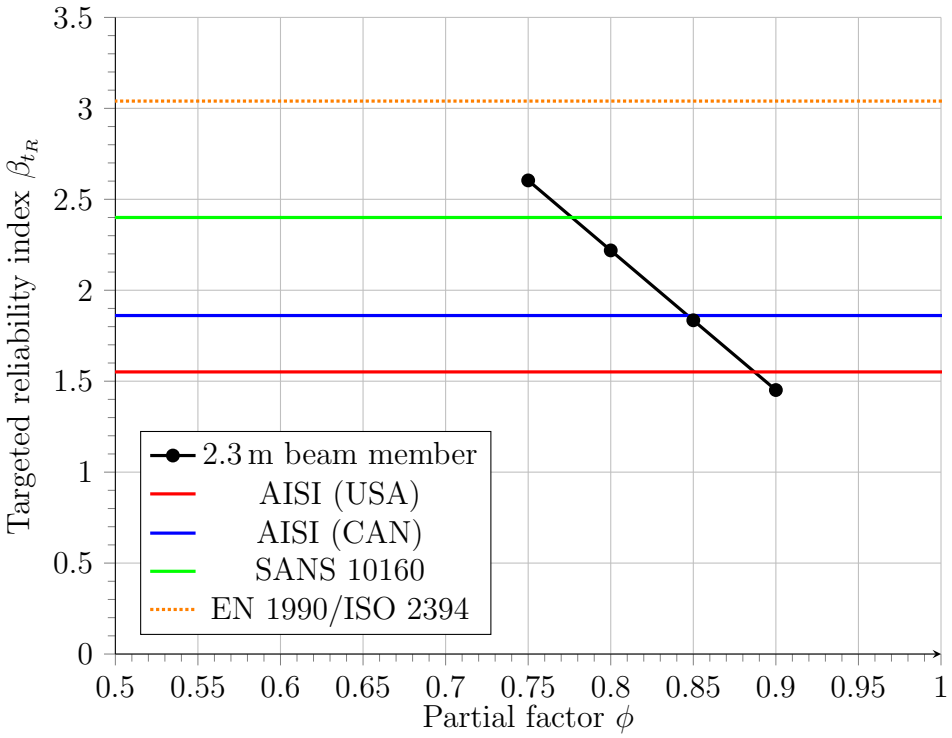

Figure 4.16: Reliability index as a function of the partial factor in comparison to the resistance side target reliability for a beam member

partial factors to achieve the aimed target reliability is much better. This can directly be related to the more prudent model factor statistics that are assumed in this thesis for the reliability analysis.

As no improved alternative for the global buckling member resistance model factor exists, a prediction for the required target reliability based on SANS basis of structural design can be made using the conservative resistance sensitivity. A value of $\phi = 0.77$ would achieve the required reliability of $\beta_{t_R} = 2.4$ for all modes of failure predicted by the DSM. Once again this is not a calibrated partial factor as it does not consider the reliability results of all member lengths nor is it economical for all cross-sections. The reliability index achieved by this partial factor value is representative for the entire DSM design method, since the model factor chosen is independent of the cross-section or failure mode. Nevertheless, the value of $\phi = 0.77$ shows that a considerable reduction of the partial factor necessary to reach SANS 10160-Basis of structural design recommended value of $\beta_t \alpha_R = 3.0 \cdot 0.8 = 2.4$.

Chapter 5

Conclusions and Recommendations

This thesis presents a procedure for calculating the reliability of cold-formed steel members designed according to the Direct Strength Method. The procedure requires the use of the Fist Order Reliability Method in combination with the constrained Finite Strip Method. Literature investigated for reliability analysis as well as the design of cold-formed steel members according to the Direct Strength Method presented no exact analysis algorithm for the combination of both procedures. An algorithm was developed considering three essential random variables from literature, namely: the thickness of a member, the yield strength of cold-formed steel as well as the model factor of the resistance predictor. The model factors considered, incorporate uncertainty associated with the use of the Direct Strength Method including procedural aspects of the design procedure.

The reliability of cold-formed members designed according to the Direct Strength Method as per SANS 10162-2 was investigated. Reliability was assessed for column members designed for pure concentric axial compression and laterally-unrestrained beam members designed for pure bending about the strong axis. Reliability indices ranging from 1.31 up to 1.67 were calculated for columns and reliability indices ranging from 1.45 up to 1.81 for beams.

All assessed reliability indices are a direct result of the statistical parameters and distributions assumed for the investigation. Although the assessed reliability results are a direct consequence of these assumptions and the cross-section investigated, similar reliability results are nonetheless expected for other profiles since the model factor uncertainty dominates and the statistics used for it are applicable for all pre-qualified sections of the Direct Strength Method. Even though reliability indices are specific to member cross-sections, loading and length, almost all mode of failure associated limiting reliability indices were calculated by increasing the slenderness of the member. Reliability

for a column member designed to resist distortional buckling failure was not determined.

This thesis also presented a discussion on what target reliability should be applicable within the South African context. A much lower sensitivity of the resistance than is expressed by the conservative EN 1990 value of $\alpha_R = 0.8$ may be suitable, if the variable load is the dominating influence for the design load case. Target values that are presented from the AISI my be accepted, if cold-formed structures are highly redundant and failure is of lower consequence. The Direct Strength Method is however not limited to structures with high redundancy and since the sensitivity of the load effect that corresponds to a low sensitivity of resistance are not considered by the load combination factor already established for SANS 10160-1, lower AISI β_{t_R} values are not motivated. Therefore the conservative approach by EN 1990 of $\alpha_R = 0.8$ and $\beta_t = 3.0$ for SANS should be targeted.

Even so, the partial factors used in SANS 10162-2 (AUS\NZ Standard) do currently not even achieve required reliability according to the sensitivity on the resistance side that were assumed by the AISI in the calibration. Target values of $\beta_t\alpha_R = 1.635$ and $\beta_t\alpha_R = 1.551$ for compression and bending design respectfully are not ensured for all the member lengths analysed and reductions in the resistance partial factors are recommended. Nevertheless, additional sufficient reliability may still be achieved form the load factors used in the South African loading standard. This depends on the ultimate loading of interest and the inherent sensitivity factors. Load effect sensitivity factors are expected to be significantly higher for load combinations with high viable load contribution. Future investigation is recommended on the load effect contribution to the reliability margin as a result.

From results obtained where global buckling is the critical failure mode, it is clear that for longer members all reliability is achieved by the partial factor. The safety relating to prescribing the yield strength as characteristic value in the design process has no influence when global buckling dominates the failure mode.

A reason for the current prescribed partial factor not ensuring the required reliability is that a single partial factor is applied for all failure modes. One partial factor for one type of member design may be uneconomical due to the fact that specific Direct Strength Method equations are better failure predictors than others. It is therefore recommended that the design procedure includes one partial factor for each type of design failure mode. Three partial factors are recommended for members designed in compression and three for members designed for bending. It may be more appropriate to apply different partial factors to the three failure modes. This is the most important conclusion of this

study. Therefore it is recommended that the partial factors be reinvestigated so that consistent reliability may be achieved across all elastic stability failure modes.

The limit state equation considered is of a simple nature, nevertheless the complexity of the reliability margin involves an integrated process of combination of the Direct Strength Method, Finite Strip Method and the First Order Reliably Method. An algorithm for this was presented in this thesis. The analysis algorithm has been critically assessed in terms or reliability index output and is deemed to oversimplify certain Direct Strength Method aspects. An analysis using one model factor across all failure modes has been presented in this thesis.

Future work should consider to evaluate the reliability using a model factor for each elastic stability mode separately. This was beyond the scope of this dissertation. Literature by Ganesan and Moen (2012) suggests such model factors for members in compression, based on various failure modes. It is suggested that model factors for different failure modes for members in bending be developed in the future.

Considering model factors that cover test-to-predictor ratios for each mode of failure can result in different reliability in certain failure modes than the ones found by this research. This depends largely on the variability of the model factor, which has significant influence on the assessed reliability due to the sensitivity of this variable. A slightly higher mean model factor model factor for columns failing in global buckling by Ganesan and Moen (2012) was found together with a significant larger variation than the variation used in this dissertation. Hence the reliably achieved by the DSM member design will be expected to especially not meet the aimed target reliability for global buckling.

For column members of the cross-section considered, distortional buckling is never the critical failure mode. When the columns fail due to local buckling the dominating variable that influences reliability is the model factor. For shorter columns the yield strength is the second most influential random variable but this decreases as member length increases and the global-local buckling interaction is more dominated by the global buckling influence. When pure global buckling is the critical mode, the yield stress has no influence. The influence of the thickness variable on the reliability is quite minor but consistent over all failure modes.

When considering beam members all Direct Strength Method associated failure modes were observed. The model factor again dominates the assessed reliability for all three failure modes. For distortional buckling the yield

strength also plays a relatively significant role in the reliability. Increased sensitivity of the Direct Strength Method beam equations to the model factor is observed for longer lengths when local buckling is critical. This is directly related to the decrease in sensitivity of yield strength that is linked with the global buckling failure mode. For even longer beams the sensitivity to the yield stress becomes zero, when global buckling, specifically elastic lateral-torsional buckling, becomes critical, which is a pure stability prediction equation. The thickness sensitivity is again relatively minor and consistently so over all failure modes.

Since model factors for various member failure modes for compression members have been developed in literature, prospective research for reliability analyses for the three failure modes presents itself. The reliability can be reassessed using failure-mode-specific model factors for column capacity predictions. However, this requires that the failure mode of the cross-section is consistent with the model factor used. Based on those outcomes, a partial factor needs to be calibrated to each mode of failure. For bending it seems no failure-mode-specific model factor statistics are present in literature that could be used for such an analysis. Another recommendation is therefore that a database of model factor statistics relating to modes of failure needs to be developed first. This can be done from testing but also by re-analysis of existing test data.

All of the above should be considered when re-investigating the partial factor. Although reliability results presented are considered independent of the specific profile used, for a failure-mode-specific partial factor calibration, a large set of cross-sections that fall within the limits of the Direct Strength Method should be investigated. A model factor based on the cross-section's failure mode must then be used to establish profile based reliability. Once a database of profiles' reliability has been created, the partial factor for each cross-section can be back calibrated to achieve the desired SANS resistance based reliability. All cross-section dependant partial factors can then be statistically analysed to find single failure- mode-dependant partial factors achieving SANS required reliability. This is suggested to provide economical partial factors for all modes of failure. Partial factors presented in this thesis aim to provide an approximation for such a partial factor, but at the same time ensure the SANS based reliability for all modes of failure.

All reliability indices were found when the probabilistic resistance and the design resistance were of the same failure mode. This is a strong advocate for the Direct Strength Method as a prediction model. Although it is not the aim of a reliability analysis to be conservative, but rather as realistic as possible, the determined reliability indices are deemed conservative estimations due to the assumption of the model factor having a normal distribution. Still reliability indices as low as 1.31 have been found for column members failing

in local buckling and thus future research in this field is warranted.

Finally, although column and beam Direct Strength Method equations follow the same fundamental concepts, it is recommended that future research is separated due to the various applicable model factors.

References

American Iron and Steel Institute, Canadian Standards Association and Camara Nacional de la Industria del Hierro y del Acero (2012). *North American specification for the design of cold-formed steel structural members.*

Bjørhovde, R. (1972). *Deterministic and probabilistic approaches to the strength of steel columns.* Ph.D. thesis, Lehigh University.

Breitung, K. (2015). 40 years FORM: Some new aspects? *Probabilistic Engineering Mechanics*, vol. 42, pp. 71–77.

British Standards Institution (2002). *Eurocode 1990 - Basis of Structural Design.* BSI, London.

Cook, R.D., Malkus, D.S., Plesha, M.E. and Witt, R.J. (2007). *Concepts and applications of finite element analysis.* John Wiley & Sons.

Ellingwood, B. and Galambos, T.V. (1983). Probability-based criteria for structural design. *Structural Safety*, vol. 1, no. 1, pp. 15–26.

Freitas, M.S., Brandão, A.L. and Freitas, A. (2013). Resistance factor calibration for cold-formed steel compression members. *Rem: Revista Escola de Minas*, vol. 66, no. 2, pp. 233–238.

Ganesan, K. and Moen, C.D. (2012). LRFD resistance factor for cold-formed steel compression members. *Journal of Constructional Steel Research*, vol. 72, pp. 261–266.

Gilbert, B.P., Savoyat, T.J.-M. and Teh, L.H. (2012). Self-shape optimisation application: Optimisation of cold-formed steel columns. *Thin-Walled Structures*, vol. 60, pp. 173–184.

Haldar, A. and Mahadevan, S. (2000). *Reliability assessment using stochastic finite element analysis.* John Wiley & Sons.

Hancock, G.J., Kwon, Y.B. and Bernard, E.S. (1994). Strength design curves for thin-walled sections undergoing distortional buckling. *Journal of Constructional Steel Research*, vol. 31, no. 2, pp. 169–186.

Holický, M. (2009). *Reliability analysis for structural design.* AFRICAN SUN MeDIA.

Holický, M., Retief, J.V. and Sỳkora, M. (2015). Assessment of model uncertainties for structural resistance. *Probabilistic Engineering Mechanics.*

International Organization for Standardization (1998). *General principles on reliability for structures - Principes généraux de la fiabilité des constructions.* ISO, Geneve.

Li, Y.-Q., Shen, Z.-Y., Wang, L., Wang, Y.-M. and Xu, H.-W. (2007 April). Analysis and design reliability of axially compressed members with high-strength cold-formed thin-walled steel. *Thin-Walled Structures*, vol. 45, no. 4, pp. 473–492.

Li, Z., Abreu, J.C.B., Leng, J., Ádány, S. and Schafer, B.W. (2014). Review: Constrained finite strip method developments and applications in cold-formed steel design. *Thin-Walled Structures*, vol. 81, pp. 2–18.

Li, Z. and Schafer, B.W. (2010). Buckling analysis of cold-formed steel members with general boundary conditions using CUFSM: conventional and constrained finite strip methods. In: *Twentieth International Specialty Conference on Cold-Formed Steel Structures. Saint Louis, Missouri, USA: November 3&4.*

Lopez, R.H. and Beck, A.T. (2012). Reliability-based design optimization strategies based on FORM: a review. *Journal of the Brazilian Society of Mechanical Sciences and Engineering*, vol. 34, no. 4, pp. 506–514.

Mori, Y., Takada, T. and Idota, H. (2002). Practical method to determine load and resistance factors used in limit state design. *1 st ASRNET.*

Nowak, A.S. and Collins, K.R. (2012). *Reliability of structures.* CRC Press.

Petschacher, M. (1997). VaP variable processor, version 1.6. *ETH Zurich.*

Rang, T.-N., Yu, W.-w. and Galambos, T.V. (1979). Load and resistance factor design of cold-formed steel statistical analysis of mechanical properties and thickness of materials combined with calibrations of the AISI design provisions of unstiffened compression elements and connections. Tech. Rep., Missouri S&T (formerly the University of Missouri-Rolla).

Retief, J.V. and Dunaiski, P. (2009). *Background to SANS 10160.* AFRICAN SUN MeDIA.

Rogers, C.A. and Hancock, G.J. (1997). Ductility of G550 sheet steels in tension. *Journal of Structural Engineering*, vol. 123, no. 12, pp. 1586–1594.

Schafer, B. (2006*a*). Direct strength method design guide. *American Iron and Steel Institute*.

Schafer, B. and Ádány, S. (2006). Buckling analysis of cold-formed steel members using CUFSM: conventional and constrained finite strip methods. In: *Eighteenth international specialty conference on cold-formed steel structures*, pp. 39–54.

Schafer, B.W. (2006*b*). Designing cold-formed steel using the direct strength method. In: *18-th International Specialty Conference on Cold-Formed Steel Structures*, pp. 26–27.

Schafer, B.W. (2008). Review: the direct strength method of cold-formed steel member design. *Journal of constructional steel research*, vol. 64, no. 7, pp. 766–778.

Schafer, B.W. (2011). Cold-formed steel structures around the world. *Steel Construction*, vol. 4, no. 3, pp. 141–149.

Schafer, B.W., Grigoriu, M. and Peköz, T. (1998). A probabilistic examination of the ultimate strength of cold-formed steel elements. *Thin-walled structures*, vol. 31, no. 4, pp. 271–288.

Schafer, B.W. and Peköz, T. (1998). Direct strength prediction of cold-formed steel members using numerical elastic buckling solutions. In: *Fourteenth international specialty conference on cold-formed steel structures.* Missouri S&T (formerly the University of Missouri-Rolla).

South African Bureau of Standards (2011). *South African National Standard 10162-2 The structural use of steel Part 2: Cold-formed steel structures.* SABS Standards Division, Pretoria.

Timoshenko, S.P. (1945). Theory of bending, torsion and buckling of thin-walled members of open cross section. *Journal of the Franklin Institute*, vol. 239, no. 4, pp. 249–268.

Timoshenko, S.P. and Gere, J.M. (1961). Theory of elastic stability. 1961. *McGrawHill-Kogakusha Ltd, Tokyo.*

Van Wyk, R. (2014). *Reliability of cold-formed steel screwed connections in tilt- and bearing.* Master's thesis, Civil Engineering, University of Stellenbosch, Stellenbosch, South Africa.

Vrouwenvelder, T., Holický, M. and Markova, J. (2001). JCSS Pobabilistic Model Code.

Yu, C. and Schafer, B.W. (2005). Distortional buckling of cold-formed steel members in bending.

Yu, W.-W. and LaBoube, R.A. (2010). *Cold-formed steel design*. John Wiley & Sons.

Ziemian, R.D. (2010). *Guide to stability design criteria for metal structures*. John Wiley & Sons.

Appendix A

Critical Global Buckling Equations

A.1 Critical elastic buckling moment

The critical buckling moment of singly symmetric sections bent about the symmetry x-axis, doubly symmetric sections and Z-sections bent about an axis perpendicular to the web is calculated by SANS 10162-2 as presented here.

$$M_{cr} = C_b A r_{oi} \sqrt{f_{oy} f_{oz}} \tag{A.1}$$

where:

C_b	= coefficient depending on moment distribution = 1 for all calculations of this document
A	= area of the full cross-section
r_{o1}	= polar radius of gyration of the cross-section about the shear centre $= \sqrt{r_x^2 + r_y^2 + x_0^2 + y_0^2}$
r_x, r_y	= radii of gyration of the cross-section about the respective axes
x_o, y_0	= coordinates of the shear centre of the cross-section
f_{oy}	= elastic buckling stress in an axially loaded compression member for flexural buckling $= \frac{\pi^2 E}{(l_{ey} r_y)^2}$
f_{oz}	= elastic buckling stress in an axially loaded compression member for torsional buckling $= \frac{GJ}{Ar_{oi}^2}\left(1 - \frac{\pi^2 E I_w}{GJ l_{ez}}^2\right)$
l_{ex}, l_{ey}, l_{ez}	= effective length for respective buckling cases
G	=shear modulus of elasticity
J	= torsion constant for the cross-section
I_w	= warping constant for the cross-section

A.2 Compressive critical elastic buckling load

The compression critical buckling load of singly symmetric sections bent about the symmetry axis, doubly symmetric sections and Z-sections bent about an axis perpendicular to the web is calculated by SANS 10162-2 as presented here.

$$P_{cr} = Af_{oc} \tag{A.2}$$

where:

A = area of the full cross-section
f_{oc} = least elastic buckling stress of f_{oy},f_{ox} and f_{oz} in an concentrically compressed member